

Spring 1996

Comparison of different signal processing algorithms to extract the respiration waveform from the ECG

David J. Caggiano
New Jersey Institute of Technology

Follow this and additional works at: <https://digitalcommons.njit.edu/theses>



Part of the [Biomedical Engineering and Bioengineering Commons](#)

Recommended Citation

Caggiano, David J., "Comparison of different signal processing algorithms to extract the respiration waveform from the ECG" (1996).
Theses. 1066.

<https://digitalcommons.njit.edu/theses/1066>

This Thesis is brought to you for free and open access by the Theses and Dissertations at Digital Commons @ NJIT. It has been accepted for inclusion in Theses by an authorized administrator of Digital Commons @ NJIT. For more information, please contact digitalcommons@njit.edu.

Copyright Warning & Restrictions

The copyright law of the United States (Title 17, United States Code) governs the making of photocopies or other reproductions of copyrighted material.

Under certain conditions specified in the law, libraries and archives are authorized to furnish a photocopy or other reproduction. One of these specified conditions is that the photocopy or reproduction is not to be “used for any purpose other than private study, scholarship, or research.” If a user makes a request for, or later uses, a photocopy or reproduction for purposes in excess of “fair use” that user may be liable for copyright infringement,

This institution reserves the right to refuse to accept a copying order if, in its judgment, fulfillment of the order would involve violation of copyright law.

Please Note: The author retains the copyright while the New Jersey Institute of Technology reserves the right to distribute this thesis or dissertation

Printing note: If you do not wish to print this page, then select “Pages from: first page # to: last page #” on the print dialog screen

The Van Houten library has removed some of the personal information and all signatures from the approval page and biographical sketches of theses and dissertations in order to protect the identity of NJIT graduates and faculty.

ABSTRACT

COMPARISON OF DIFFERENT SIGNAL PROCESSING ALGORITHMS TO EXTRACT THE RESPIRATION WAVEFORM FROM THE ECG

by
David J. Caggiano

Power spectral analysis of heart rate variability is a powerful tool to measure the activity of the parasympathetic division of the autonomic nervous system non-invasively. To determine the parasympathetic activity, the frequency of respiration must be known. However, during ambulatory studies, the frequency of respiration is not acquired. To alleviate this problem, methods have been proposed in the past to derive the respiration from the ECG. Unfortunately, these previous methods are unreliable if the subject's breathing rate is uncontrolled.

In this study, four methods to derive the respiration waveform from the electrocardiogram (ECG) were developed. Two leads of ECG and a measure of respiration were taken from nine healthy subjects during rest, paced breathing, and exercise. To determine the optimum method, the respiration was then derived using all four methods and compared to the measured respiration in the time domain and frequency domain using cross-correlation and coherence, respectively. The results of this study indicate that three of the four methods developed can accurately and reliably derive the respiration during every section of the experimental protocol. In addition, the respiration waveform derived using the variable QRS window, dependent leads method is quantitatively identified as the most accurate.

**COMPARISON OF DIFFERENT SIGNAL PROCESSING ALGORITHMS TO
EXTRACT THE RESPIRATION WAVEFORM FROM THE ECG**

by
David J. Caggiano

**A Thesis
Submitted to the Faculty of
New Jersey Institute of Technology
in Partial Fulfillment of the Requirements for the Degree of
Master of Science in Biomedical Engineering**

Biomedical Engineering Committee

January 1996

Blank Page

APPROVAL PAGE

**COMPARISON OF DIFFERENT SIGNAL PROCESSING ALGORITHMS TO
EXTRACT THE RESPIRATION WAVEFORM FROM THE ECG**

David J. Caggiano

Dr. Stanley S. Reisman, Thesis Advisor Date
Professor of Electrical Engineering and Associate
Chairperson for Graduate studies, NJIT

Dr. David Kristol, Committee Member Date
Professor of Chemistry and Director of Biomedical
Engineering Program. NJIT

Dr. Thomas W. Findley, Committee Member Date
Associate Professor of Medicine, UMDNJ
Director of Research, Kessler Institute for
Rehabilitation

BIOGRAPHICAL SKETCH

Author: David J. Caggiano

Degree: Master of Science in Biomedical Engineering

Date: January 1996

Date of Birth: December 7, 1971

Place of Birth: Summit, NJ

Undergraduate and Graduate Education:

- Master of Science in Biomedical Engineering,
New Jersey Institute of Technology, Newark, NJ, 1996
- Bachelor of Science in Electrical Engineering,
New Jersey Institute of Technology, Newark, NJ, 1994
- Minor in Applied Mathematics,
New Jersey Institute of Technology, Newark, NJ, 1994

Major: Biomedical Engineering

This thesis is dedicated to my beloved parents, Karen and Joseph Caggiano, and my beloved grandmother, Catherine Goduti, for all their support, guidance, and encouragement throughout my education

ACKNOWLEDGMENT

The author wishes to express his sincere gratitude to his advisor, Dr. Stanley S. Reisman, for his guidance, friendship, and moral support throughout this research. Without his help, this thesis would never have been completed.

Special thanks are extended to Dr. David Kristol and Dr. Thomas W. Findley for serving as members of the committee.

The author is also grateful to the Kessler Institute for Rehabilitation for providing the facility for this research. Thanks also to John Andrews for his time and patience in helping me with the computer network, to Lynne Hendrickson for technical support, and to everyone who participated in the experimental protocol.

The author also appreciates the timely help, suggestions, and friendship from Dr. Alan Davis and Dr. Hallie Robbins.

And finally, a special thank you to Chris O'Bara for his help, suggestions, encouragement, and, most of all, friendship throughout my college career and especially during the research for this thesis.

TABLE OF CONTENTS

Chapter	Page
1 INTRODUCTION	1
1.1 The Heart	1
1.2 The Electrocardiogram	6
1.3 Cardiac Depolarization, Repolarization and Mean Electrical Vector	9
1.3.1 Cardiac Action Potentials	9
1.3.2 Cardiac Electrical Vector	11
1.4 The Basis for ECG Derived Respiration	15
1.5 The Nervous System	18
1.5.1 The Autonomic Nervous System	20
1.6 Heart Rate Variability	25
1.6.1 Physiology of Changes in Heart Rate	25
1.6.2 Heart Rate Variability as a Measure of Autonomic Function	27
1.6.3 Power Spectral Analysis of Heart Rate Variability	28
1.7 Literature Review	32
1.7.1 Previous Research on Power Spectral Analysis of Heart Rate Variability ...	32
1.7.2 Previous Research on ECG Derived Respiration	35
1.8 Scope of Thesis	37

TABLE OF CONTENTS
(Continued)

Chapter	Page
2 METHODS	39
2.1 Theory of Power Spectral Analysis	39
2.2 Analog-to-Digital Conversion	43
2.3 Subjects and Experimental Protocol	46
2.4 Data Acquisition	48
2.4.1 Acquisition of the Original Respiration Waveform	48
2.4.2 Acquisition of ECG	53
2.4.2.1 Determination of Sampling Frequency	57
2.5 Data Analysis	60
2.5.1 Converting Data from Binary Format to ASCII Format	60
2.5.2 Analysis of ECG to Obtain Power Spectrum of Heart Rate Variability	61
2.5.3 Analysis of Original Respiration Waveform	68
2.6 Methods for Deriving the Respiration from the ECG	69
2.6.1 The Method Presented by Mark and Moody	69
2.6.1.1 Zhao's Software to Implement Mark and Moody's Method	70
2.6.1.2 Problems with Zhao's Software	73
2.6.2 Fixed QRS Window, Independent Leads Method	78
2.6.2.1 Software Implementation of the Fixed QRS Window, Independent Leads Method	80

TABLE OF CONTENTS
(Continued)

Chapter	Page
2.6.3 Method Based on the Amplitude Modulation of the R-Waves.....	82
2.6.3.1 Software Implementation of the Method Based on the Amplitude Modulation of the R-Waves	83
2.6.4 Variable QRS Window, Independent Leads Method.....	84
2.6.4.1 Software Implementation of the Variable QRS Window, Independent Leads Method.....	86
2.6.5 Variable QRS Window, Dependent Leads Method	89
2.6.5.1 Software Implementation of the Variable QRS Window, Dependent Leads Method.....	89
2.7 Developed Methods That Were Unsuccessful.....	91
3 RESULTS.....	94
3.1 Theory of Cross-Correlation	94
3.1.1 Understanding the Cross-Correlation Function	97
3.2 Theory of Coherence	102
3.3 Visual Comparison.....	104
3.4 Cross-Correlation of the ECG Derived Respiration with the Measured Respiration	107
3.5 Coherence Between the ECG Derived Respiration and the Measured Respiration	113
3.6 Cross-Correlation of the Spectra.....	117
3.7 Comparison of the Standard Method to Compute Parasympathetic Activity to a More Theoretical Method.....	121

TABLE OF CONTENTS
(Continued)

Chapter	Page
4 DISCUSSION AND CONCLUSIONS.....	126
4.1 General Summary of the Work in This Thesis.....	126
4.2 Comparison of the Different Methods Developed to Derive the Respiration	128
4.3 Factors Affecting the ECG Derived Respiration Results	133
4.4 Comparison of the Parasympathetic Activity When Calculated by the Traditional Method and With a More Theoretical Method.....	134
4.5 Future Work.....	134
APPENDIX A SOME FIGURES FOR CHAPTER 3.....	139
APPENDIX B A COPY OF THE IRB PROPOSAL TO CONDUCT AN EXPLORATORY STUDY INVOLVING HUMAN SUBJECTS.....	149
APPENDIX C PROCEDURE FOR A/D CONVERSION OF A HOLTER CASSETTE.....	160
APPENDIX D ANALYSIS PROCEDURES TO OBTAIN POWER SPECTRUM OF HRV	163
APPENDIX E ANALYSIS PROCEDURES AND PROGRAM TO ANALYZE THE ORIGINAL RESPIRATION WAVEFORM.....	166
APPENDIX F PROGRAM “CORRECTH” TO CORRECT R-WAVE DETECTION	168
APPENDIX G “IMPQRSCA” PROGRAM LISTING	169
APPENDIX H “ADRESP” PROGRAM LISTING	175
APPENDIX I “VQRSIND” PROGRAM LISTING.....	181
APPENDIX J “VQRSDEP” PROGRAM LISTING	187
APPENDIX K S-PLUS PROGRAM DEVELOPED TO CALCULATE CROSS-CORRELATION.....	192

TABLE OF CONTENTS
(Continued)

Chapter	Page
APPENDIX L S-PLUS PROGRAM DEVELOPED TO CALCULATE COHERENCE.....	194
REFERENCES	196

LIST OF FIGURES

Figure	Page
1.1 The Heart.....	2
1.2 The Systemic and Pulmonary Circulations.....	3
1.3 The Conducting System of the Heart	4
1.4 The Sequence of Cardiac Excitation	5
1.5 Illustration of a Typical Electrocardiogram	6
1.6 Standard ECG Limb Leads to Form Einthoven's Triangle.....	7
1.7 Comparison of Different ECG Tracings with Emphasis on the QRS Complex	8
1.8 A Cardiac Action Potential and the Associated Changes in Membrane Permeabilities	10
1.9 Comparison of Action Potentials in a Ventricular Muscle Cell to a SA Nodal Cell....	11
1.10 Diagrammatic Explanation of the Voltage Induced by a Dipole at a Distant Point P.....	13
1.11 The Spatial Vectorcardiogram Formed by the Termini of an Infinite Number of Instantaneous Heart Vectors.....	14
1.12 The Three Vectorcardiographic Loops and Their Mean Vectors	15
1.13 Respiration Induced Modulation of the ECG.....	16
1.14 ECG Modulated by Respiration	17
1.15 Right and Left Axis Deviation of the Mean QRS Vector	19
1.16 The Sympathetic Nervous System and Parasympathetic Nervous System	22
1.17 Autonomic Innervation of the Heart.....	26
1.18 Effect of Autonomic Stimulation on the Slope of the Pacemaker Potential	27

**LIST OF FIGURES
(Continued)**

Figure	Page
1.19 Typical Power Spectrum of HRV	30
2.1 Block Diagram of an Analog-to-Digital Converter	43
2.2 Spectrum of the Measured Signal, Sampled Signal, and Improperly Sampled Signal.	45
2.3 Placement of the Electrodes to Record Respiration Using the RESPI.....	50
2.4 Example of Three Cycles of a RESPI Respiration Waveform Showing the Waveshape and Typical Recording Quality.....	52
2.5 ECG Electrode Locations	55
2.6 Plot of the Average Amplitude of the R-Wave Peaks vs. Sampling Frequency.....	60
2.7 Figure Depicting the Construction of the IBI Signal.....	62
2.8 IBI Signal and IIBI Signal.....	64
2.9 Power Spectrum of IIBI Signal in Figure 2.8	66
2.10 Smoothed Power Spectrum of Figure 2.9.....	67
2.11 Plot of the Split Cosine Bell Taper Used as a Window in the FFT Calculation.....	67
2.12 Estimation of the Mean Cardiac Vector by Taking the Arctangent of the Areas Under the QRS Complex of Leads I and III.....	71
2.13 Figure Showing the Algorithm to Detect the Q-wave.....	72
2.14 Figure Showing the Calculation of the QRS Complex Area.....	73
2.15 Construction of the Derived Respiration Waveform from the QRS Complex Areas from Two Orthogonal Leads.....	74
2.16 Close-Up of an R-Wave Showing an Incorrect Detection.....	75

**LIST OF FIGURES
(Continued)**

Figure	Page
2.17 Illustration of the Origin of the Phase Shift Between the R-waves of Leads I and III for a Simplified Case in Which the QRS Loop Has a Constant Magnitude and Constant Change in Direction	77
2.18 One QRS Complex of Lead I and Lead III Showing Different Time of R-waves.....	78
2.19 An Example of the S-wave as the Minimum of the QRS Complex.....	79
2.20 Example of “adresp” Output of Amplitude Modulation of the R-waves.....	84
2.21 Different Waveshapes for Closely Spaced Lead Connections.....	85
2.22 Illustration of the Algorithm to Detect the S-wave	88
2.23 An Example of How the Times of the Q, R, and S-Waves from the Dominant Lead Were Used to Correspond to the Times of the Q, R, and S-Waves in the Non-Dominant Lead.....	90
3.1 Illustration of the Cross-Correlation Calculation	96
3.2 Cross-Correlation of Two Sine Waves with the Same Frequency, in Phase, and with Different Amplitudes	99
3.3 Cross-Correlation Between Two Sine Waves, One Which Contains a DC Component.....	99
3.4 Cross-Correlation of Two Sine Waves with Different Frequencies	100
3.5 Cross-Correlation Between Two Sine Waves, One Which Contains a Frequency Component of the Other	101
3.6 Cross-Correlation of Two Signals with the Same Frequency, but Different Waveshapes.....	102
3.7 Cross-Correlation of the ECG Derived Respiration with the Measured Respiration	108

LIST OF FIGURES
(Continued)

Figure	Page
3.8 Example of Coherence Between the Measured Respiration and the ECG Derived Respiration	114
3.9 Cross-Correlation Between Two Spectra.....	118
4.1 Comparison of the Spectra for the Respiration Derived from the Fixed QRS Window, Independent Leads Method to the Respiration Derived With Zhao's Program	127
4.2 Illustration of the Central Frequency Calculation.....	129
4.3 Examples of the RESPI Recording During Exercise	131
A.1 Comparison of the Measured Respiration with the ECG Derived Respiration for All Four Methods for Each Section of Each Section of the Experimental Protocol	140
A.2 Boxplots for Data in Chapter 3	146

LIST OF TABLES

Table	Page
1.1 The Nervous System.....	20
1.2 Autonomic Effects on Selected Organs of the Body	24
2.1 General Information of Each Subject	47
2.2 Average Amplitude of the Peak in the R-Waves at Different Sampling Frequencies of an Actual ECG.....	58
2.3 Average Amplitude of the Peak in the R-Waves at Different Sampling Frequencies of a Simulated ECG.....	59
3.1 Cross-Correlation Between the Derived Respiration and the Measured Respiration for the Fixed QRS Window, Independent Leads Method	108
3.2 Cross-Correlation Between the Derived Respiration and the Measured Respiration for the Method Based on the Amplitude Modulation of the R-Waves ..	110
3.3 Cross-Correlation Between the Derived Respiration and the Measured Respiration for the Variable QRS Window, Independent Leads Method.....	111
3.4 Cross-Correlation Between the Derived Respiration and the Measured Respiration for the Variable QRS Window, Dependent Leads Method	111
3.5 Average Correlation Coefficient Between the Derived Respiration and the Measured Respiration for the Four Methods, for Each Section of the Experimental Protocol	112
3.6 Average Cross-Correlation Coefficients for Each Method	112
3.7 Coherence Between the Derived Respiration and the Measured Respiration for the Fixed QRS Window, Independent Leads Method.....	114
3.8 Coherence Between the Derived Respiration and the Measured Respiration for the Method Based on the Amplitude Modulation of the R-Waves	115
3.9 Coherence Between the Derived Respiration and the Measured Respiration for the Variable QRS Window, Independent Leads Method	115

LIST OF TABLES
(Continued)

Table	Page
3.10 Coherence Between the Derived Respiration and the Measured Respiration for the Variable QRS Window, Dependent Leads Method	115
3.11 Average Coherence at the Frequency of Respiration Between the Derived Respiration and the Measured Respiration for the Four Methods, for Each Section of the Experimental Protocol.....	117
3.12 Cross-Correlation Between the Spectra of the Derived Respiration and the Measured Respiration for the Fixed QRS Window, Independent Leads Method...	119
3.13 Cross-Correlation Between the Spectra of the Derived Respiration and the Measured Respiration for the Method Based on the Amplitude Modulation of the R-Waves	120
3.14 Cross-Correlation Between the Spectra of the Derived Respiration and the Measured Respiration for the Variable QRS Window, Independent Leads Method	120
3.15 Cross-Correlation Between the Spectra of the Derived Respiration and the Measured Respiration for the Variable QRS Window, Dependent Leads Method.	120
3.16 Average Cross-Correlation of the Spectra of the Derived Respiration and the Measured Respiration for the Four Methods, for Each Section of the Experimental Protocol.....	121
3.17 Values Indicating the Parasympathetic Activity Computed by the Traditional Method and by Coherence.....	123

CHAPTER 1

INTRODUCTION

Biomedical engineering is the application of the principles of engineering, science, and mathematics to medicine and biology. Therefore, in order to conduct biomedical engineering research, the relevant physiological systems must be understood. The purpose of this chapter is to provide a general, but concise, introduction to the physiological systems that are relevant to the work in this thesis.

1.1 The Heart

The cardiovascular system consists of blood vessels and the heart. In 1628, British physiologist William Harvey discovered that the cardiovascular system forms a circle, or circuit, so that blood pumped out of the heart through one set of vessels returns to the heart via a different set of vessels[1]. In actuality, there are really two circuits, both originating and terminating in the heart. Therefore, the heart, illustrated in Figure 1.1, is divided into two functional halves, each half containing two chambers: an atrium and a ventricle. The atrium of each side empties into the ventricle on that side. There is no direct flow between the two atria or the two ventricles in a healthy individual.

Blood is pumped by the pulmonary circuit from the right ventricle through the lungs and then into the left atrium. The blood is then pumped by the systemic circuit, from the left ventricle, through all the tissues of the body except the lungs, and then to the right atrium. In both circuits, the vessels carrying blood away from the heart are called arteries,

and those carrying blood from either the lung or all other parts of the body back to the heart are called veins. Figure 1.2 illustrates the heart with the systemic and pulmonary circulations.

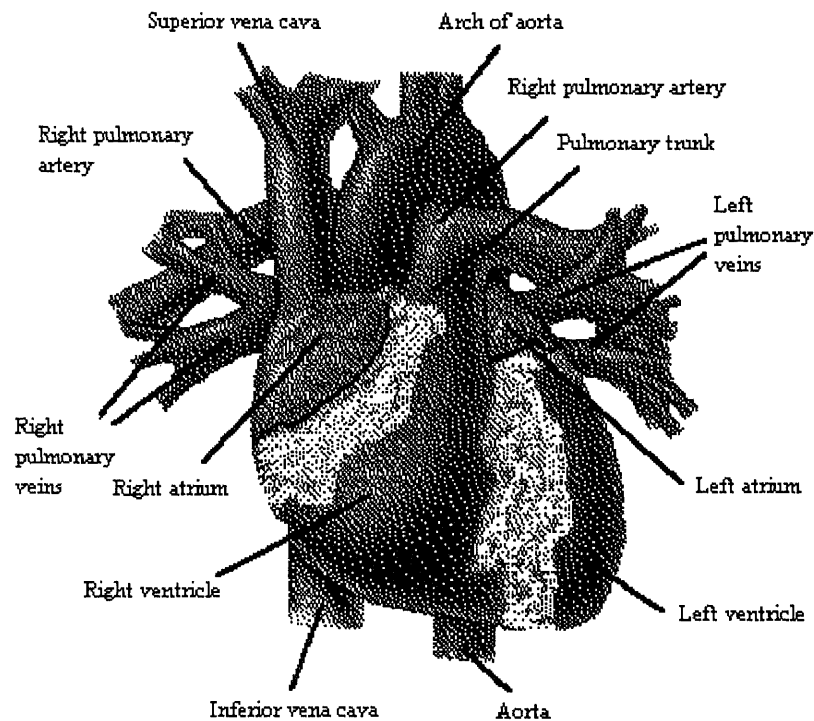


Figure 1.1 The Heart (from A.J. Vander, J.H. Sherman, and D.S. Luciano, *Human Physiology*, 1994)

The heart, located in the chest, is a muscular organ which is enclosed in a fibrous sac called the pericardium[2]. The walls of the heart are primarily composed of cardiac-muscle cells called the myocardium. Cardiac-muscle cells combine properties of both skeletal muscle and smooth muscle. However, even more important, approximately one percent of the cardiac-muscle fibers have specialized features that are essential for normal heart excitation[1]. They constitute a network known as the conducting system of the

heart and are connected to other cardiac-muscle fibers by gap junctions. The gap junctions allow action potentials to spread from one cardiac-muscle cell to another. Thus, the initial excitation of one myocardial cell results in excitation of all cells, and as a result, the pumping action of the heart. The conducting system of the heart is illustrated in Figure 1.3.

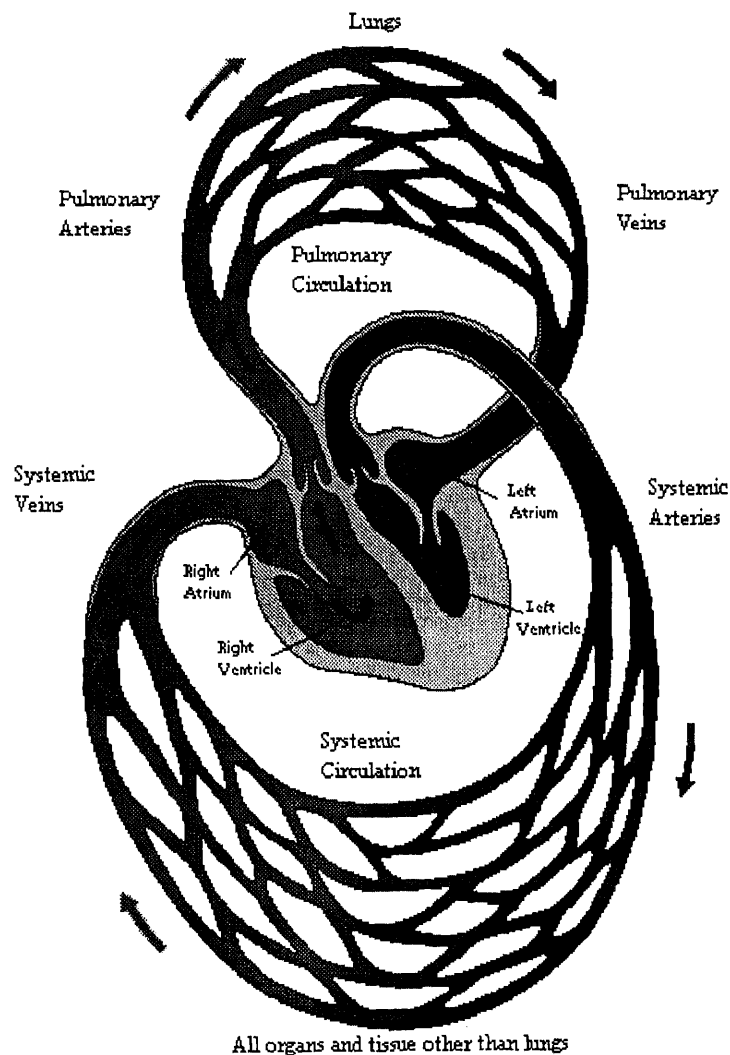


Figure 1.2 The Systemic and Pulmonary Circulations
(from A.J. Vander, J.H. Sherman, and D.S. Luciano, *Human Physiology*, 1994)

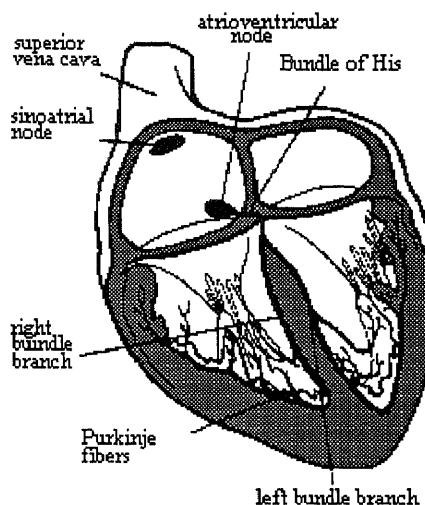


Figure 1.3 The Conducting System of the Heart
 (from A.J. Vander, J.H. Sherman, and D.S. Luciano, *Human Physiology*, 1994)

The initial depolarization normally arises in a small group of conducting-system cells called the sinoatrial (SA) node. The SA node is located in the right atrium near the entrance of the superior vena cava (the vein returning from the body tissues that are above the heart). The SA node has the fastest inherent discharge rate of any of the myocardial cells with pacemaker activity. Therefore, the SA node is the normal pacemaker for the entire heart[1]. The action potential initiated in the SA node spreads throughout the myocardium, passing from cell to cell by way of gap junctions. The spread throughout the right atrium and the left atrium does not depend on fibers of the conducting system. The spread is rapid enough that the two atria are depolarized and contract at essentially the same time.

The spread of the action potential from the atria to the ventricles involves a portion of the conducting system called the atrioventricular (AV) node. The AV node is located at the base of the right atrium. The AV node has an important characteristic that makes

the cardiac cycle more efficient. For several reasons related to the electrical properties of the cells that make up the AV node, the propagation of action potentials through the AV node results in a delay of approximately 0.1 seconds[1]. This delay allows the atria to finish contracting and, therefore, completely emptying their contents of blood into their respective ventricles before ventricular excitation occurs.

Upon leaving the AV node, the action potential then travels to the septum, the area between the two ventricles, by the conducting-system fibers called the bundle of His[2]. The bundle of His then divides into the left and right bundle branches which eventually leave the septum and enter the walls of their respective ventricles. These fibers then make contact with the Purkinje fibers which are large conducting cells that rapidly distribute the action potential throughout most of the ventricles. The rapid conduction along the Purkinje fibers and the distribution of these fibers cause the depolarization of the left and right ventricular cells approximately simultaneously, thus resulting in a single coordinated contraction. Figure 1.4 illustrates the sequence of cardiac excitation.

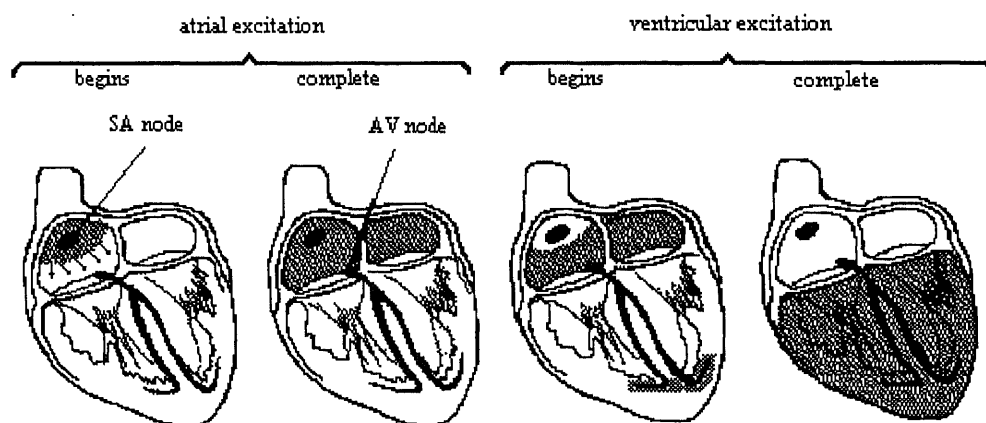


Figure 1.4 The Sequence of Cardiac Excitation
(from A.J. Vander, J.H. Sherman, and D.S. Luciano, *Human Physiology*, 1994)

1.2 The Electrocardiogram

The electrocardiogram (ECG) is primarily a tool for evaluating the electrical events within the heart. The action potentials of cardiac muscles can be viewed as batteries that cause charge to move throughout the body fluids. These moving charges, or currents, represent the sum of the action potentials occurring simultaneously in many individual cells and can be detected by recording electrodes at the surface of the skin[1]. Figure 1.5 illustrates a typical normal ECG recorded between the right and left wrists for one heart beat.

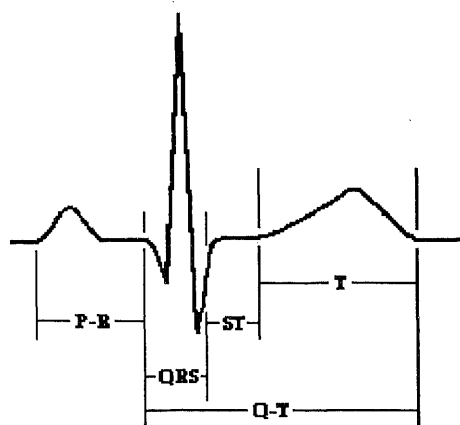


Figure 1.5 Illustration of a Typical Electrocardiogram.

The first deflection, the P wave, corresponds to the current flow during atrial depolarization (contraction). The second deflection, the QRS complex, is a result of ventricular depolarization. The third and final deflection is the T wave. The T wave is a result of ventricular repolarization (relaxation). It should be noted that atria repolarization is usually not evident in the ECG because it occurs at the same time as the QRS complex.

As mentioned earlier, the ECG is a measure of the electrical activity of the heart measured on the skin. In order to measure the ECG, bipolar leads are required. A “lead”

is not a single wire attached to the body. The bipolar method of acquiring ECG detects electrical variations at two different locations on the skin and displays the difference to obtain one waveform. Figure 1.6 is an illustration of the standard limb lead connections that form Einthoven's triangle. In addition, the diagram also shows the names of the respective leads. To record lead I, the negative terminal of the ECG monitor is connected to the right arm (RA) and the positive terminal is connected to the left arm (LA). To record lead II, the negative terminal of the ECG monitor is connected to the right arm and the positive terminal is connected to the left leg. To record lead III, the negative terminal of the ECG monitor is connected to the left arm and the positive terminal is connected to the left leg (LL). The reference point or ground is connected to the right leg (RL).

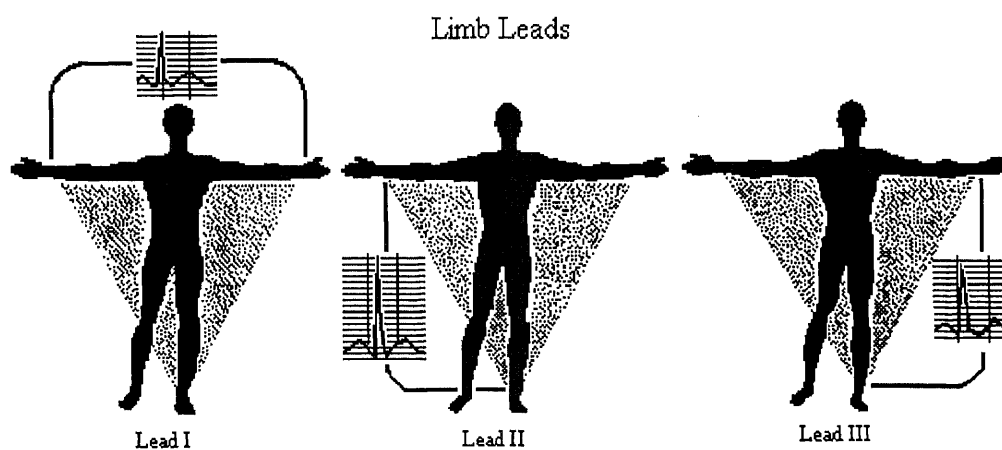


Figure 1.6 Standard ECG Limb Leads to Form Einthoven's Triangle (from F. Netter. *The CIBA Collection of Medical Illustrations Volume 5, The Heart*, 1981)

It is important to realize that depending on where the electrodes are attached, a different waveshape will be obtained for the same electrical events occurring in the heart. In other words, Leads I, II, and III all have a different waveform shape. In addition to

obtaining different waveforms depending on the location of the electrodes, each individual has a unique ECG.

Figure 1.7 illustrates two different waveshapes frequently acquired from the leads which constitute Einthoven's triangle. It is necessary to devise a terminology which differentiates between these two types of ECG waveforms so they can be referred to throughout the remainder of the thesis. It should be noted that this terminology is specific to this thesis and is not standardly used. The tracing in Figure 1.7(a) is termed "dominant" by the author because when it is compared to the tracing in Figure 1.7(b), the QRS complex is mainly above the baseline of the ECG and the R wave has a higher peak than in the other tracing.

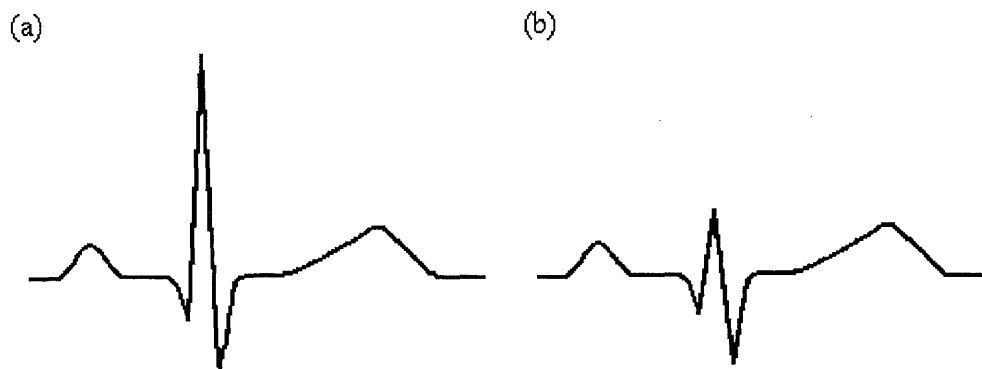


Figure 1.7 Comparison of Different ECG Tracings With Emphasis on the QRS Complex.
(a) Dominant Lead (b) Non-Dominant Lead

It should be noted that certain leads can not be considered dominant when compared to another lead on a consistent basis. For example, lead I is not always dominant when compared to lead III. The explanation of this fact is described in section 1.4 and is related to the motion of the heart in the thoracic cavity.

1.3 Cardiac Depolarization, Repolarization, and Mean Electrical Vector

1.3.1 Cardiac Action Potentials

The typical resting cardiac cell, like any other cell of excitable tissues (skeletal muscle, smooth muscle, and nerve) maintains the separation of charged particles (ions) across its membrane[2]. Negatively charged particles (anions) are distributed along the inside of the cardiac cell membrane and positively charged particles (cations) are distributed along the outside of the cardiac cell membrane. Action potentials result when the membrane permeabilities change, resulting in an inrush of cations and an export of anions from the cell membrane. Figure 1.8 illustrates a cardiac action potential and the associated changes in the membrane permeabilities.

As in skeletal-muscle cells and neurons, the resting membrane is much more permeable to potassium than to sodium[1]. Therefore, the resting membrane potential is closer to the potassium equilibrium potential (-90 mV) than to the sodium equilibrium potential (+60 mV). The depolarization phase of the action potential is due to a positive-feedback increase in sodium permeability, which is caused by the opening of voltage-sensitive sodium channels. Occurring almost simultaneously, the permeability to potassium decreases as potassium channels close, adding to the depolarization.

In skeletal muscle cells and neurons, the return of sodium permeability toward its resting value is accompanied by repolarization (toward the resting membrane potential of approximately -90 mV). However, with cardiac muscle cells this is not the case. The cardiac muscle cell membrane remains depolarized at a plateau of about 0 mV. There are two reasons for the plateau. One reason is that the potassium permeability stays below the

resting value. The second, more important, reason for the plateau in the depolarization is because there is an increase in the permeability to calcium. Repolarization occurs when the permeabilities of calcium and potassium return to their original resting states.

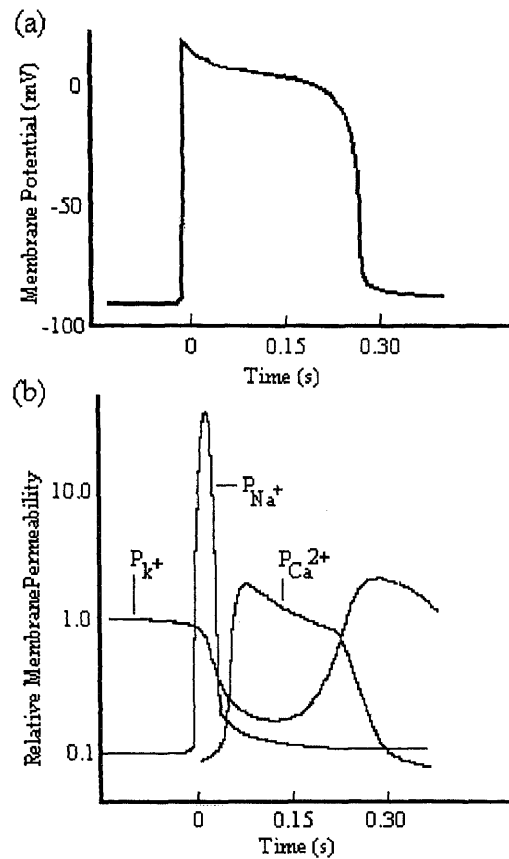


Figure 1.8 A Cardiac Action Potential and the Associated Changes in Membrane Permeabilities. (a) Ventricular Muscle Cell Membrane Potential. (b) Simultaneously Measured Permeabilities P to Potassium, Sodium, and Calcium. (from A.J. Vander, J.H. Sherman, and D.S. Luciano, *Human Physiology*, 1994)

It should be noted that there is a distinct difference between the action potentials of the vast majority of the myocardial cells, as just described, and the action potentials of the SA node[1,2]. Figure 1.9 illustrates both the cardiac action potential and the action potential occurring in the SA node. Note that the resting potential of the SA-node is not

steady, and has a slow depolarization known as a pacemaker potential. This slow depolarization brings the membrane potential to a threshold, at which point an action potential occurs. Following the action potential, the membrane repolarizes, and the gradual depolarization begins again. The pacemaker potential provides the SA node with automaticity, the capacity for spontaneous rhythmical self-excitation. The inherent rate of the SA node, that is, the rate exhibited in the total absence of an neural or hormonal input to the node, is approximately 100 depolarizations per minute [1].

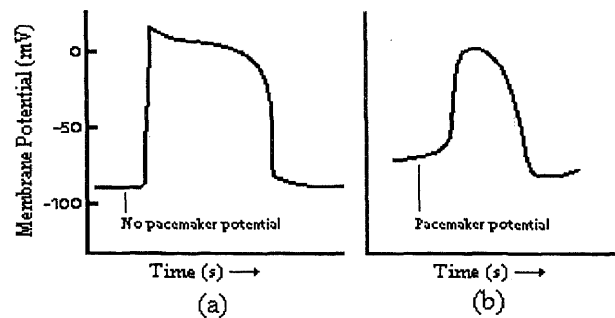


Figure 1.9 Comparison of Action Potentials in a (a) Ventricular Muscle Cell to (b) a Sinoatrial (SA) Nodal Cell. (from A.J. Vander, J.H. Sherman, and D.S. Luciano, *Human Physiology*, 1994)

1.3.2 Cardiac Electrical Vector

When charges are separated by a distance, such as is the case with the cardiac cell in its resting state, the result is an electric dipole[3]. When the cardiac cell is depolarizing or repolarizing, the strength and magnitude of the dipole are changing. Each cardiac cell, consisting of anions and cations separated by a cell membrane, can be modeled by a dipole with a positive and negative terminal. During every cardiac cycle, every cardiac cell of the heart depolarizes and repolarizes in an orderly manner and, therefore, each dipole changes

magnitude and direction every cardiac cycle. At any one instant, by vectorally summing up every dipole from each cardiac cell, an instantaneous mean cardiac vector can be calculated that corresponds to the total electrical activity of the heart.

Due to the chemical nature of the tissue fluids, the body is essentially a volume conductor with the boundary being the body surface[3]. A volume conductor is a medium that permits the conduction of electricity in three dimensions. Therefore, a dipole (instantaneous cardiac vector) on the inside of a volume conductor (body) induces an electric field on the surface of the volume conductor (skin), and potential variations within this field are easily measured (ECG).

In a volume conductor, the paths taken by the current depend upon the geometry and structure of the volume conductor[4]. When the volume conductor is homogeneous, isotropic, and large compared to the dipole and when the dipole is located centrally within the conductor, then the distribution of currents, and thus potentials, is symmetrical and obeys the simple law for voltage induced at a distant point by a dipole. Thus, the electrical potential at any point P in a volume conductor is

$$V_P = \frac{\mu \cos\theta}{4\pi\epsilon R^2} \quad (1.1)$$

where μ is the dipole moment, which is equal to the product of the charge Q and the length of the dipole d, R is the distance from the center of the dipole to the point P, ϵ is the dielectric constant or permittivity of the material between the dipole and the point P, and θ is the angle between the dipole axis and the line to that distant point P[3,4] (Figure 1.10).

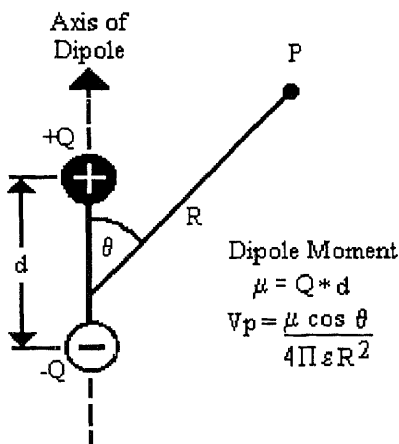


Figure 1.10 Diagrammatic Explanation of the Voltage Induced by a Dipole at a Distant Point P

The formula mentioned above is for an isotropic, homogeneous, relatively large conductor compared to the size of the dipole[4]. In addition, it assumes that the dipole is located centrally within the conductor. Unfortunately, this is not the case of the human body. The heart dipole is located eccentrically within the body. Also, the human body is anisotropic, inhomogeneous, finite sized, and irregular-shaped volume conductor. In modeling, this inhomogeneity seems to be rather unimportant except perhaps for the low resistance and consequent short circuiting effect of blood within the heart cavities[3]. The short circuiting effect of blood within the heart presumably diminishes the effect of all separate sources and leads to a unification of electrical activity, which lends further support to the hypothesis that the heart behaves as a single dipole[3].

The origin of the cardiac vector is assumed to be in the center of the heart mass and remains there throughout the entire cardiac cycle[3]. The magnitude and direction of the vector changes throughout the cycle depending on the sum of all the individual cardiac-cell dipole moments. For the entire cardiac cycle there are an infinite number of

instantaneous heart vectors. Consequently, the instantaneous vector plotted over time forms a continuous loop in 3-dimensional space. This loop is called the spatial vectorcardiogram and is illustrated in Figure 1.11.

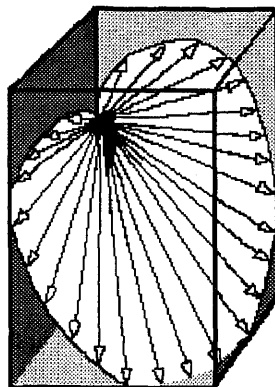


Figure 1.11 The Spatial Vectorcardiogram Formed by the Termini of an Infinite Number of Instantaneous Heart Vectors

The spatial vectorcardiogram consists of 3 successive loops, namely: the “P loop”, the “QRS loop”, and the “T loop”[3]. The P loop represents the time course of each instantaneous cardiac vector produced during atrial depolarization. The QRS loop represents the time course of each instantaneous cardiac vector produced during ventricular depolarization. The T loop represents the time course of each instantaneous cardiac vector produced during ventricular repolarization. Figure 1.12 illustrates the three vectorcardiographic loops as well as their respective mean vectors. It should be noted that the mean cardiac vector is different from the resultant vector. The resultant vector is the vectorial sum of all the instantaneous vectors. It will have the same direction as the mean vector and the magnitude will be the sum of each component of all the instantaneous

vectors in that direction. On the other hand, the magnitude of the mean cardiac vector is the magnitude of the resultant vector divided by the number of instantaneous vectors.

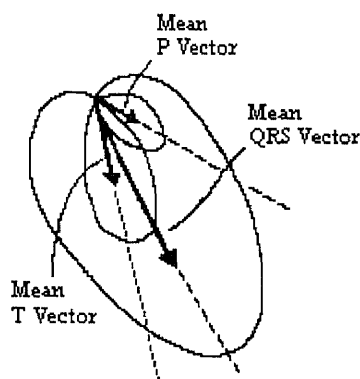


Figure 1.12 The Three Vectorcardiographic Loops and Their Mean Vectors

1.4 The Basis for ECG Derived Respiration

Due to the interaction of the many different biological systems, a specific biological signal, such as the ECG, is mostly influenced directly by the specific biological system being measured, as well as by other systems which act indirectly. Because the respiratory system influences the cardiovascular system, it is possible to derive a respiratory signal from an ECG signal. For example, it is very common to see an amplitude modulation of the R-wave peaks of an ECG tracing as illustrated in Figure 1.13. The specific interaction of the respiratory system on the ECG is described below.

ECG signals recorded from surface electrodes that are mounted on the chest are influenced by two different factors[5]. One factor affecting the ECG is the change in the electrical impedance of the thoracic cavity while breathing. The expansion and contraction

of the thoracic cavity, caused by the filling and emptying of the lungs with air while breathing, results in a change in the electrical impedance between the electrical activity of the heart and the recording electrodes of the chest. Not only does the distance change between the electrodes and the heart, but the composition of the thoracic cavity changes due to the inhalation and exhalation of air. Because air is a good insulator, or conversely, a bad conductor, it is easy to understand why the inhalation of air increases the electrical impedance of the thoracic cavity. Therefore, one would suspect that regardless of the ECG lead being monitored, when the person breathes in, the ECG amplitude would decrease. Likewise, when the person exhales, one would suspect that the ECG amplitude would increase, as is the case in Figure 1.13. However, Figure 1.14 indicates that this is not the case.

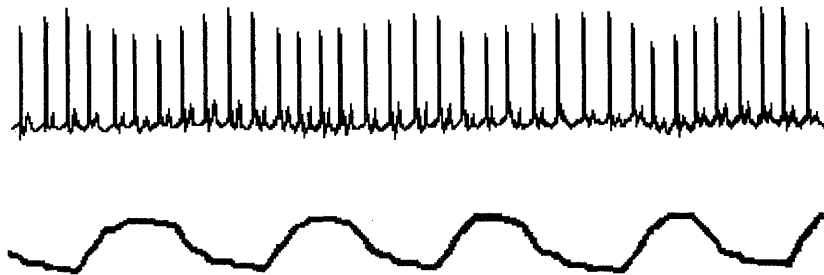


Figure 1.13 Respiration Induced Modulation of the ECG. Upper Trace: ECG; Lower Trace: Respiration Waveform Measured by Impedance Pneumography Device.

In Figure 1.14, when the person inhales, the amplitude of Lead I decreases while the amplitude of Lead III increases. Also when the person exhales, the amplitude of Lead I increases, and the amplitude of Lead III decreases. Using our reasoning that the impedance of the thoracic cavity increases during inhalation and decreases during

exhalation, it appears that the change in amplitude of lead III should be the opposite of what is shown. Clearly, there is another factor affecting the amplitude modulation of the ECG. This other factor is the change in the direction of the mean cardiac vector. The mean electrical axis of the QRS wave often reflects the anatomic position of the heart in the chest. Thus, it is important to understand the relationship between the position of the heart in the chest and the electrocardiogram because the heart's position has a profound affect on the ECG[6].

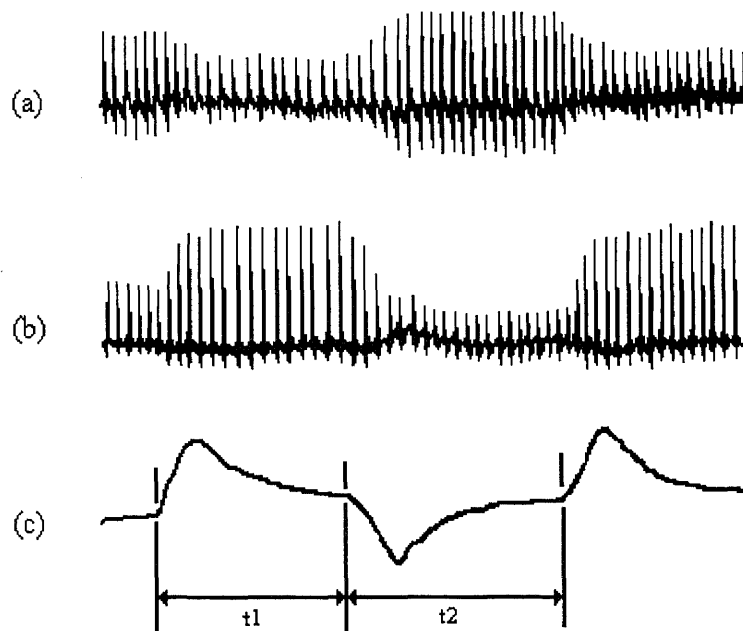


Figure 1.14 ECG Modulated by Respiration. (a): Lead I ECG; (b): Lead III ECG; (c) Respiration; t1: Deep Inhalation and Hold; t2: Deep Exhalation and Hold (from S. Shin, W. Tapp, S. Reisman, and B. Natelson, "Assessment of autonomic regulation of HRV by the method of complex demodulation," *IEEE Trans. on Biomed. Eng.*, 1989)

During inspiration and expiration, the lungs fill and empty with air, which consequently changes the position of the heart within the thoracic cavity. The change in

the position of the heart is very complex because the heart can rotate around an anteroposterior axis, a transverse axis, and an anatomical axis which runs from the base to the apex of the heart[6]. In addition, the heart can rotate from front to back, side to side, and around the anatomic axis simultaneously. The rotation around the anatomic axis is often best described as being either clockwise or counterclockwise. This description of rotation refers to the observer looking at the base or bottom of the heart along the anatomic axis which runs from the base of the heart, through the septum (which is between the ventricles), and finally emerges at the apex.

There are two different axis deviations that are apparent in the leads that constitute Einthoven's triangle[6]. These deviations are termed the right axis deviation and the left axis deviation and are illustrated in Figure 1.15. In right axis deviation, the QRS loop is directed downward. Electrocardiographically, this results in large R waves in leads II and III. Because of the geometry, if the QRS loop is directed downward, the loop would be orthogonal to Lead I. Therefore, right axis deviation results in a small amplitude R wave in Lead I. In left axis deviation, the QRS loop points toward the left shoulder blade. This results in a large R wave in Lead I, and depending on the specific ECG, relatively small R wave amplitude in Leads II and III.

1.5 The Nervous System

Human behavior is controlled and regulated by two major communication systems, the endocrine system and the nervous system. The nervous system can be divided into two separate, but interconnected, parts. The first part consists of the brain and spinal cord and

is called the central nervous system. The second part, which consists of nerves which extend from the brain and the spinal cord out to all points of the body, is called the peripheral nervous system.

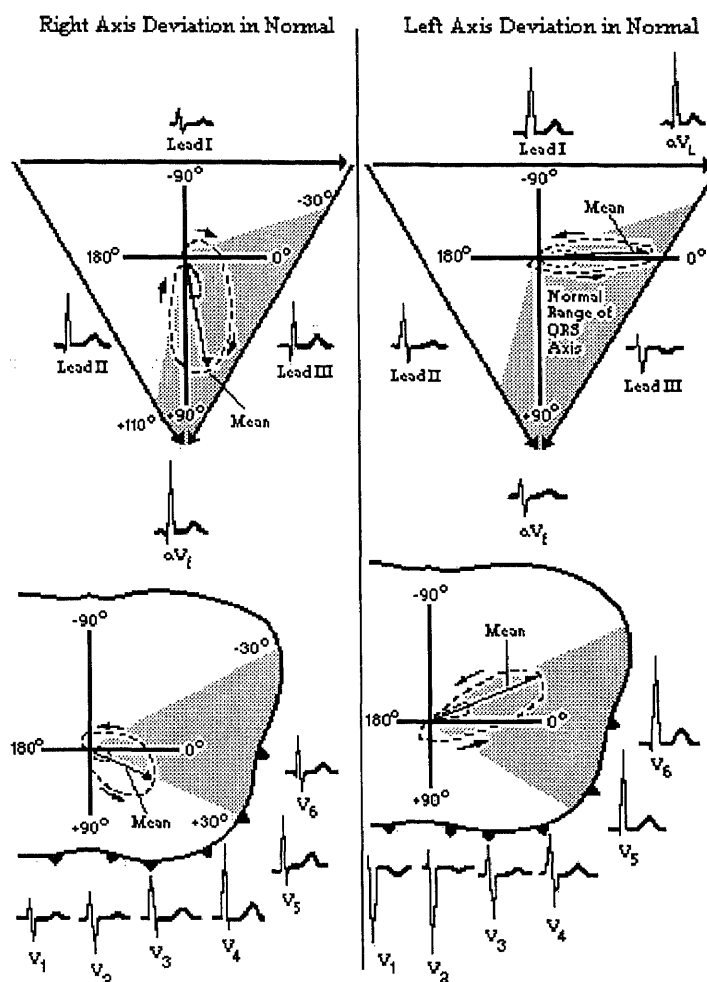


Figure 1.15 Right and Left Axis Deviation of the Mean QRS Vector (from F. Netter. *The CIBA Collection of Medical Illustrations Volume 5, The Heart*, 1981)

The peripheral nervous system consists of both an afferent division and efferent division. The afferent division conveys information from primary receptors to the central nervous system. The efferent division carries signals from the central nervous system out to effector cells such as muscles and organs. The efferent division is subdivided into a

somatic nervous system and an autonomic nervous system. The somatic nervous system consists of all the nerve fibers going from the central nervous system to skeletal-muscle cells. The efferent innervation of all tissues other than skeletal muscle is done by the autonomic nervous system. Table 1.1 illustrates the organization of the human nervous system.

Table 1.1 The Nervous System

- I. Central Nervous System
 - A. Brain
 - B. Spinal Cord
- II. Peripheral Nervous System
 - A. Afferent Division
 - B. Efferent Division
 - 1. Somatic Nervous System
 - 2. Autonomic Nervous System
 - a. Sympathetic Nervous System
 - b. Parasympathetic Nervous System

1.5.1 The Autonomic Nervous System

Cardiac muscle cells, smooth muscle cells, and glands are innervated by the autonomic nervous system. Although it is not entirely true, the autonomic nervous system controls bodily functions that one often assumes to be automatically controlled. Such functions are heart rate, blood pressure, and body temperature. For example, when one is placed under a lot of physical stress such as climbing three flights of stairs, the person's heart rate and respiration rate automatically increase to supply the body with the energy needed on demand. Likewise, when a person is resting, the heart rate and respiration rate slows down due to the decrease in energy expenditure. Therefore, one can assume that the body automatically controls heart rate and respiration rate. However, it is possible to override

the autonomic nervous system and consciously control some of its functions. A good example of this is that under certain meditation techniques, it has been shown that some people can actually lower their heart rate substantially below their resting rate, or even stop their heart from beating for a brief period of time. In addition, some people can slow their breathing rate to only one breath for every few minutes during deep meditation.

As shown in Table 1.1, the autonomic nervous system is divided into two anatomically and physiologically different systems[1,2]. These two systems are termed the sympathetic nervous system and the parasympathetic nervous system. Anatomically, the sympathetic and parasympathetic nervous systems differ for two reasons. One difference is that the nerve fibers of each system leave the central nervous system at different levels. The sympathetic nerve fibers leave the central nervous system from the thoracic and lumbar sections of the spinal cord. The parasympathetic nerve fibers leave the central nervous system from the brain through cranial nerves III, V, VII, IX, and X and the second and third sacral spinal nerves. Cranial nerve X is also called the vagus nerve. The parasympathetic innervation of much of the thorax and abdomen, and especially the heart, is done by the nerve fibers which leave from the brain through cranial nerve X. Therefore, parasympathetic activity related to the heart is often called vagal activity. Figure 1.16 illustrates the anatomic difference between the sympathetic nervous system and parasympathetic nervous system as well as some of their respective effector organs.

The second anatomical difference between the sympathetic and parasympathetic nervous systems has to do with the location of the ganglia. Each connection of the autonomic nervous system between the central nervous system and the effector cells

consists of two-neuron chains connected by a synapse. Most, but not all, of the sympathetic ganglia are located close to the spinal cord and form two chains of ganglia, one on each side of the spinal cord, called the sympathetic trunk. Conversely, the parasympathetic ganglia lie within the organs innervated by the postganglionic neurons.

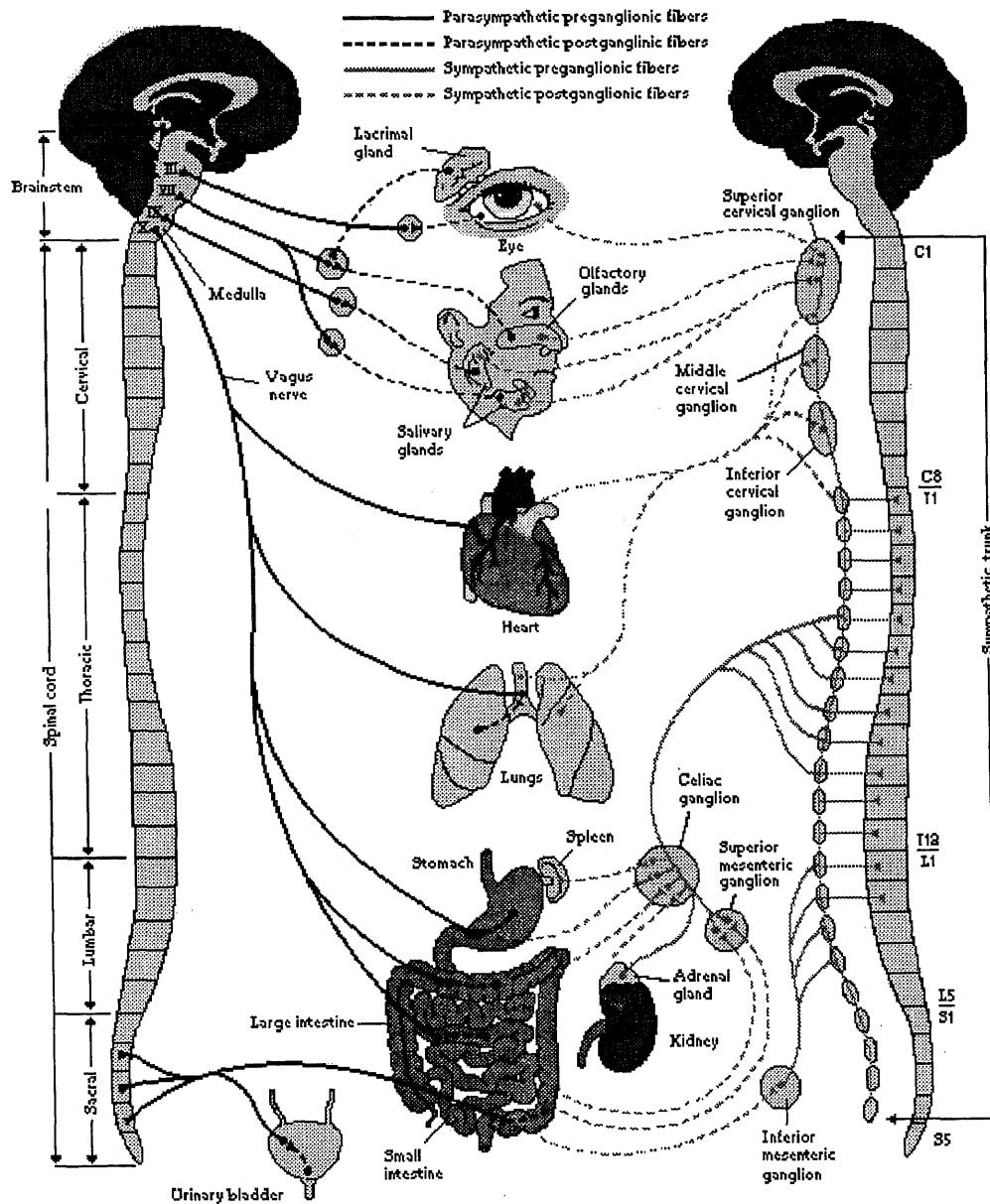


Figure 1.16 The Sympathetic Nervous System (right) and Parasympathetic Nervous System (left). (from A.J. Vander, J.H. Sherman, and D.S. Luciano, *Human Physiology*, 1994)

Physiologically, the sympathetic and parasympathetic nervous systems are also different[2]. One common physiological characteristic is that the major neurotransmitter released between the pre- and post-ganglionic fibers is acetylcholine. However, in the sympathetic division, the major neurotransmitter between the postganglionic fiber and the target cell is usually norepinephrine, a neurotransmitter that activates excitatory receptors, but in some cases can inhibit certain organs. In the parasympathetic division, the major neurotransmitter between the postganglionic fiber and the target cell is the same as the pre- and post- ganglionic neurotransmitter, acetylcholine. Although acetylcholine generally has an excitatory effect, it is also known to have inhibitory effects as well, such as the slowing of the heart by the vagus nerve. In Figure 1.16, it is important to realize that some organs, such as the heart, eyes, and stomach, receive autonomic activity from both the sympathetic and parasympathetic nervous systems. This is often called “dual innervation”. Usually, but not always, whatever effect the sympathetic nervous system has on the effector cells, the parasympathetic nervous system has the opposite effect[2]. In general, the sympathetic nervous system increases its response under conditions of stress. It is responsible for what is known as the fight-or-flight response. On the other hand, activity of the parasympathetic nervous system is associated with relaxing and the storing of energy. For example, heart rate increases with sympathetic activity and decreases with parasympathetic activity. Table 1.2 summarizes the effects of the autonomic nervous system on selected organs.

Dual innervation by nerve fibers that cause opposite responses provides a very fine degree of control over the effector organ- it is like equipping a car with both an

accelerator and a brake[1]. One can slow the car simply by decreasing the pressure on the accelerator; however, the combined effects of releasing the accelerator and applying the brake provides faster and more accurate control. Analogously, the sympathetic and parasympathetic divisions are usually activated reciprocally; that is, as the activity of one division is increased, the activity of the other is decreased.

Table 1.2 Autonomic Effects on Selected Organs of the Body.
(from A.J. Vander, J.H. Sherman, and D.S. Luciano, *Human Physiology*, 1994)

Effector Organ	Effect of Sympathetic Stimulation	Effect of Parasympathetic Stimulation
Eyes		
Iris muscles	contracts (dilates pupil)	relaxes (constricts pupil)
Ciliary muscle	Relaxes (flattens lens)	Contracts
Heart		
SA node	Increases heart rate	Decreases heart rate
Atria	Increases contractility	Decreases contractility
AV node	Increases conduction velocity	Decreases conduction velocity
Ventricles	Increases contractility	Decreases contractility slightly
Arterioles		
Coronary	Dilates (β_2); constricts (α)	Dilates
Skin	Constricts	None
Skeletal muscle	Dilates (β_2); constricts (α)	None
Abdominal viscera	Dilates (β_2); constricts (α)	None
Salivary glands	Constricts	Dilates
Lungs		
Bronchial Muscle	Relaxes	Contracts
Stomach		
Motility, tone	Decreases	Increases
Sphincters	Contracts	Relaxes
Secretion	Inhibits (?)	Stimulates

In addition to dual innervation, another important physiological characteristic is that the sympathetic and parasympathetic nervous system are continually active. These basal rates of sympathetic and parasympathetic activity are often referred to as

sympathetic and parasympathetic tone. Without tone, each nervous system would only be able to produce one desired output, such as increasing heart rate. For instance, when sympathetic tone increases, heart rate increases. Conversely, when sympathetic tone decreases below its basal rate, the heart rate will decrease because of less sympathetic influence.

1.6 Heart Rate Variability

1.6.1 Physiology of Changes in Heart Rate

Change in heart rate is sensitive to changes in body temperature, plasma electrolyte concentrations, and hormones[1]. However, the most important influence of beat-to-beat variations of heart rate comes from the autonomic nervous system. More specifically, sympathetic activity increases heart rate, whereas activity in the parasympathetic (vagus) nerves causes the heart rate to decrease. Due to considerably more parasympathetic activity to the heart than sympathetic activity in the resting state, the normal resting heart rate is below the inherent rate of 100 beats/minute.

The autonomic nervous system innervates the heart in a number of places. The sympathetic nervous system terminates at the SA node, the conduction system, atrial and ventricular myocardium, and coronary vessels. The parasympathetic fibers terminate in the SA and AV nodes, atrial and ventricular musculature, and coronary vessels. Interplay between the two systems will cause the heart to speed up or slow down, depending on which system is more active[7]. Figure 1.17 illustrates the autonomic innervation of the heart.

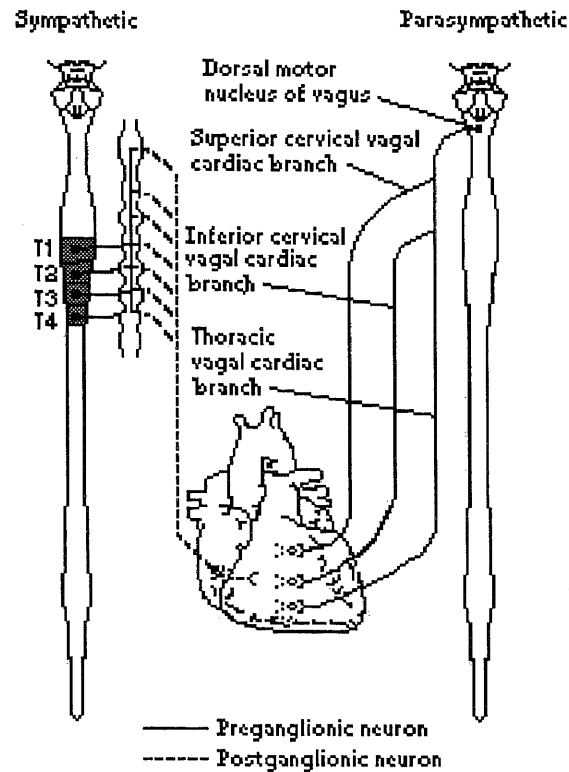


Figure 1.17 Autonomic Innervation of the Heart (from M.D. Kamath and E.L. Fallen, "Power spectral analysis of heart rate variability," *Crit. Rev. in Biomed. Eng.*, 1993)

Perhaps the most important site of innervation of the autonomic nervous system on the heart occurs at the SA node. As was mentioned in section 1.3.1, the SA node possesses an inherent discharge rate, often referred to as the pacemaker potential. The pacemaker potential is a slow depolarization of the cells of the SA node as was illustrated in Figure 1.9. The innervation of the sympathetic and parasympathetic nervous system on the SA node changes the characteristics of depolarization within the SA node cells, thus changing heart rate. Figure 1.18 illustrates these changes due to autonomic innervation.

For comparative purposes, the pacemaker potential labeled 'a' is the control. From the figure, one can observe that sympathetic stimulation increases the slope of the pacemaker potential. As a result, the SA node cells reach the threshold more rapidly, thus

increasing the heart rate. Conversely, parasympathetic stimulation decreases the slope of the pacemaker potential. Consequently, the SA node cells reach the threshold more slowly, and heart rate decreases. In addition to decreasing the slope of the pacemaker potential, parasympathetic stimulation also hyperpolarizes the plasma membrane of the SA node cells so that the pacemaker potential starts from a more negative membrane potential. As a result, the time it takes the SA node cells to reach the threshold increases, which decreases heart rate.

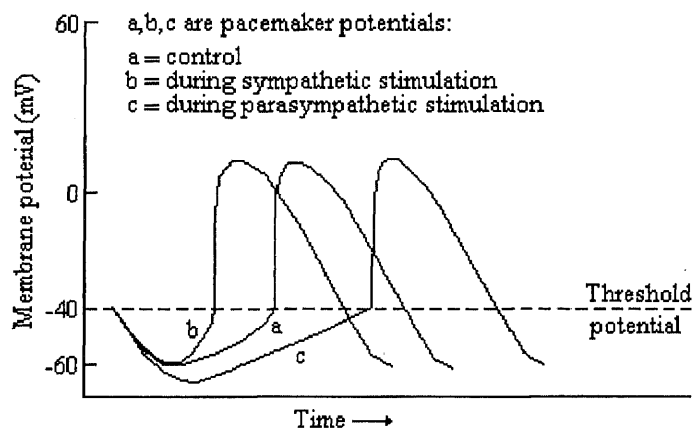


Figure 1.18 Effect of Autonomic Stimulation on the Slope of the Pacemaker Potential (from A.J. Vander, J.H. Sherman, and D.S. Luciano, *Human Physiology*, 1994)

1.6.2 Heart Rate Variability as a Measure of Autonomic Function

Changes in heart rate usually involve the reciprocal action of the two divisions of the autonomic nervous system. An increased heart rate is the result of reduced parasympathetic tone and a concomitant increase in sympathetic activity. A decrease in heart rate is usually the result of increased parasympathetic tone and a simultaneous decrease in sympathetic tone. Therefore, changes in heart rate reflect the action of the sympathetic and parasympathetic nervous systems on the heart. However, under certain

conditions, it is possible for heart rate to change by activity of only one division of the autonomic nervous system, independent of the other division, rather than reciprocal changes in both.

Initially, the effect of the autonomic nervous system on the heart was estimated by utilizing the traditional technique of average heart rate[7]. As a reference, the average heart rate was measured under normal resting conditions. Then the average heart rate was measured under the administration of drugs. The drugs used were atropine, which blocks the effects of the parasympathetic nervous system, and propranolol, which masks the effects of the sympathetic nervous system. A qualitative assessment can then be made of the autonomic nervous system by comparing the reference heart rate to the heart rate while under the administration of the drugs. This method looks at the average over time of heart rate. However, when the ECG is looked at on a beat-to-beat basis, rather than over a period of time, fluctuations in the heart rate are observed[7]. Recent research indicates that fluctuations in heart rate are a healthy sign. In fact, one hypothesis is that the larger variations in the heart rate correlate to a healthier autonomic nervous system. By contrast, a number of physiologic and disease states produce alterations in autonomic function which reduce the variability in heart rate[8] (see section 1.7 for a literature review).

1.6.3 Power Spectral Analysis of Heart Rate Variability

Power spectral analysis of heart rate variability is a potentially powerful tool for evaluating the activity of the autonomic nervous system noninvasively. Power spectral analysis is a

technique which transforms a signal from the time domain to the frequency domain. It is based on the theory proposed by Fourier which states that all periodic functions can be represented as a sum of sines and cosines at a fundamental frequency and its harmonics. This sum is referred to as a Fourier series. Since heart rate variability is not periodic, a similar technique called the Fourier transform is applied.

The time domain signal used for computing the heart rate variability power spectrum is known as the interbeat interval (IBI). The following is a brief description of how to obtain the IBI signal. A detailed description of the process is discussed in Section 2.5.2. To obtain the IBI signal, every R wave in the ECG is detected with software after the ECG has been acquired. The proper analog to digital techniques for data acquisition are discussed in Section 2.2. The difference in time between successive R waves is then converted to an IBI amplitude. Because the Fourier transform requires that the samples be evenly spaced[9], the IBI samples, which occur at different lengths of time, are interpolated with a backward step technique. This interpolated signal is often referred to as the interpolated interbeat interval (IIBI). The Fourier transform is then taken to convert the IIBI from the time domain to the frequency domain. Figure 1.19 illustrates a typical power spectrum of the IIBI signal.

In Figure 1.19, three distinct peaks are visible. These peaks are defined as: a very low frequency peak (0.0033 Hz to 0.04 Hz), a low frequency peak (0.04 Hz to 0.15 Hz), and a high frequency peak (0.15 Hz to 0.4 Hz). Sometimes, a fourth peak is identified as the ultra low frequency peak which consists of frequencies less than 0.0033 Hz.

Past research in power spectral analysis of heart rate variability correlates the three distinct peaks with certain physiological parameters[7]. The very low frequency band is associated with vasomotor control and temperature control. The low frequency band is associated with baroreceptor-mediated blood pressure control. The high frequency band has been linked with respiration.

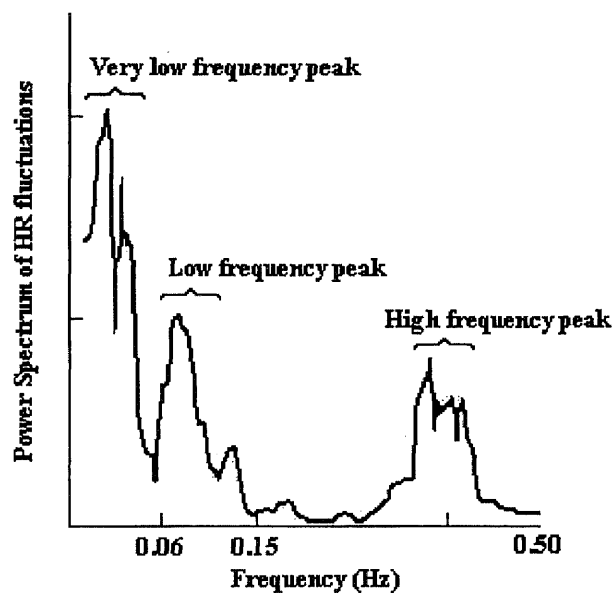


Figure 1.19 Typical Power Spectrum of HRV. (from M. Kamath and E. Fallen, "Power spectral analysis of heart rate variability," *Crit. Rev. in Biomed. Eng.*, 1993)

To date, the best known and best defined peak in power spectral analysis of heart rate variability is the high frequency peak. The high frequency peak reflects changes in the interbeat interval that cycles up and down at the same frequency as respiration. This influence of respiration on heart rate has been known for more than one century and is called respiratory sinus arrhythmia (RSA). Properly defined, RSA is a rhythmical fluctuation in heart periods at the respiratory frequency that is characterized by a

shortening and lengthening of heart periods in a phase relationship with inspiration and expiration, respectively[10]. RSA is being used increasingly as a measure of vagal control of the heart. As a result, the high frequency peak, which often occurs at the same frequency as the respiration peak, corresponds approximately to the RSA and it is purely parasympathetic in origin[11].

From experience, one might contest that the frequency of respiration is not limited to within the narrow band of 0.15 Hz to 0.4 Hz. The normal respiration rate can be as low as only a few breaths per minute at rest and as high as up to 40 breaths per minute during intense exercise[2]. This stresses the fact that, when doing research on heart rate variability to determine parasympathetic activity, the frequency of respiration must be known. More specifically, the power spectrum of the respiration waveform should be computed. Once the power spectrum of the respiration is obtained, the coherence between the respiration spectrum and the heart rate variability spectrum could be computed. Frequencies with a high coherence (i.e. >0.9) could then be considered of parasympathetic origin. Although this is the theoretical approach, in the field, the area under the frequencies of 0.15 to 0.4 Hz is considered parasympathetic in origin.

Unlike parasympathetic activity, the sympathetic activity is not easily separated from the power spectrum of heart rate variability[7]. It has been hypothesized that the low frequency peak (0.04 to 0.15 Hz) is a mixture of both parasympathetic activity and sympathetic activity. A better concept that is used to isolate the sympathetic activity is that of “sympatho-vagal balance” which recognizes both reciprocal and non-reciprocal parasympathetic and sympathetic influences on heart rate by computing the low frequency

to high frequency ratio[12]. An increase in the low frequency to high frequency ratio indicates either an increase of sympathetic activity, a decrease in parasympathetic activity, or a reciprocal change in both.

1.7 Literature Review

Research on heart rate variability is a relatively new area of study. Therefore, the results of many studies are still a major topic for discussion. For example, some groups of researchers feel the low frequency peak is purely sympathetic in nature, whereas most of the results appear to state that the low frequency region is a mixture of both the sympathetic and parasympathetic nervous systems. Despite this conflict, all researchers agree that the high frequency peak is an indicator of parasympathetic activity, and is directly related to the respiratory sinus arrhythmia. The following is a review of a small sampling of the research in the area of heart rate variability, the autonomic nervous system, and ECG derived respiration. The main point behind this short literature review is that increased parasympathetic activity is an indication of increased health and that certain disease conditions are accompanied by decreased vagal activity.

1.7.1 Previous Research on Power Spectral Analysis of Heart Rate Variability

In one of the earlier studies, O'Brien et al. conducted an experiment to see how age affects autonomic function [13]. The study was designed to investigate the effect of age on heart rate variability during four different situations: at rest, in response to a single deep breath, the Valsalva maneuver, and standing. Although O'Brien did not calculate the

power spectrum of HRV, his group investigated the variance of the R to R interval. In each procedure, heart rate variation showed a skewed distribution and a statistically significant negative correlation with age[13]. In other words, heart rate variation decreases with increasing age.

In another pioneering study involving diabetics, Pagani et al. subjected 49 uncomplicated diabetics and 40 age-matched controls to supine and tilt conditions while recording their heart rate variability (HRV)[14]. Pagani investigated R-R variance of the ECG and found that the R-R variance in diabetics was less than the control's R-R variance during both rest and tilt conditions. This study indicated that HRV could someday be used as an indicator of disease conditions such as diabetes.

In another pioneering study, Kleiger et al. observed that in a large sample (N=808) of post myocardial infarction (MI) patients, a low (<50 msec) standard deviation of mean R-R interval over 24 hour duration, 2 weeks after the MI, had the strongest univariate correlation with mortality[15]. The relative risk of mortality was 5.3 times higher in the group with low HRV (<50 msec) than the group with high HRV (>100 msec). It is hypothesized that decreased HRV correlates with increased sympathetic tone and decreased vagal tone and thus predisposes the patient to ventricular fibrillation[16].

In a study conducted in Japan, the short-term and long-term effects of cigarette smoking on autonomic cardiac regulation were investigated by power spectral analysis of heart rate variability under controlled respiration (15 breaths per minute)[17]. The short-term effects were examined in 9 smokers without evidence of cardiopulmonary disorders after an overnight abstinence from smoking. The heart rate spectral component which

reflects vagal cardiac control (0.25 Hz - the frequency of respiration equivalent to 15 breaths per minute) decreased 3 minutes after smoking 1 cigarette and the low frequency spectral component (0.04 to 0.15 HZ), indicative of sympathetic activity, increased after 10 to 17 minutes. The long-term effects were examined in 81 normal subjects comprising 25 nonsmokers, 31 moderate (1 to 24 cigarettes/day) smokers, and 25 heavy (>25 cigarettes/day) smokers after an overnight abstinence. Although the magnitude of the low frequency component was unaffected by the smoking status, the respiratory component in the supine position was smaller in the young (<30 yrs old) heavy smokers than in the young nonsmokers or moderate smokers. Also, postural changes in the components, a decrease in the respiratory component and an increase in the low frequency component with standing, were observed in the nonsmokers but not in the heavy smokers. These results suggest that smoking causes an acute and transient decrease in vagal cardiac control, and that heavy smoking causes long-term reduction in vagal cardiac control in young people and blunted responses in autonomic cardiac regulation[17].

In 1992, Bigger et al. conducted a study that compared the 24 hour parasympathetic activity in aerobically trained and untrained healthy young men[18]. In this study, parasympathetic activity was assessed from 24 hour ECG recordings by calculating the high frequency (0.15 to 0.4 Hz) beat to beat heart period variability in eight endurance-trained men and eight age-matched untrained men. The data were analyzed separately for sleeping hours when parasympathetic activity is dominant and also for waking hours. The results concluded that the parasympathetic activity is substantially greater in trained men than in untrained men, and that this effect is present during both

waking and sleeping hours. These data suggest that exercise training may increase parasympathetic activity over the entire day.

1.7.2 Previous Research on ECG Derived Respiration

The problem of extracting a quality representation of the respiration waveform from ECG tracings is an open problem for which the published literature gives no consistent and reliable solution. Even more striking, the application of ECG derived respiration to assess autonomic function is another scarcely written about topic. The following is a review of the few attempts that have been made to extract the respiratory waveform from the ECG.

In 1985, Pinciroli et al. published two papers, one about obtaining “virtual ECG Leads” and the other about the extraction of electrical axis variation for the derivation of the respiratory waveform[19,20]. Pinciroli tried to create “virtual ECG leads” which would represent what would be obtained from electrodes fixed in position relative to the heart. The virtual leads were mathematically derived from the original leads. The conclusions of his study on virtual leads was that they do not exist on a consistent basis. Although only two orthogonal leads were taken into consideration, Pinciroli suggests that using a third orthogonal lead might yield better results. The insight of deriving the respiration with the virtual leads stems from the fact that the virtual leads could yield a somewhat strong variation of the heart’s position in the chest. In his group’s second paper about the extraction of the electrical axis variation of the heart, he applies his techniques of virtual leads to three orthogonal leads to derive the respiratory waveform. As a comparison, a respiratory wave was recorded with a band impedance meter.

Although he did have some success on deriving a respiration waveform similar to the one recorded directly, his results were inconsistent. In his conclusion, Pinciroli agrees that the aim of deriving the respiratory waveform from the ECG is attainable and should be researched further.

In 1985, Moody et al. published a paper that describes a method to derive the respiratory waveform from two-leads of ECG[5]. In 1986 he followed his original work up with a paper that validates the clinical significance of his work[21]. The method presented in these papers involved estimating the mean cardiac vector during each QRS loop to derive the respiration. Although the specifics of the method will be presented in section 2.6.1, the results obtained with this method appeared to work on a consistent basis when trying to diagnose sleep apnea. In addition, it should be mentioned that Moody did not describe in detail why he chose to do the method the way he did. In other words, there was no explanation for doing the specifics of his method as opposed to other possible slight modifications to his method.

In 1994, Lingeng Zhao presented a thesis to the biomedical engineering committee at NJIT that utilized the method presented by Moody[22]. In addition, Zhao et al. published two papers describing his work[23,24]. In this study, data were taken from 9 healthy subjects during rest, paced breathing, and exercise. The respiration was derived from the recorded ECG signals and was compared with the original respiration recorded through an impedance pneumography device. Zhao reported an excellent correlation between the derived respiration and the original respiration for rest and paced breathing. However, during exercise, the results indicate that there is room for improvement.

1.8 Scope of Thesis

The ultimate goal of power spectral analysis of heart rate variability is to utilize the results of the past, present, and future research to be able to characterize certain disease states by measuring the function of the autonomic nervous system non-invasively. At the present time, there are many variables, some of which are known and some that are not known, which adversely affect the signal processing, as well as the autonomic nervous system itself. One known variable that affects the autonomic nervous system is that when subjects are surrounded by technological equipment such as an ECG cart or impedance pneumograph, they tend to get nervous, which is a sympathetic response. Perhaps even the surroundings, such as a hospital or rehabilitation facility, make people nervous. Therefore, it is difficult to get an accurate measure of the subject's usual autonomic activity. The solution to this problem is to measure the autonomic activity of an individual in their natural, every day environment over a course of 24 hours using a Holter monitor. As previously mentioned, in order to compute the parasympathetic activity, the frequency of respiration must be known.

The purpose of this thesis is to determine the optimum signal processing algorithm to extract the respiration waveform from the ECG for a variety of activities. Once the respiration waveform is known, the ECG can be processed and the autonomic activity can be calculated. Therefore, this would enable accurate ambulatory measurement of the autonomic nervous system.

Although previous research has been conducted to estimate the mean cardiac vector, and thus, derive the respiration from the change in angle of the mean cardiac

vector in the frontal plane, nobody has investigated the specifics to determine the optimum method. Therefore, in this research, four software algorithms were developed and tested to determine the best possible technique. The software was used to derive the respiration waveform from 9 subjects who were exposed to a specific experimental protocol consisting of resting, controlled breathing, and exercise. During the experiment, two leads of ECG were collected using a Holter monitor and the subject's actual respiration was measured as a reference for the derived waveforms. The derived respiration methods were then compared to the measured respiration in both the time domain and frequency domain using cross correlation and coherence, respectively.

In addition, the traditional method of computing parasympathetic activity by calculating the area under the power spectrum of the IIBI between 0.15 and 0.4 Hz was compared to a more theoretical method. Theoretically, the parasympathetic activity should be calculated by determining the specific frequency band of respiration and calculating the power in the heart rate variability spectrum within those frequencies.

CHAPTER 2

METHODS

The purpose of this chapter is to thoroughly explain the methods used to acquire the biological signals of interest, namely the electrocardiogram and respiration rate, and to explain the equipment used to acquire these signals. To begin the chapter, a basic description is given of the theory behind the signal processing techniques used to analyze and acquire the signals. Because of the complexity of the signal processing, references are provided for more specific explanations. Also in this chapter is an explanation of the experimental protocol, as well as the different signal processing algorithms developed to derive the respiration from the ECG.

2.1 Theory of Power Spectral Analysis

In the early 1800's, a French mathematician named Jean Baptiste Joseph Fourier (1768-1830) discovered that a periodic function can be represented by an infinite sum of sine and cosine functions that are harmonically related[9]. That is, the period of any trigonometric term in the infinite series is an integral multiple, or harmonic, of the fundamental period T of the periodic function. This series of trigonometric terms is called the Fourier series. Stated another way, the Fourier series says that all periodic functions can be represented as a sum of sines and cosines at a fundamental frequency and its harmonics.

Mathematically, the Fourier series of a function $f(t)$ is represented as [25]:

$$f(t) = a_0 + \sum_{n=1}^{\infty} (a_n \cos[n\omega_0 t] + b_n \sin[n\omega_0 t]) \quad (2.1)$$

where a_v , a_n , and b_n are the Fourier coefficients and are defined as:

$$a_v = \frac{1}{T} \int_{t_0}^{t_0+T} f(t) dt \quad (2.2)$$

$$a_n = \frac{2}{T} \int_{t_0}^{t_0+T} f(t) \cos[n\omega_o t] dt \quad (2.3)$$

$$b_n = \frac{2}{T} \int_{t_0}^{t_0+T} f(t) \sin[n\omega_o t] dt \quad (2.4)$$

Once a_n and b_n are known, the amplitude and phase angle of each harmonic is known. The description of a periodic function in terms of the amplitude and phase angle of each term in the Fourier series of $f(t)$ can be represented graphically. The plot of the amplitude of each term versus the frequency is called the amplitude spectrum of $f(t)$, and the plot of the phase angle versus the frequency is called the phase spectrum of $f(t)$. Because the amplitude and phase angle data occur at discrete values of the frequency, these plots are also referred to as line spectra[25]. The distance between components in the frequency domain is an integer multiple of the fundamental frequency.

In general, the Fourier series can be thought of as a tool which helps convert a signal from the time domain to the frequency domain. In the time domain, the amplitude of the signal is known over all times; however, the frequency content is unknown. In the graphical representation of the amplitude of each frequency term in the Fourier series, the frequency content of the wave is known. The relative contribution of each frequency is proportional to the amplitude of each frequency term.

Using some basic trigonometric rules, the Fourier series can be expressed in an exponential form. To derive this form, the sine and cosine functions must be replaced with their exponential equivalents:

$$\cos[n\omega_o t] = \frac{e^{jn\omega_o t} + e^{-jn\omega_o t}}{2} \quad (2.5)$$

$$\sin[n\omega_o t] = \frac{e^{jn\omega_o t} - e^{-jn\omega_o t}}{2j} \quad (2.6)$$

After substituting equations (2.5) and (2.6) into equation (2.1) and simplifying, the exponential form of the Fourier series is obtained:

$$f(t) = \sum_{n=-\infty}^{\infty} C_n e^{jn\omega_o t} \quad (2.7)$$

where

$$C_n = \frac{1}{T} \int_{t_o}^{t_o+T} f(t) e^{-jn\omega_o t} dt \quad (2.8)$$

The Fourier series is a good technique to transform nonsinusoidal, periodic functions from the time domain to the frequency domain. However, if the function $f(t)$ is non-periodic, the Fourier series can not be used. Instead, a technique is used called the Fourier transform. Unlike the Fourier series, frequency components of a non-periodic function may be present at all frequencies in the Fourier transform.

The derivation of the Fourier transform is a limiting case of a Fourier series[9]. The transition from a periodic function to an aperiodic function is accomplished by allowing the fundamental period T to increase without limit. In other words, if T becomes infinite, the function never repeats itself and, therefore, the function is aperiodic. Also as

T increases, the separation between adjacent harmonic frequencies becomes smaller because the fundamental frequency is directly equal to the inverse of the period T. Therefore, in the frequency domain, the frequency in a Fourier series is a discrete variable, whereas in the Fourier transform, the frequency is a continuous variable.

Mathematically, the Fourier transform is obtained by:

$$F(\omega) = \int_{-\infty}^{\infty} f(t)e^{-j\omega t} dt \quad (2.9)$$

In the above equation used to calculate the Fourier transforms, the time signal $f(t)$ is continuous. However, when working on a computer, the signals are converted from analog to digital form and are discrete. Therefore, to compute the power spectrum of a discrete, non-periodic signal a method called the discrete Fourier transform(DFT) is used. In addition, computationally efficient algorithms for computing the DFT have been developed and are known as fast Fourier transform (FFT) algorithms.

Although the complete theory behind FFTs is beyond the scope of this thesis, there are a few subtle points of importance. One important point is that when performing FFTs on a computer, the time signal is a discrete signal, sampled at a particular sampling frequency. In order to compute the FFT, the discrete points in the sampled signal must be evenly spaced. The theory of converting an analog signal to a discrete signal is presented in Section 2.2. In addition, because the calculation is performed by a digital computer on a discrete signal, the resulting spectrum is not continuous, but discrete[9]. The frequency resolution is proportional to the sampling frequency divided by the number of FFT points. Therefore, in order to increase the frequency resolution, one has to increase the number of

FFT points. If the desired number of FFT points is longer than the number of points in the signal, zero padding should be used to increase the length of the signal to equal the number of FFT points.

2.2 Analog-to-Digital Conversion

A discrete time signal is defined by specifying the value of an analog signal only at discrete times, called sampling instants[26]. Once the sampled values are quantized and encoded, a digital signal results. A digital signal is formed from a continuous-time, analog signal by a process called analog-to-digital(A/D) conversion. A block diagram of an analog-to-digital converter is shown in Figure 2.1.

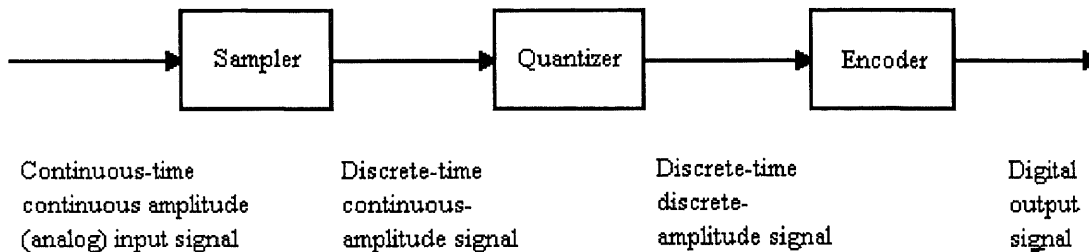


Figure 2.1 Block Diagram of an Analog-to-Digital Converter (from R. Ziemer, W. Tranter, and R. Fannin, *Signals and Systems: Continuous and Discrete*, 1989)

The first component is a sampler that extracts sample values from a continuous time, continuous amplitude (analog) input signal at specified sampling instants. The output of the sampler is a discrete time signal with a continuous amplitude because the sampled values assume the same continuous range of values assumed by the input signal.

The second component in an A/D converter is a quantizer, which quantizes the continuous amplitude range of samples into a finite number of amplitude values. The last component of an A/D converter is an encoder which maps each quantized sample value onto a digital word. For a binary representation, the number of quantizing levels q and the digital wordlength n are related by

$$q = 2^n \quad (2.10)$$

In order to be able to reconstruct the original signal from the sampled signal, there are three important points that must be followed. The first point involves the sampling rate, and is covered by the sampling theorem which states that a bandlimited signal, having no frequency components above f_h hertz, is completely specified by samples that are taken at a uniform rate with a frequency greater than $2f_h$ hertz. In other words, the time between samples is no greater than $1/2f_h$ seconds. The frequency $2f_h$ is known as the Nyquist frequency. To understand why the sampling frequency must be greater than twice the highest frequency in the signal, the spectrum of the input signal and the spectrum of the sampled signal are displayed in Figure 2.2. The spectrum of the input signal is double sided, consisting of power at both positive and negative frequencies. The spectrum of the sampled signal contains the spectrum of the original signal repeating at integer multiples of the sampling frequency. Figure 2.2(c) shows the effect of sampling at too low of a sampling rate. This effect is known as aliasing, and makes it impossible to recover the original signal.

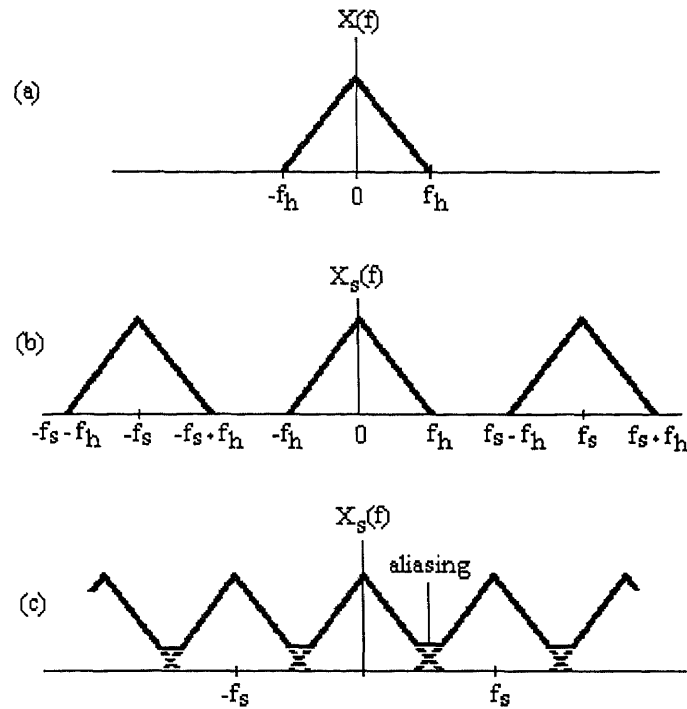


Figure 2.2 Spectrum of (a) the Original Signal (b) Sampled Signal and (c) Improperly Sampled Signal (from R. Ziemer, W. Tranter, and R. Fannin, *Signals and Systems: Continuous and Discrete*, 1989)

The second important point to be made about the reconstructing of the original wave from the sampled wave, is that a low pass filter must be used to pass only those frequencies involved in the original spectrum. The final point concerns the number of quantization levels. Since the quantizing level is the only value retained after sample values are quantized, errors are induced by the quantizing process that can not be removed by additional processing[26]. To reduce the quantization error, it is important to have enough quantization levels and to make sure the amplitude range of the signal uses all the quantization levels.

2.3 Subjects and Experimental Protocol

Because our purpose was to derive the respiratory waveform from the ECG signal and apply it to power spectral analysis of heart rate variability, the experimental protocol was designed to include sections that stimulate both the parasympathetic and sympathetic nervous systems. In addition, the form of exercise used included a lot of upper and lower body movement to determine if the derived respiration methods were consistently reliable.

A total of nine subjects, three females and six males, participated in the study. The age of the subjects ranged from 20 to 37 years. All subjects were considered normal. In other words, they suffered from no known illnesses such as diabetes, heart disorders, etc. The only restriction on subjects were: (1) the subjects were between 18 and 40 years old, (2) subjects did not suffer from any breathing disorders, and (3) pregnant women were not allowed. Some general information on the subjects is shown in table 2.1. The subjects were considered smokers if they had at least one cigarette per day and were considered regular exercisers if they exercised at least 3 times a week, for a minimum of 45 minutes.

Two leads of EKG (lead I and lead III) and an original respiration waveform were collected on the subjects during six 4-minute test conditions: 1) sitting, non-paced breathing, 2) sitting, paced breathing at 8 breaths per minute(bpm), 3) sitting, paced breathing at 12 bpm, 4) sitting, paced breathing at 16 bpm, 5) walking on a treadmill at 3.5 mph, and 6) walking on a treadmill at 3.5 mph with a 5% incline. At the initiation of each phase of the protocol, the ECG signals were synchronized with the respiration signals by pressing the event marker button on the ECG monitor.

Table 2.1 General Information of Each Subject

Subject #	Sex	Age	Height	Weight	Smoker	Regular Exerciser
1	M	24	6' 1"	180	no	no
2	M	21	6' 2"	190	no	yes
3	M	20	5' 7"	135	no	yes
4	M	37	5' 8"	150	no	no
5	F	24	5' 5"	130	no	yes
6	M	24	5' 10"	150	yes	yes
7	M	23	6'	200	no	yes
8	F	21	5' 9"	130	yes	no
9	F	21	5' 10"	125	yes	no

For test conditions 1 through 4, the subjects were sitting in a comfortable chair and were facing a wall. For test conditions five and six, when walking on the treadmill, the subjects were allowed to either hold on to the treadmill or walk swinging their hands at their side. The difference between test conditions five and six was to increase the subjects breathing rate, breathing volume, or both, depending on the individual.

In this protocol, the sitting non-paced breathing represents a period of time when the subject can breath at his own comfortable breathing rate. Usually when a person is sitting and relaxing, their breathing rate might fluctuate around their nominal breathing rate. In addition, it is not unusual for people to stop breathing for periods up to 10 seconds when resting. During this time, the subject's parasympathetic activity is at a nominal level, perhaps slightly decreased because the subject might be nervous.

The three sections of the protocol when the subject is sitting and paced breathing represent periods of time when the subject's respiration rate was voluntarily controlled. It should be noted that the subjects were free to breathe at whatever volume was comfortable in each of the three tests involving paced breathing. The subject's breathing

rate was paced using a box that contains a column of 16 light emitting diodes that emitted either green or red light. The subjects were asked to match their inhalation and exhalation to the rate at which the lights proceeded up the column. For example, when the lights were green and traveling up, the person was asked to pace himself so that one inhalation took the same amount of time as the lights to reach from the bottom of the column to the top of the column. Then, the lights would turn red, and would proceed from the bottom of the column to the top of the column which represented the time for the subject to exhale. Generally, during paced breathing, parasympathetic activity increases above a person's nominal parasympathetic activity.

The final two sections of the experimental protocol involved walking on a treadmill. The purpose of this section was to increase the person's breathing rate and heart rate, with upper and lower body movement. Exercise represents a period of decreased parasympathetic activity because there is physical stress on the body.

The experiments were conducted in the autonomic research lab at the Kessler Institute for Rehabilitation under experimental protocol #P-205-95. The Institutional Review Board(IRB) application to conduct an exploratory study involving human subjects is provided in Appendix B.

2.4 Data Acquisition

2.4.1 Acquisition of the Original Respiration Waveform

In order to compare the results of the derived respiration methods developed in this study, the original respiration waveform was recorded using a method called impedance

pneumography. A RESP I impedance pneumograph (UFI, Morrow Bay, CA) was used to measure trans-thoracic impedance changes which result from respiration. To produce a signal proportional to the trans-thoracic impedance, the RESP I causes a safe, high-frequency (30 KHz) alternating current to flow between two electrodes. As a result of the current, a voltage is produced which reflects the changes in impedance in the segment between the two electrodes. The RESP I senses this voltage and makes it available as its output in analog form.

For this study, two diagnostic ECG adhesive silver/silver chloride surface electrodes (Medtronic, Haverhill, MA) were placed trans-thoracically on the patients, as shown in Figure 2.3. Note that the electrodes were placed on the sides of the subject. In addition, the electrode on the side of the heart was placed on the lowest rib and the electrode on the opposite side was placed on the highest rib that was approximately two inches below the armpit. This is an important point because if the electrode on the side of the heart is placed approximately two inches below the armpit, there will be some ECG content in the respiration waveform. It was important that the electrodes were placed directly over the nearest rib bone to reduce the effects of EMG which can be recorded from muscles.

To obtain a clean respiration signal, each skin site was prepared before the electrode application. The skin site was thoroughly scrubbed with an alcohol prep to remove the outermost layer of dead skin (stratum corneum). This helps reduce the dc offset and motion artifact from the skin-electrode interface. Next, a dry piece of gauze pad was used to remove any alcohol and dead skin. Finally, application of the electrode to

the prepared site was performed by placing the electrode on the skin, making sure that the gel makes contact with the skin first, and then smoothing the electrode from the center out.

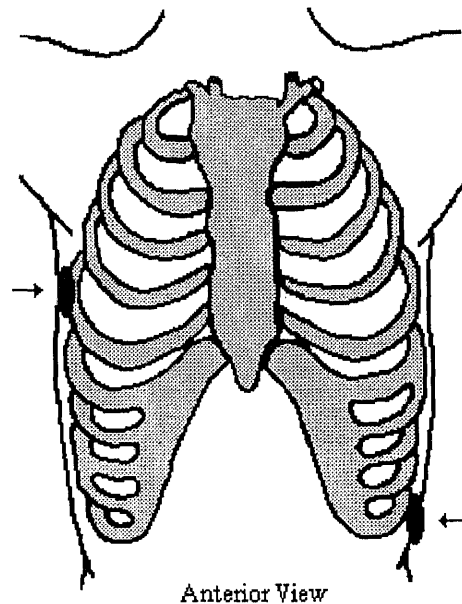


Figure 2.3 Placement of the Electrodes to Record Respiration Using the RESPI

The analog voltage output of the RESPI was input to a DAS-16 analog-to-digital converter (Keithley Metrabyte/Asyst, Natick, MA) which was installed in an IBM compatible 286, 25 MHz computer with 1 Mb of RAM and 107 Mb hard drive. However, before the output of the RESPI entered the DAS-16, it was isolated from the acquisition computer by an isolation amplifier which protects the subject from the 120V source required to power the acquisition computer. The connection between the RESPI and the isolation amplifier and the isolation amplifier and the A/D board were made with shielded cables.

The DAS-16 was configured to accept 8 different channels of data, each having an amplitude in the range of - 5 Volts to + 5 volts. Each sample of data requires 2 bytes of hard disk space. Twelve of the sixteen bits are used for encoding the amplitude of the input signal, providing 2048 different quantization levels. One of the twelve bits is used to indicate if the signal has a positive or negative voltage. The remaining four bits are used to identify the different channels. Therefore, each quantization level is equivalent to 2.44 mV (5 Volts/ 2048).

The respiration is sampled at 200 samples per second and is stored in binary format. Because there is no filtering between the RESPI and the data acquisition board, the respiration was sampled at 200 samples per second to avoid aliasing due to 60 Hz noise. To make sure there were no harmonics above 60 Hz, the respiration was sampled at 400 Hz, and the power spectrum was computed for frequencies up to 200 Hz. The highest frequency that contained any indication of power was at 60 Hz; therefore, it is safe to sample the RESPI signal at 200 Hz. Before the signal was acquired, the connection between the RESPI and the A/D board was checked with a program that plots the input to the A/D board on the screen. Once confirmed that the connection was okay, the signal was acquired using Streamer v3.25 data acquisition software (Keithley MetraByte/Asyst, Natick, MA).

Figure 2.4 shows a typical RESP I recording. Note that the resistance increased during inhalation and decreased during exhalation. The resistance increases during inhalation because the chest volume increases and the lungs fill up with air which is a very poor conductor due to a high resistivity. It should be noted that the respiration was

monitored on an oscilloscope during the experiment to determine the amplitude range of the voltage from the RESPI. The RESPI includes an internal amplifier that was set to maximum amplification during all the experiments. Before each section of the experimental protocol, the amplitude of the subject's respiration waveform for that section was monitored. If there appeared to be a possibility for the amplitude to exceed five volts, the amplitude of the respiration was decreased using the amplifier provided on the isolation amplifier. If the voltage exceeds five volts, information is lost because the signal is quantized to the highest quantization level regardless of the excess over five volts.

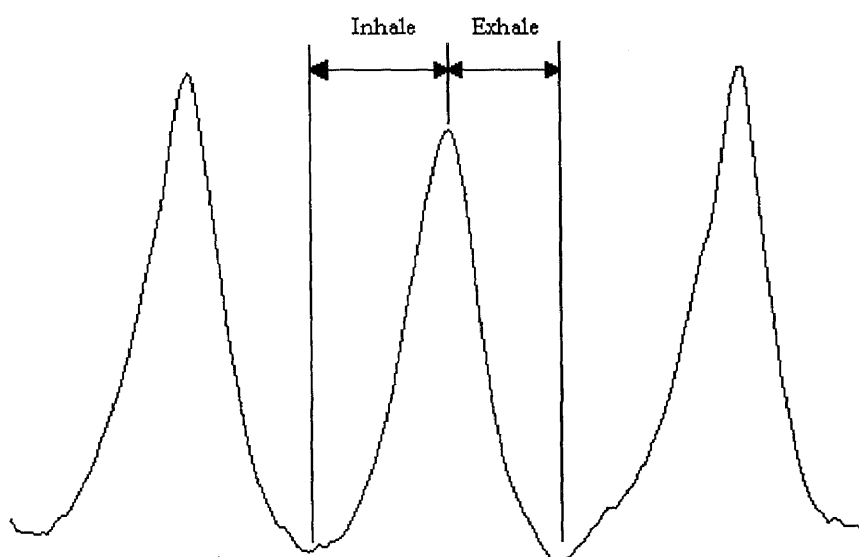


Figure 2.4 Example of Three Cycles of a RESPI Respiration Waveform Showing the Waveshape and Typical Recording Quality

It should be mentioned that the RESPI is really an indirect measure of respiration. However, it is referred to as the direct measure of respiration throughout the thesis because it is an indication of the actual respiration waveform. A direct measure of

respiration would measure the air flow in and out of the lungs through the nose and mouth which would indicate both respiration rate and volume. The only way to do this is to place a mask over the subject's nose and mouth and connect the subject through a flexible tube to a spirometer or metabolic cart. Although this was an option, the RESPI was chosen for its simplicity to implement and comfort. Another method considered to measure the respiration waveform was that of nasal thermistors. However, during exercise, people tend to breathe from both their nose and mouth. Unfortunately, the nasal thermistor would not measure the flow of air through the mouth. One possible solution to this problem is to put the nasal thermistor in the opening of a mask which covers the nose and mouth. Although this is a viable solution, it was never experimented with to determine the accuracy of such a setup. An advantage of the methods to measure respiration other than by impedance pneumography, is that they provide a very clean respiration tracing during all test conditions. Conversely, the RESPI tends to get noisy during exercise because of muscle electromyography, skin movement, and movement of the skin-electrode interface.

2.4.2 Acquisition of ECG

The ECG was recorded using a Holter recorder (Del Mar Avionics, Irvine, CA). The Model 423 Dynacord Cassette Holter Recorder is a small cassette, three-channel recorder, designed to record an ambulatory patient's ECG continuously for up to 24 hours. The Model 423 includes a patient event button, an automatic calibrator, and a carrying case. A 9-volt disposable battery supplies power.

In this study, two leads of ECG were collected, namely, lead I and lead III. It should be noted that the standard limb lead connections that form Einthoven's triangle were not used. The electrodes were not hooked up in the standard limb lead connections for two reasons. One reason was to minimize electromyographic noise produced by the limb muscles. The second reason was because the method to derive the respiration by estimating the mean cardiac electrical vector assumes that the two leads of ECG are orthogonal. Therefore, lead I and lead III were connected to the patient as shown in Figure 2.5. The same electrodes and preparation techniques used to apply the electrodes for the acquisition of the respiration waveform were used for the application of the ECG electrodes. An important detail about the lead connections is that for lead I, the positive terminal is on the left clavicle bone and the negative terminal for lead III is also on the left clavicle. It was discovered that of the two electrodes on the subject's left clavicle, if the positive terminal of lead I was connected to the electrode that is closest to the subjects side, a larger R-wave will result in lead I.

When the 9 Volt battery is inserted, the Holter recorder turns on and six minutes of 1 mV calibration pulses are automatically recorded on two channels. During the calibration period, the Holter recorder does not record any input signals. However, the internal calibration signal can be terminated by pressing the patient event button. Once the calibration signal stops, the Holter recorder begins to record input signals. In order to distinguish different segments of the experimental protocol when the data is recovered from the Holter tape, the patient event button was pressed at the beginning of each segment of the experimental protocol.

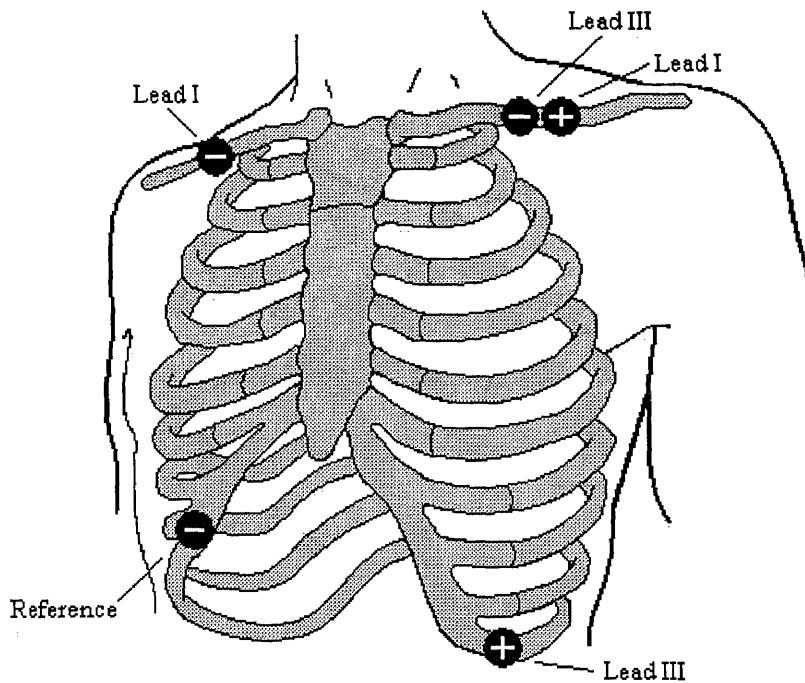


Figure 2.5 ECG Electrode Locations

During the experiment, the two leads of ECG were recorded in analog form onto an audio cassette. For this study, the tape cassette was a Radio Shack Type I Normal Bias XR60. To recover the two leads of ECG, the cassette was played back after the experiment using a JVC TD-W10 consumer quality cassette player. The frequency range of the cassette player was from 20 Hz to 16000Hz. The two channel analog output of the JVC TD-W10 cassette player was then input into a two channel amplifier. In order to be able to identify what channel was lead I and what channel was lead III, the same setup was used each time for playback. The left output of the cassette player was always inserted into channel 1 on the amplifier and the right output of the cassette player was always inserted into channel 2 on the amplifier. With this setup, it was determined that the

outputs of channel 1 and 2 were leads I and III respectively. The amplifier had a variable gain between 1 and 100 and a constant frequency response for frequencies above 7 Hz and up to at least 5 KHz. The amplifier was necessary to reduce the quantization error in the analog to digital conversion. The gain was adjusted during playback for each section of the protocol to yield a signal with maximum absolute amplitude no greater than 4 volts.

The outputs of the amplifier were then converted into a digital signal by a DAS-16 analog-to-digital converter. An important point to be made is that the Holter monitor records 48.35 times slower than a standard cassette player. This slower recording speed enables the Holter monitor to record for up to 24 hrs continuously. However, because the playback is 48.35 times faster, this changes the frequency of the waves being played back. The frequency content of an ECG signal is between 0.01 and 60 Hz. Therefore, during playback the frequency band is 0.4835 and 2901 Hz. Thus the DC offset and very low frequencies might not be passed by the JVC TD-W10 cassette player and amplifier. However, this will have no significant affect on the acquired signal because all the important waves of the ECG are higher in frequency.

In this study, the sampling frequency used to sample the ECG was 500 Hz. However, because of the faster playback, the adjusted sampling frequency used to sample the playback of the ECG from the JVC-W10 was 24.175 KHz. The sampled data were stored in binary format on the same acquisition computer used to acquire the respiration waveform. The two ECG leads were also acquired using Streamer v3.25 data acquisition software. The procedure to perform the above steps on the data acquisition computer are detailed in Appendix C.

2.4.2.1 Determination of Sampling Frequency

Normally, 200 Hz is the standard sampling frequency used when performing A/D conversion of an ECG signal. Because the highest frequency in the ECG is approximately 60 Hz, a sampling frequency of 200 Hz is 80 Hz more than the Nyquist frequency. However, when the ECG is sampled at 200 Hz, the exact peak of the R-wave is not always sampled on a consistent basis because the width of the peak occurs in a very small period of time. Therefore, the maximum time error that can be made, is half the time between samples, or 2.5 ms. Although this might seem like a short period of time, the amplitude of the R-wave can change significantly during that time. In this study, the peak of the R-wave is rather important. Therefore, two experiments were performed to determine the optimum sampling frequency to accurately sample the peak of the R-wave.

In the first experiment, one minute of an actual ECG recorded with a Holter monitor was played back and sampled at 1000, 900, 800, 700, and 600 Hz. To simulate sampling frequencies below 600 Hz, the signal sampled above at each of the different sampling frequencies was downsampled by a factor of two using software (every other point was taken). This provided the same signal sampled at 500, 450, 400, 350, 300, 250, 225, and 200 Hz. Next, the highest point in the R-wave was detected using software, and the mean of the highest points in the R-wave was calculated. The results are shown in Table 2.2 below. Because the ECG was played back from a Holter cassette for each of the 5 different sampling frequencies, care was taken to include the same portion of ECG during each analog-to-digital conversion.

Table 2.2 Average Amplitude of the Peak in the R-Waves at Different Sampling Frequencies of an Actual ECG.

Sampling Frequency (Hz)	Average Amplitude of R-Waves
1000	1368.566
900	1365.590
800	1365.525
700	1365.721
600	1365.459
500	1365.475
450	1321.246
400	1360.656
350	1359.311
300	1357.328
250	1354.295
225	1308.557
200	1345.262

From table 2.2, it can be seen that when the sampling frequency is below 500 Hz, the average height of the R-waves became inconsistent. For example, the real mean of the highest point in the R-wave appears to be approximately 1365. At 500 Hz, the mean is 1365.475. At 450 Hz, the mean is 1321.246 which is a significant difference. However, at 400 Hz, the mean is 1360.656 which is a relatively small error. As it turns out, the mean of the highest point in the R-waves for an actual ECG depends a lot on whether or not the few peaks that are accurately detected are high in amplitude or low in amplitude (remember there is a modulation of the ECG from breathing). Therefore, to obtain more accurate results, an ECG that is not modulated by the frequency of breathing is needed.

For the second experiment, one minute of simulated ECG was recorded from a Quinton Q4000 Stress Test Monitor (manufactured by Quinton Instrument Co. of Seattle, WA). It was assumed that the Quinton ECG cart output was a stable simulated ECG. In this case, the meaning of stable is consistent R-wave amplitude. Similar to the previous

experiment, the simulated ECG was sampled at 1000, 900, 800, 700, and 600 Hz. Then, to simulate sampling frequencies below 600 Hz, the simulated ECG signal sampled above at each of the different sampling frequencies was downsampled by a factor of two using software (every other point was taken). This provided the same signal sampled at 500, 450, 400, 350, 300, 250, 225, and 200 Hz. Next the highest point in the R-waves was detected, and the mean of the these points was computed. Table 2.3 contains the results. In addition, the mean of the highest point in the R-waves was plotted against sampling frequency in Figure 2.6.

Table 2.3 Average Amplitude of the Peak in the R-Waves at Different Sampling Frequencies of a Simulated ECG.

Sampling Frequency (Hz)	Average Amplitude of R-Waves
1000	626.5667
900	626.5085
800	626.3667
700	626.1356
600	626.1356
500	625.7833
450	625.2542
400	624.8500
350	624.6780
300	623.4746
250	621.8971
225	619.7797
200	618.4167

One can see from the table and graph that when the sampling frequency is less than 500 Hz, the accuracy of sampling the maximum peak of the R-wave decreases. Based on these two experiments, the optimum sampling frequency to detect the R-wave peaks has been chosen to be 500 Hz. This means that the time between samples is 2 msec, or the maximum time error of not detecting the peak in the R-wave is 1 msec.

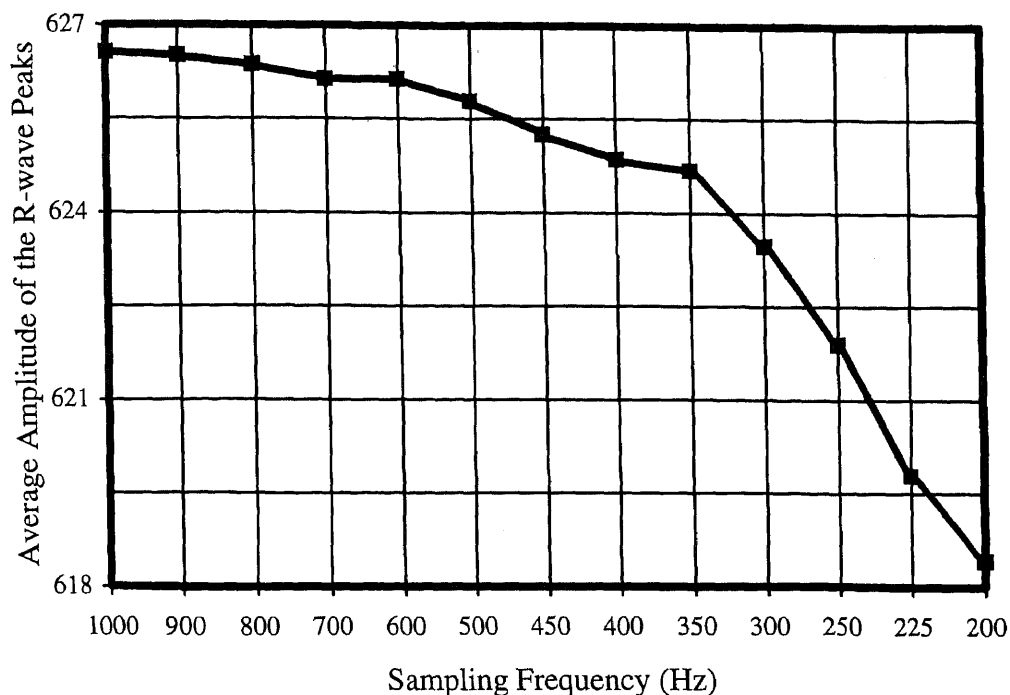


Figure 2.6 Plot of the Average Amplitude of the R-Wave Peaks vs. Sampling Frequency

2.5 Data Analysis

2.5.1 Converting Data from Binary Format to ASCII Format

Both the respiration signal and the ECG leads were collected using Streamer data acquisition software and a DAS16 data acquisition board. The signals were quantized to 12 bit words, and were stored on the root directory in a binary format that utilizes 2 bytes per sample. The software programs used for analysis, S-Plus v3.1 (Statistical Sciences, Inc., Seattle, WA) and MATLAB v4.2b (Math Works Inc., Natick, MA), can not convert

the data from binary format into ASCII format. Therefore, a program called unpack was utilized to convert the data from binary to ASCII format for S-Plus and a program called kunpack1 was utilized to convert the data from binary to ASCII format for MATLAB. The difference between unpack and kunpack1 is that unpack converts the binary file to ASCII format separated by commas, whereas the kunpack1 program converts the binary file to an ASCII file where each channel of data is represented as a column in a matrix and the columns are separated by spaces. Because the unpack program separates the samples by only a comma, it is necessary to tell it how many channels were collected, to be able to separate the channels. The unpack program is a utility that Keithley MetraByte/ Asyst provided with the Das16 analog-to-digital conversion board. The kunpack1 program is a modified version of the unpack program.

2.5.2 Analysis of ECG to Obtain Power Spectrum of Heart Rate Variability

As mentioned in section 2.4.2, the ECG is converted from analog to digital form and stored in binary format on the data acquisition computer. The data is then transferred over the network to a signal processing computer. In this study, the computer used to do the signal processing was an IBM compatible with a 90 Mhz Pentium processor with 65 Mb of RAM and a 2 GB hard drive. The initial step in the data analysis is to unpack the data from binary format to ASCII format using the unpack program. Once in ASCII format, S-Plus is used to scan in the data into a matrix form and then previously developed software algorithms in S-Plus were used to obtain the HRV power spectrum. The following is a description of the necessary steps to obtain the power spectrum of HRV.

To begin the analysis, one of the two leads of ECG must be chosen. Although both leads contain the same heart rate information, one lead usually works better than the other with the existing software. The lead which works best is the dominant lead (see section 1.2), because the first step to obtain the power spectrum of HRV is to detect every R-wave in the ECG. Because the R-wave complex is more pronounced in the dominant lead, the analysis proceeds more smoothly.

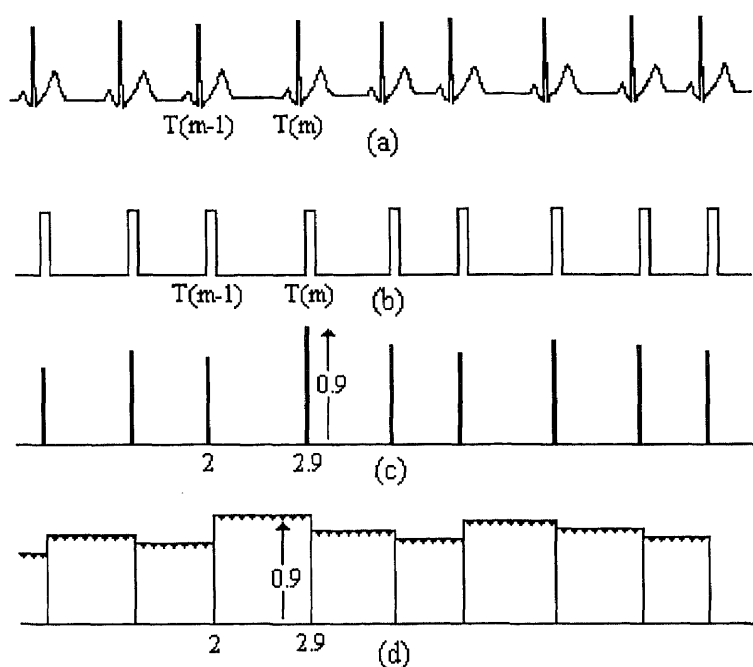


Figure 2.7 Figure Depicting the Construction of the IBI Signal (from S.J. Shin, W.N. Tapp, S.S. Reisman, and B.H. Natelson, "Assessment of autonomic regulation of heart rate variability by the method of complex demodulation," 1989)

Before trying to detect the R-waves, the ECG signals were detrended using a locally weighted robust regression algorithm. To help detect each R-wave, a vertical threshold (which the R-wave must exceed) and a horizontal threshold (to prevent detecting an R-wave for a period of time after one was detected) can be varied. If an

error occurs during the R-wave detection, the analyst can use existing software to manually detect or undetect the mis-detected R-waves. Appendix D contains the syntax of the commands involved in the analysis procedure.

Once the R-waves are properly detected, an interbeat interval (IBI) signal can be constructed. To obtain the IBI signal, the distance in time between a specific beat(T_m) and the beat previous in time(T_{m-1}) is calculated. This value of time difference then becomes the amplitude of the IBI signal at that specific beat. Mathematically, the IBI signal is computed by the formula $IBI_m = T_m - T_{m-1}$. See Figure 2.7 for a graphical representation.

Although the IBI represents the heart period at discrete points, the IBI signal is not suitable for FFT analysis because the discrete points, located at each R-wave, are not evenly spaced. In order to produce equidistant IBI samples suitable for analysis, the IBI signal must be interpolated. The interpolation method used was that of a backward step function. This method assumes no new information about the direction of the time series is available until the next heart beat occurs. Therefore, the amplitude of all of the interpolated values between a beat at time T_{m-1} and the beat at T_m were set equal to the time difference between T_m and T_{m-1} . The interpolated interbeat interval(IIBI) is then sampled to produce an IIBI with evenly spaced samples. For example, in Figure 2.7(c) if a beat occurs at a time equal to 2 seconds and the next beat occurs at a time equal to 2.9 seconds, then the interpolated values between time 2 seconds and 2.9 seconds are all 0.9 seconds as shown in Figure 2.4(d). After the IIBI signal is obtained, it is detrended using a locally weighted robust regression algorithm. Essentially, this removes low frequency components below 0.05 Hz. If these low frequency components are not removed, they

can dominate the power spectrum and decrease the detail of the components in the frequencies above 0.05 Hz. Another example of an IBI signal and an IIBI signal is shown in Figure 2.8.

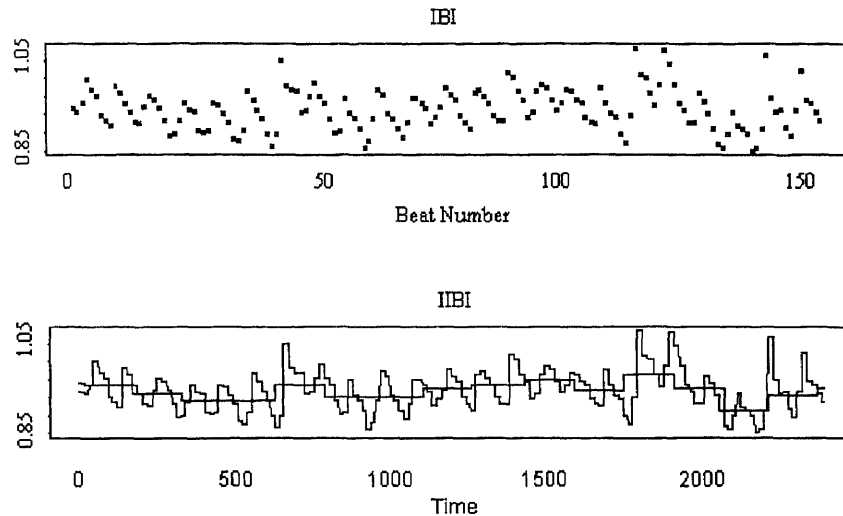


Figure 2.8 IBI Signal and IIBI Signal

The final step to obtain the power spectrum of HRV is to take the FFT of the detrended IIBI signal. In the existing software, this is done by decimating the IIBI signal by a factor of twenty five (the ECG is sampled at 500 Hz) and taking an 8192 point FFT of the decimated IIBI signal. When the signal is decimated by a factor of twenty five, every twenty fifth point of the original signal is kept, and the twenty four points in between every twenty fifth point are not used. In a time series of samples, every twenty fifth point occurs at the same time as in the undecimated signal, except that there are no samples in between. In effect, decimating is similar to down-sampling. In other words, because the

length of the IIBI signal is approximately the same length of the sampled ECG, which is acquired using a sampling frequency of 500 Hz, decimating the IIBI by a factor of 25, is similar to sampling the IIBI at 20 Hz. This can be done because the IIBI signal contains no frequency components above 6 Hz.

The IIBI signal is detrended to improve the frequency resolution in the power spectrum of the FFT. The software is programmed to take an 8192 point FFT by default regardless of the input signal length. In the experiments, 120 seconds of ECG were collected. At a sampling frequency of 500 Hz, this corresponds to 60,000 samples. Recall that the IIBI is approximately the same length as the ECG. If an 8192 point FFT is taken, only the first one-eighth of the IIBI would be represented in the spectrum. In addition, the frequency resolution would be $500/8192 = 0.061$ Hz and the spectrum would be between 0 Hz and 250 Hz. However, the spectrum of the IIBI, the heart rate variability spectrum, consists of low frequencies less than 6 Hz; therefore, a better frequency resolution would be desired and the spectrum does not need to be calculated up to 250 Hz. As a result, the IIBI is decimated by a factor of twenty five. In this case, the IIBI signal would then be 2,400 samples long for a 120 sec long ECG signal. Note in Figure 2.8 that the length of the IIBI signal is 2400 points long. The length of the IBI signal depends on the number of heart beats. Now, in order to take an 8192 point FFT of a signal that has only 2,400 samples, a technique called zero padding must be used. Essentially all samples from 2,401 to 8192 are given the value of zero. The only effect this has on the spectrum is that it increases the frequency resolution. When the FFT is calculated, we limited our spectrum from 0 Hz up to 10 Hz. The frequency resolution is now $20/8192 = 0.00244$ Hz. Once the

power spectrum is obtained, it is smoothed twice by applying a modified Daniell (Rectangular) smoothing algorithm. Figure 2.9 illustrates the power spectrum of the IIBI signal in Figure 2.8. Figure 2.10 illustrates the smoothed version of the power spectrum illustrated in Figure 2.9.

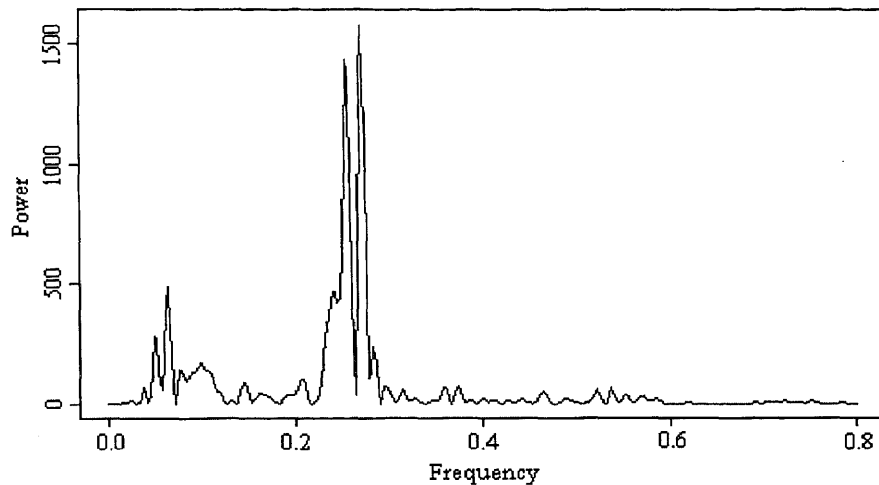


Figure 2.9 Power Spectrum of IIBI Signal in Figure 2.8.

It should also be noted that when performing the FFT, the IIBI signal is windowed by applying a split cosine bell taper. The taper begins at 20 percent from each end of the time signal. The application of the split cosine bell taper is done before the zero padding takes place so as to provide a smooth transition to zero rather than a sharp discontinuity. It should be noted that if the window is a simple rectangular function, then discontinuities would result due to the discontinuity of the window, which would add additional spectral components in the spectrum. The purpose of the split cosine bell taper window is to reduce any additional spectral components that result from the shape of the window. The

windowing is done by multiplying the time signal by the window function. The split cosine bell taper for a 2400 point long signal is shown in Figure 2.11.

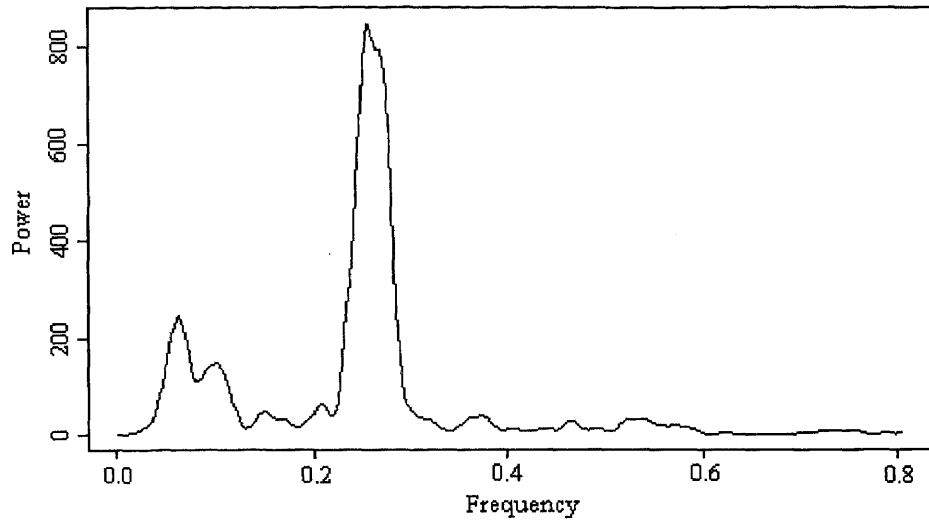


Figure 2.10 Smoothed Power Spectrum of Figure 2.9

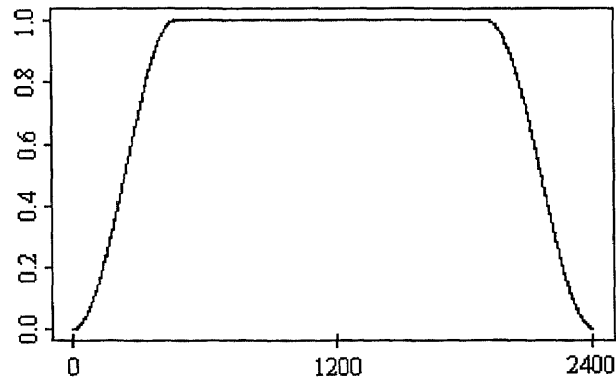


Figure 2.11 Plot of the Split Cosine Bell Taper Used as a Window in the FFT Calculation

2.5.3 Analysis of Original Respiration Waveform

The power spectrum of the original respiration waveform was needed for two reasons in this study. The power spectrum of the respiration waveform is needed to properly locate the parasympathetic activity in the heart rate variability power spectrum. However, more important, for this study the power spectrum of the original respiration was compared to the power spectrum of the respiration derived from the ECG. Therefore, a program was written to compute the power spectrum of the original respiration waveform. The program, which executes in S-Plus, and the analysis steps to obtain the power spectrum of the original respiration waveform are shown in Appendix E.

To begin the analysis of the original respiration waveform, the data file is unpacked in DOS using the kunpack1 program. The ASCII file is then loaded into MATLAB and decimated by a factor of ten. This decimation is done in MATLAB because the MATLAB decimation program contains an eighth order Chebyshev type I lowpass filter with cutoff frequency equal to $.8*(F_s/2)$. At F_s , the filter response is approximately 30 dB down. Recall that the RESPI signal was acquired with no filtering and a sampling frequency of 200 Hz. There is a frequency component due to noise at 60 Hz. Therefore, the Nyquist frequency of the respiration waveform is 120 Hz. If the signal is downsampled to 20Hz without filtering first, aliasing will occur. Therefore, the program first applies the lowpass filter with cutoff frequency equal to 8 Hz (the Nyquist frequency is 10 Hz), and then decimates the signal by a factor of ten which effectively downsamples the signal to a sampling frequency of 20 Hz. The signal is then written to an ASCII file, which then can be loaded into S-Plus and the power spectrum of the RESPI signal can then be taken.

The basics of taking the FFT of the respiration waveform are the same as those described in sections 2.1 and 2.5.2. The respiration waveform is 120 seconds long and is acquired at a sampling frequency of 200Hz. Therefore, the respiration signal is 24000 points long before the decimation, and 2400 points long after the decimation. An 8192 point FFT is taken by first windowing the 2400 points, then zero padding the remainder of the points between 2401 and 8192. The frequency resolution of the respiration spectrum is 0.00244 Hz ($20/8192$). The spectrum of the respiration waveform is also smoothed twice by performing a modified Daniell (Rectangular) smoothing algorithm.

2.6 Methods for Deriving the Respiration from the ECG

As mentioned in section 1.4, the heart's position changes during respiration due to the filling and emptying of air in the lungs. Thus, the mean cardiac vector changes from beat to beat. All the following methods derive the respiration waveform from the change in angle of the mean cardiac vector in the frontal plane.

2.6.1 The Method Presented by Mark and Moody

In a paper presented in 1985 by Moody et al.[S], a method to estimate the mean cardiac vector during each QRS loop was presented to attempt to derive the respiration waveform. The basis for this method is that the mean cardiac vector changes during inhalation and exhalation due to the rotation of the heart in the chest. As a result of the rotation, the amplitude of each ECG lead changes. By using two orthogonal leads of ECG, the mean cardiac vector can be approximated in the plane defined by the two leads.

To measure this change in amplitude, the area under each normal QRS complex in the two orthogonal leads is calculated over a fixed window. The baseline area for each QRS is subtracted from the area calculation. Since the window width is fixed, the area is proportional to the mean amplitude of the signal over the course of the window, and hence, to the projection of the mean cardiac electrical vector on the lead axis. By assuming that the two leads are orthogonal, the arctangent of the ratio of the areas measured in the two leads gives the angle of the mean axis with respect to one of the lead axes. Even if the two leads are not truly orthogonal, a systematic but harmless error in the axis direction estimation results. See Figure 2.12 for a graphical interpretation.

From a signal processing viewpoint, the axis direction measurement during each QRS complex provides one sample of the ECG derived respiratory signal per cardiac cycle. Assuming that the heart rate is always greater than twice the frequency of respiration, the respiration waveform can be measured well in both the time domain and frequency domain from this limited set of samples. To produce a continuous respiration waveform, cubic spline interpolation is used.

2.6.1.1 Zhao's Software to Implement Mark and Moody's Method

In order to perform the analysis of the ECG, Zhao[22] created some programs that executed in S-Plus to perform the steps necessary to derive the respiration from the method presented by Moody. The programs written by Zhao require that the HRV analysis to be done prior to their execution, because Zhao's programs rely on the HRV analysis program which detects the R waves in one of the two ECG leads.

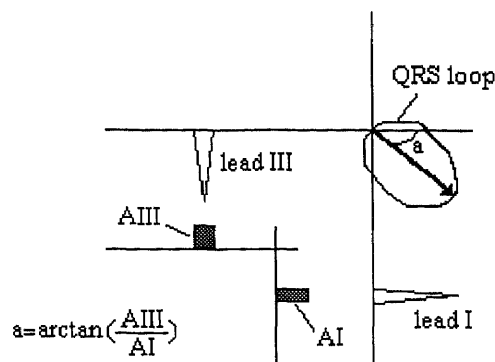


Figure 2.12 Estimation of the Mean Cardiac Vector by Taking the Arctangent of the Areas Under the QRS Complex of Leads I and III.

Once the location of each R wave is known, the first step is to calculate the average fixed window width of each QRS complex. To do this, Zhao locates what he calls the “PQ junction”. In actuality, the “PQ junction” is the Q-wave. The algorithm to detect the Q-wave is explained in Figure 2.13. Based on the position of each R-wave peak, a time period a_c was set backward from the R peak. Within this time period a_c , the minimum value b was detected as the point of the Q-wave.

To obtain the width of each QRS, the S-wave is not detected. Instead, the interval from the Q-wave to the R-wave is assumed to be the same as the interval from the R-wave to the S-wave. Therefore, after all the Q-waves are detected, the average length from the Q-wave to the R-wave is calculated. The window width is determined by doubling the average length between the Q-wave and the R-wave as in the following equation

$$W = 2 \sum_{i=1}^n L_{qr}[i] / n \quad (2.11)$$

where W is the time window width of each QRS complex, L_{qr} is the time interval between the Q-wave and the R-wave, and n is the number of QRS complexes.

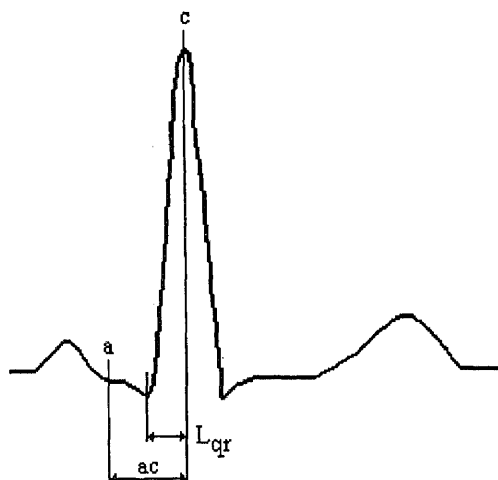


Figure 2.13 Figure Showing the Algorithm to Detect the Q-Wave.

Once the window width is calculated, the area for each QRS complex can be computed. Because the ECG is a discrete signal, the area is a sum of the samples that are within the window. To calculate the baseline area, Zhao uses the Q-wave as the minimum point. Thus, once all the QRS complex samples are summed, the product of the amplitude of the Q-wave and the window width is then subtracted. See Figure 2.14 for an illustration of the QRS complex area calculation.

Once the areas of each QRS is computed, the values represent samples of the respiration waveform which occur at the time of the R-wave. Figure 2.15 illustrates the procedure. Figures 2.15 (c) and (d) are the areas under the QRS complexes for their respective leads. Figure 2.15 (e) illustrates the arctangent of the two leads. In Figure 2.15 (f), the arctangent values are interpolated, and (g) represents the spectrum.

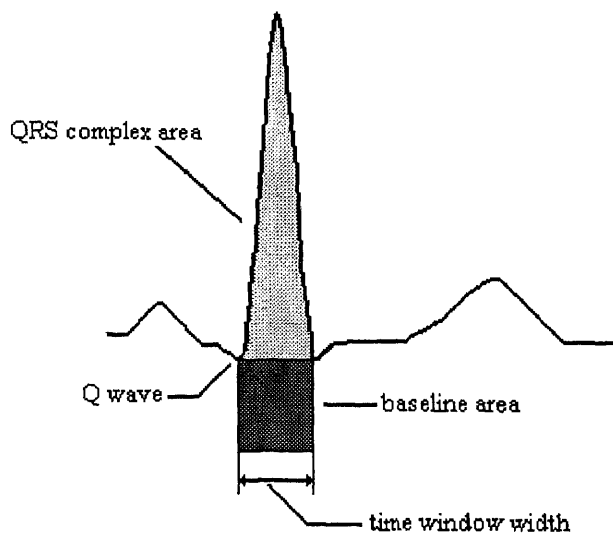


Figure 2.14 Figure Showing the Calculation of the QRS Complex Area

2.6.1.2 Problems With Zhao's Software

The process of deriving the respiration by the method described above was implemented by Zhao using a multi-step process. The areas under the QRS complexes for each lead were computed by the same program, but required a command for each lead. Additionally, the arctangent and interpolation were done in another program, and the spectrum in a third command. Ideally, the programs are not time efficient, and would be more user friendly if all the steps existed in one program.

Besides that subtle detail, there were a few other problems with Zhao's algorithms that could yield an incorrect respiration waveform. To begin, it was discovered that the software used to do the heart rate variability analysis did not properly detect the R-waves consistently. Often, the R-waves were misdetected by a few points. If some of the R-waves are misdetected by even a few points, the average window width for the QRS

complex will then be calculated incorrectly. To alleviate this problem, a program called “correcth” was written that properly detects the R-waves. The program is an additional step in the heart rate variability analysis (see Appendix D). The program is listed in Appendix F. Figure 2.16 is an example of an improperly detected R-wave.

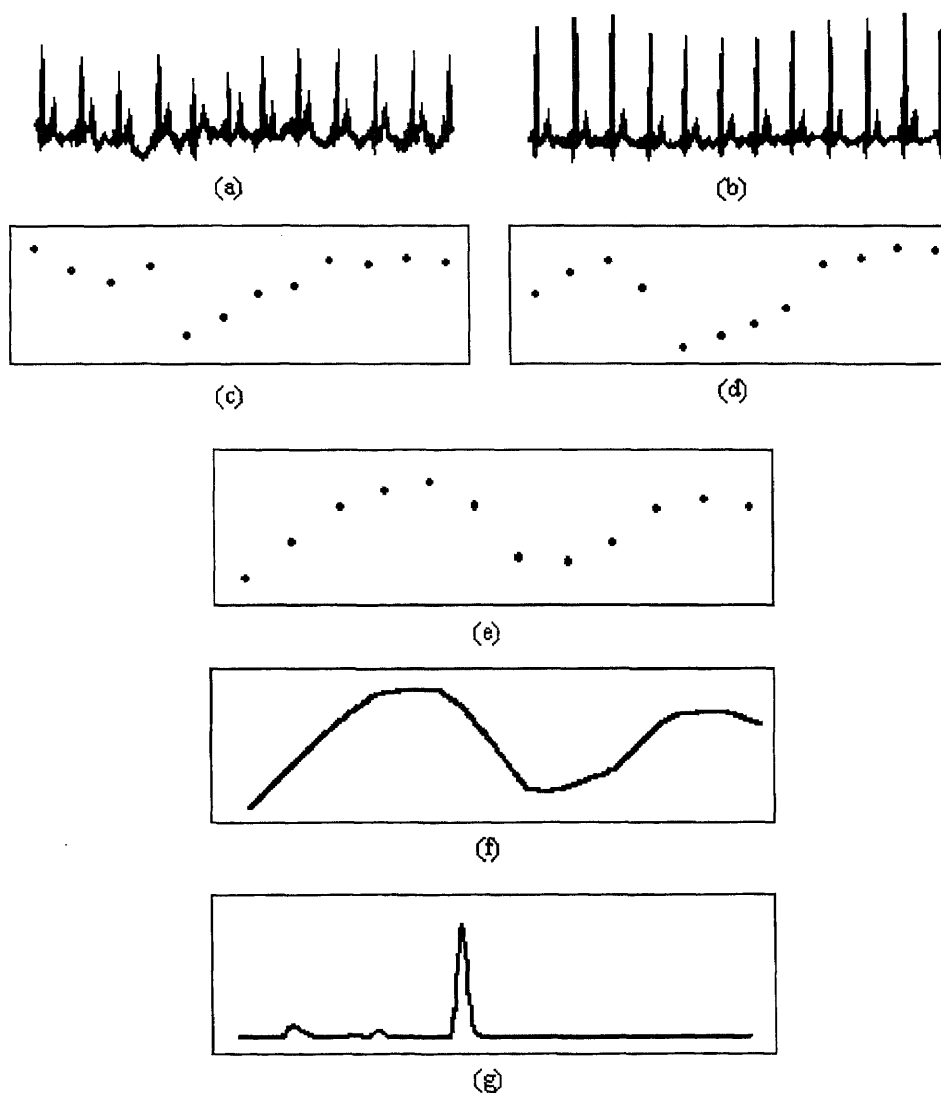


Figure 2.15 Construction of the Derived Respiration Waveform from the QRS Complex Areas from Two Orthogonal Leads

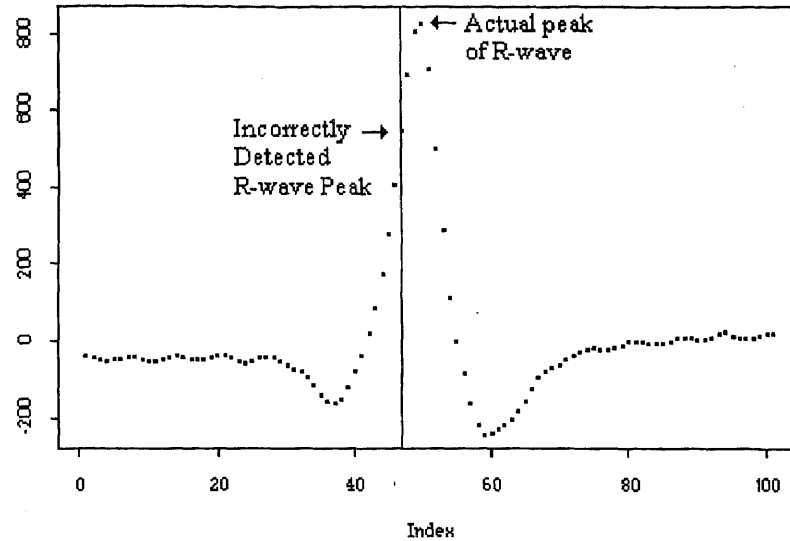


Figure 2.16 Close-Up of an R-Wave Showing an Incorrect Detection.

Another problem with Zhao's algorithms concerns the phase shift that exists between the R-waves of two different leads. It is important to remember that when doing the heart rate variability analysis, only one lead is used to detect the R-waves, and thus, to construct the interpolated interbeat interval. However, the ECG derived respiration method implemented by Zhao uses two leads of ECG. One detail about the ECG that was ignored by Zhao when designing his software, is that the R-waves occur at different times in different leads. Because the leads involved in the method, leads I and III, are orthogonal, there exists a phase shift between the R-waves in the two leads. In addition, because the magnitude of the mean cardiac vector is also changing, the amplitude of the R-waves is also different in the two leads.

To better understand this point, imagine the instantaneous cardiac vector to be of constant magnitude and rotating 360 degrees in a circular pattern in the frontal plane as in Figure 2.17. The resulting waveform in a particular lead is the projection of the

instantaneous cardiac vector on that lead over time. Therefore, for the case shown in Figure 2.17, the waveform of lead I will lead the waveform of lead III by 90 degrees as shown. If one extends this case to the instantaneous cardiac vector during the QRS loop, which changes in amplitude during the cycle, it is clear why the R-wave appears at different times and in different forms in leads I and III. Figure 2.18 illustrates an example of the phase shift between the R-waves in lead I and lead III.

The problem that exists in Zhao's software is that it assumes that the R-waves occur at the same time in the different leads. By doing so, Zhao's software creates an error in the QRS complex window width for the lead that was not used in the heart rate variability analysis. To alleviate the problem, the R-waves should also be detected for the lead that was not used in the heart rate variability analysis. In addition, because the areas will be placed at different periods of time, which are representative of each R-wave, the arctangent can not be taken between the points. Instead, each area waveform must be interpolated first, and then the arctangent of the interpolated signals can be taken.

A third problem that exists in Zhao's software occurs when the area under the QRS is calculated. The ECG is a discrete signal at the time of data processing. To approximate the area under a discrete signal that contains evenly spaced samples, one can simply sum the amplitude of each point in the part of the signal of interest. However, the signal should be completely above zero, or area will be subtracted when it is below zero. To begin the software analysis, Zhao's program detrends the ECG using a locally weighted robust algorithm. As a result, the baseline of the ECG is close to zero with some points being positive and some points negative. Unfortunately, Zhao's programs do

not shift the signal above zero, and in some instances, the software calculates the area incorrectly.

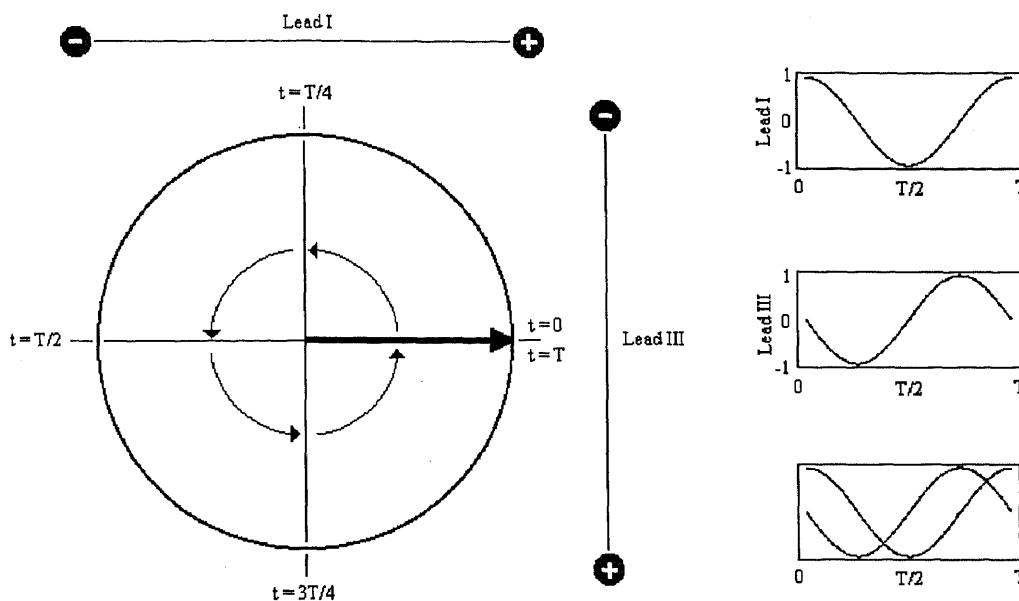


Figure 2.17 Illustration of the Origin of the Phase Shift Between the R-Waves of Leads I and III for a Simplified Case in Which the QRS Loop Has a Constant Magnitude and Constant Change in Direction

The fourth and final problem with Zhao's software has to do with subtracting the baseline area. To find the baseline area of each QRS complex, the minimum of each QRS complex is multiplied by the window width. To find the minimum, Zhao's software takes the minimum point between the Q-wave and the R-wave and assumes that this point is the minimum for the QRS complex. However, this is not always the case as shown in Figure 2.19. If the S-wave is less than the Q-wave, Zhao's software incorrectly computes the baseline area, and therefore, computes the area of the QRS complex incorrectly.

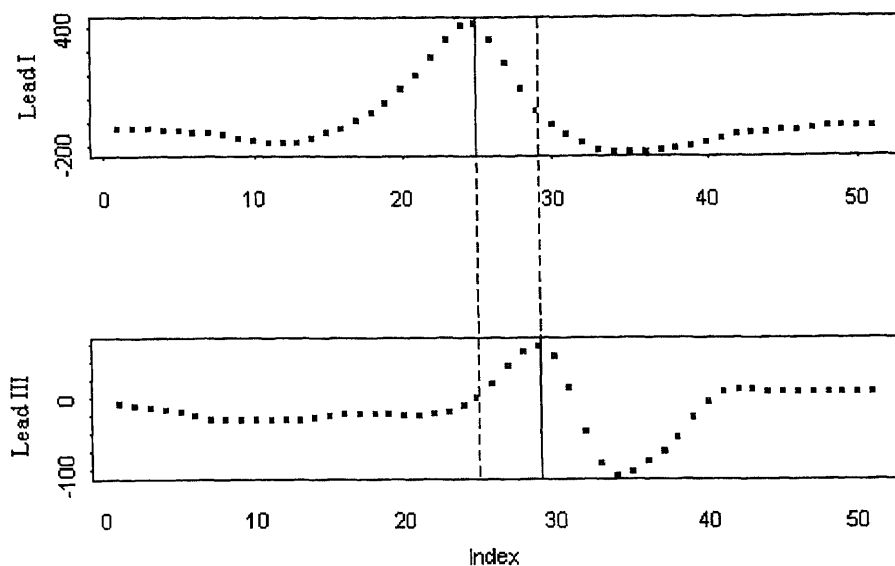


Figure 2.18 One QRS Complex of Lead I and Lead III Showing Different Time of R-Waves. The Solid Line Indicates the R-Wave in Each Lead.

2.6.2 Fixed QRS Window, Independent Leads Method

This method is an improvement on the software written by Zhao. It is called a fixed QRS window, independent leads method for two reasons. One reason is because the width of each QRS complex is fixed for each lead. In other words, the same average window width is used for each QRS complex within each lead. The second reason is because the width of the QRS complexes in lead I is independent of the width of the QRS complexes in lead III.

The improvements made are the corrections to the problems mentioned in Section 2.6.1.2. The first correction involves the dc offset of the ECG. At the beginning of each program, both leads of ECG are detrended. Once they are detrended, the minimum point of each ECG is found and each ECG is shifted vertically by 1.1 times the absolute value of

the minimum point. This provides all samples of the ECG to be positive, and therefore, no errors will occur when calculating the area of each QRS complex.

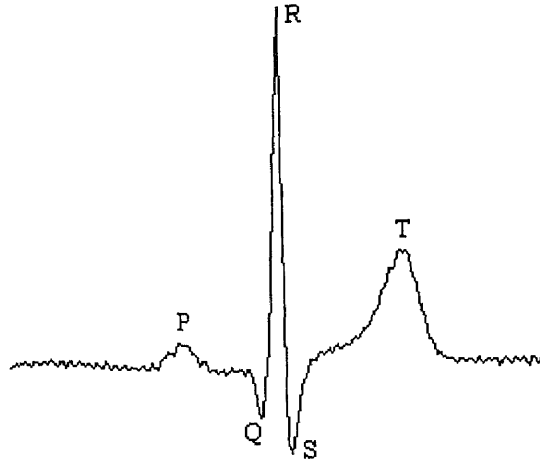


Figure 2.19 An Example of the S-Wave as the Minimum of the QRS Complex

The second correction made is that the program detects the R-waves independently for the two leads because a slight shift in time might be present between the R-waves. This will provide for a more accurate estimate of the average width of the QRS complexes for each lead. The width of the QRS complex for each lead is calculated by equation 2.11. The average width of the QRS complexes in each lead is equal to twice the average of the Q-wave to R-wave width in each lead. Note that this assumes that the QRS complex is symmetrical around the R-wave.

To detect the R-waves, the program relies on the HRV analysis to be done so the location of the R-waves in one lead will already be detected. Because the R-waves occur at different points in time in different leads, it is incorrect to take the arctangent of the areas under the QRS complexes of the two leads. Therefore, the areas are first interpolated for each lead, and the arctangent of the interpolated signals is taken.

Another improvement included in this method is that for each QRS complex, the minimum value is found for the samples within the average window width. This minimum value is used in the baseline area calculation. Zhao's software used the minimum between the R-wave and the Q-wave for the calculation of the baseline area which could be erroneous.

2.6.2.1 Software Implementation of the Fixed QRS Window, Independent Leads Method

The fixed QRS window, independent leads method was implemented in a software program called "impqrsca" which executes in S-Plus. The title of the program stands for an improved version of qrsca, which was the program written by Zhao. The software was written to be user friendly, requiring only one command to obtain the output. The impqrsca program is listed in Appendix G. The command lines preceded by the # sign are not performed by the program and are considered comment lines. During execution, the program gives a few general checks that are a good indication of the integrity of the analysis. The following is a brief description of how the critical steps involved to perform the fixed QRS window, independent leads method were performed with the software, as well as the general information of the inputs to and the outputs of the program

In order to execute the program properly, the dominant lead, which was used to detect the R-waves in the preliminary heart rate variability analysis, must precede the non-dominant lead in the program command line. Other inputs to the program include the final file from the HRV analysis, five variables named w, rq, nfft, sr, decim, and the title for the output plots. The variables w and rq will be described later. The variable nfft is the size

of FFT to take when computing the power spectra of the derived respiration signals. The default for `nfft` is 8192. The variable `sr` refers to the sampling frequency of the ECG signals and the default is 500 Hz. The variable `decim` is an integer that indicates the decimation factor for the interpolated respiration waveform. The respiration waveforms are interpolated to be equal to the number of points in the ECG signals and are then decimated to improve the frequency resolution in the power spectra. The default for the variable `decim` is 25.

To detect the R-waves for the two leads, the R-waves of the dominant lead are first checked to make sure that the peak is detected properly. This process is done by looking for a local minimum whose width is proportional to the input variable `w`. To detect the R-waves of the other lead, another local minimum is performed based on the location of the R-wave in the dominant lead.

Once all the R-waves are properly detected, the Q-waves for each QRS complex for each lead must be detected. To do this, a time period equal to `rq` (whose value is in points) is set back from each R-wave. To identify the Q-wave, the program looks for the minimum between the R-wave and the time period `rq` before the R-wave. This algorithm is analogous to that used by Zhao's software and the idea is illustrated in Figure 2.13 (the variables shown are those used in Zhao's program).

The outputs of the program, saved to a file given at the time of execution, are the original, uninterpolated areas under each QRS complex for each lead. These outputs are called "qrsca1" and "qrsca2". These are output in case there was a problem with the ECG which would cause outliers to be present. If this is the case, the outliers are removed

manually. The program also outputs the detrended, decimated, interpolated areas for each lead. These signals are also representative of the respiration waveform and are called “d.iqrscal” and “d.iqrscal2”. The respiration signal computed from the arctangent operation is saved as “d.iqrscal”. The power spectrum of these three respiration signals is also saved and are called “d.iqrscas”, “d.iqrscal1s”, and “d.iqrscal2s”, respectively.

2.6.3 Method Based on the Amplitude Modulation of the R-Waves

In clinical practice, the existence of an amplitude modulation in an ECG is often observed. An example of this modulation was shown in Figure 1.13. This method was developed to determine if the respiratory waveform can be constructed on a consistent basis from the amplitude modulation of the R-waves. In addition, because the other three methods in this study rely on the area under the QRS complex, which is dependent on the amplitude of the R-waves, this method can be used for comparative purposes.

Whereas the fixed QRS window, independent leads program derives time path of the mean cardiac vector from samples of the QRS loop, this method derives the time path of the mean cardiac vector from one sample of the QRS loop, namely, the peak of the R-wave. It should be reminded that the peak of the R-waves can occur at different periods of time in different leads. Therefore, this results in one sample of the QRS loop for each lead, although the samples might occur at slightly different periods in time. The arctangent of the interpolated waveforms is taken to predict the time path of the mean cardiac vector.

2.6.3.1 Software Implementation of the Method Based on the Amplitude Modulation of the R-Waves

The method based on the amplitude modulation of the R-waves was implemented in a software program called “adresp” which executes in S-Plus. The title of the program stands for “amplitude derived respiration”. The adresp program is listed in Appendix H. The command lines preceded by the # sign are not performed by the program and are considered comment lines. Some of the code has been commented out but left in the listing because this part of the code can be easily used to get a real specific graphical check for the detection of each R-wave in each lead. The following is a brief description of how the software works, as well as the general information of the inputs to and the outputs from the program.

In order to execute the program properly, the dominant lead, which was used to detect the R-waves in the preliminary heart rate variability analysis, must precede the non-dominant lead in the program command line. Other inputs to the program include the final file from the HRV analysis, four variables named *w*, *nfft*, *sr*, *decim*, and the title for the output plots. The description of these inputs, what they do, and their default values are the same as in the fixed QRS window, independent leads program. Therefore, for an explanation of these inputs and an explanation on how the program finds the peak in the R-waves, see Section 2.6.2.1.

During execution the program outputs several checks on the ECG processing to detect the R-waves. The first output is a series of close-ups showing the detection of each of the R-waves. The program shows five detections as a check. Another check on the integrity of the R-wave peak detection is an output of the entire two minutes, broken up in

one minute halves and plotted one above the other, that shows the outline of the amplitude modulation of the detected R-waves. An example of this output is shown in Figure 2.20.

The outputs of the program are saved to a file which is named at the time of execution. The outputs are the modulation waveform and its spectrum for each lead as well as the arctangent of the modulating waveforms and its spectrum. The time signal outputs are called "ampmod1", "ampmod2", and "ampmod". Their respective outputted spectrums are called "ampmod1.spec", "ampmod2.spec", and "ampmod.spec".

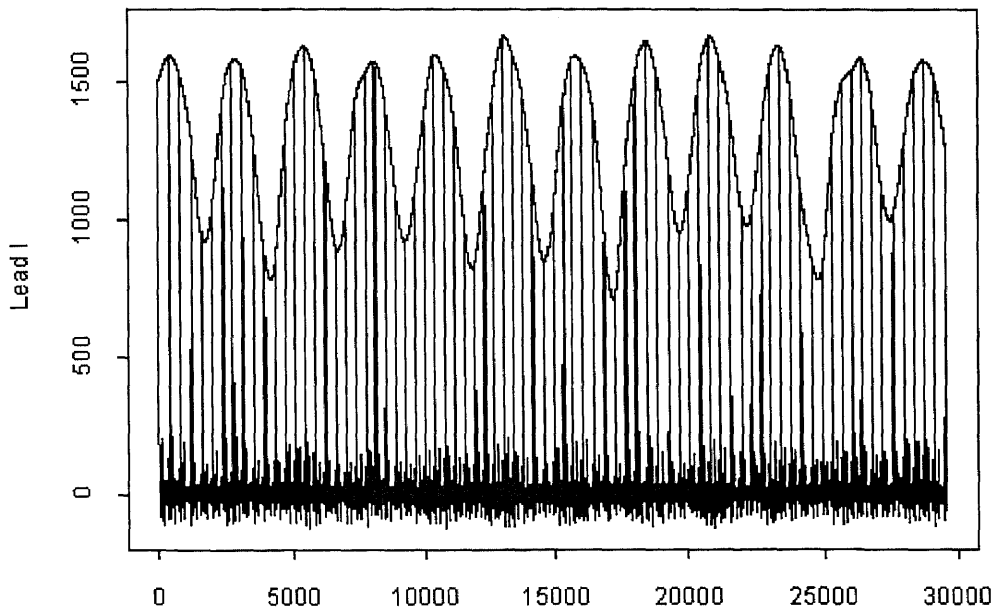


Figure 2.20 Example of "adresp" Output of Amplitude Modulation of the R-waves.

2.6.4 Variable QRS Window, Independent Leads Method

This method is very similar to the fixed QRS window, independent leads method, except for one subtle detail. The fixed QRS window, independent leads method assumes the QRS complex is symmetrical and does not detect the S-wave, whereas, this method

detects the S-wave. It is called a variable QRS window, independent leads method because the width of each QRS complex is dependent on the waveshape of each QRS complex. In other words, it is possible to have different window widths for different QRS complexes in the same lead. In addition, the widths of the QRS complexes in lead I are independent of the widths of the QRS complexes in lead III.

The reason for investigating this method is because sometimes the width of the QRS complexes in a particular lead changes by a slight amount. One possible reason for this change can be attributed to the position of the heart slightly changing in the chest. To better understand this point, a portion of Figure 1.15 is shown in Figure 2.21 for illustrative purposes.

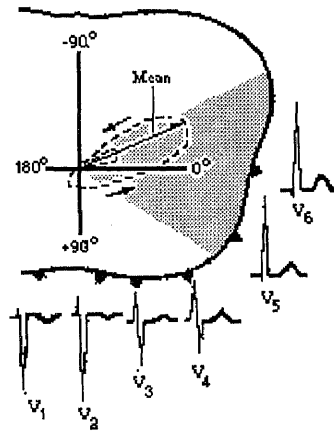


Figure 2.21 Different ECG Waveshapes for Closely Spaced Lead Connections

In Figure 2.21, the leads V_1 through V_6 are shown in a top view of a horizontal slice through a human's abdomen. The representative waveshapes are for the same QRS-wave and T-Wave. Note that as the position of the lead changes on the body, the waveshape changes in a systematic way. In other words, when comparing the waveshapes

from V_1 to V_6 , the R-wave deflection gets bigger, the S-wave deflection gets smaller, and the Q-wave deflection becomes slightly bigger and more defined. Although this logic applies to the same QRS-wave and different places on the body, it can be used to reason why a slightly different waveshape would be recorded for the same position on the body and a change in position of the heart. Although the change in waveshape might be small, it is additional information on the movement of the heart in the thoracic cavity, and therefore, on the direction of the mean cardiac vector.

In this method, the program detects the R-waves independently for the two leads because once the areas are calculated for each QRS complex, the value representing that area is placed at the R-waves. In the fixed window, independent leads method the exact detection of the R-waves was important to increase the accuracy of the window width. Any error in the Q-wave to R-wave length caused a twofold error in the QRS window width assuming a symmetric QRS complex. In this method, the location of the R-wave in the QRS complex does not affect the detected width of the QRS complex.

2.6.4.1 Software Implementation of the Variable QRS Window, Independent Leads Method

The variable QRS window, independent leads method was implemented in a software program called "vqrsind" which executes in S-Plus. The software was written to be user friendly, requiring only one command to obtain the output. The vqrsind program is listed in Appendix I. As in the previous program, the command lines preceded by the # sign are not performed by the program and are considered comment lines. They were left in the listing because this part of the code can be easily used to get a real specific graphical check

for the proper operation of the program. However, during execution, the program gives a few general checks that are a good indication of the integrity of the analysis. The following is a brief description of how the critical steps involved to perform the variable QRS window, independent leads method were performed with the software, as well as the general information of the inputs to and the outputs of the program.

In order to execute the program properly, the dominant lead, which was used to detect the R-waves in the preliminary heart rate variability analysis, must precede the non-dominant lead in the program command line. Other inputs to the program include the final file from the HRV analysis, six variables named *w*, *rq*, *rs*, *nfft*, *sr*, *decim*, and the title for the output plots. The description of *w*, *rq*, *nfft*, *sr*, and *decim*, what they do, and their default values are the same as in the fixed QRS window, independent leads program. Therefore, for an explanation of these inputs and an explanation on how the program detects the peak in the R-waves, see Section 2.6.2.1.

To detect the R-waves, the program relies on the HRV analysis to be done so the location of the R-waves in one lead will already be detected. Because the R-waves occur at different points in time in different leads, it is incorrect to take the arctangent of the areas under the QRS complexes of the two leads. Therefore, the areas are first interpolated for each lead, and the arctangent of the interpolated signals is taken.

The Q-wave detection is the same for the fixed QRS window, independent leads method. Once all the R-waves and Q-waves are properly detected, the S-waves for each QRS complex for each lead needs to be detected. To do this, a time period equal to *rs* (whose value is in points) is set ahead from each R-wave. To identify the S-wave, the

program looks for the minimum between the R-wave and the time period r_s after the R-wave. An example of this algorithm is shown in Figure 2.22.

The outputs of the program, saved to a file given at the time of execution, are the original, uninterpolated areas under each QRS complex for each lead. These outputs are called “qrsca1” and “qrsca2”. These are output in case there was a problem with the ECG which would cause outliers to be present in them. If this is the case, the outliers are removed manually. The program also outputs the detrended, decimated, interpolated areas for each lead. These signals are also representative of the respiration waveform and are called “d.iqrsca1” and “d.iqrsca2”. The respiration signal computed from the arctangent operation is saved as “d.iqrsca”. The power spectrum of these three respiration signals is also saved. When either of these variables are followed with an s, this indicates that it is a power spectrum.

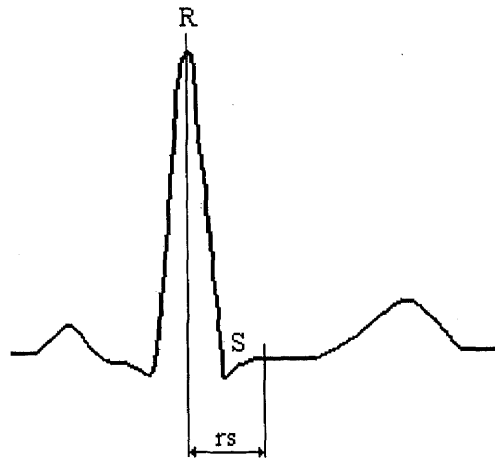


Figure 2.22 Illustration of the Algorithm to Detect the S-Wave

2.6.5 Variable QRS Window, Dependent Leads Method

This method is called a variable QRS window, dependent leads method because the width of each QRS complex is dependent on the waveshape of each QRS complex. In addition, the width of the QRS complexes in one lead are dependent of the width of the QRS complexes in the other lead. In other words, the width of the QRS complexes can vary from cardiac cycle to cardiac cycle, but are the same width in each lead.

If the widths of the variable QRS complexes are the same in each lead, and the QRS waves occur at the same time, then the samples of the QRS are the same for each lead. Consequently, the reason this method was developed was to sample the QRS loop at the same time, rather than at two separate times. The reason a variable window was used is explained in section 2.6.4.

At first, the above paragraph might be confusing because it has been shown that the Q-wave, R-wave, and S-wave occur at different times in different leads. To solve this problem, the detected times of the Q, R, and S-waves from the dominant lead were used to correspond to the time of the Q, R, and S-waves in the non-dominant lead. Therefore, in reality, the times corresponding to the Q, R, and S-waves in the non-dominant lead are not really correct. Figure 2.23 illustrates an example.

2.6.5.1 Software Implementation of the Variable QRS Window, Dependent Leads Method

The variable QRS window, dependent leads method was implemented in a software program called “vqrsdep” which executes in S-Plus. The software was written to be user friendly, requiring only one command to obtain the output. The vqrsdep program is listed

in Appendix J. As in the previous programs, the command lines preceded by the # sign are not performed by the program and are considered comment lines. They were left in the listing because this part of the code can be easily used to get a real specific graphical check for the proper operation of the program. During execution, the program gives a few general checks that are a good indication of the integrity of the analysis. The following is a brief description of the program and its inputs and outputs.

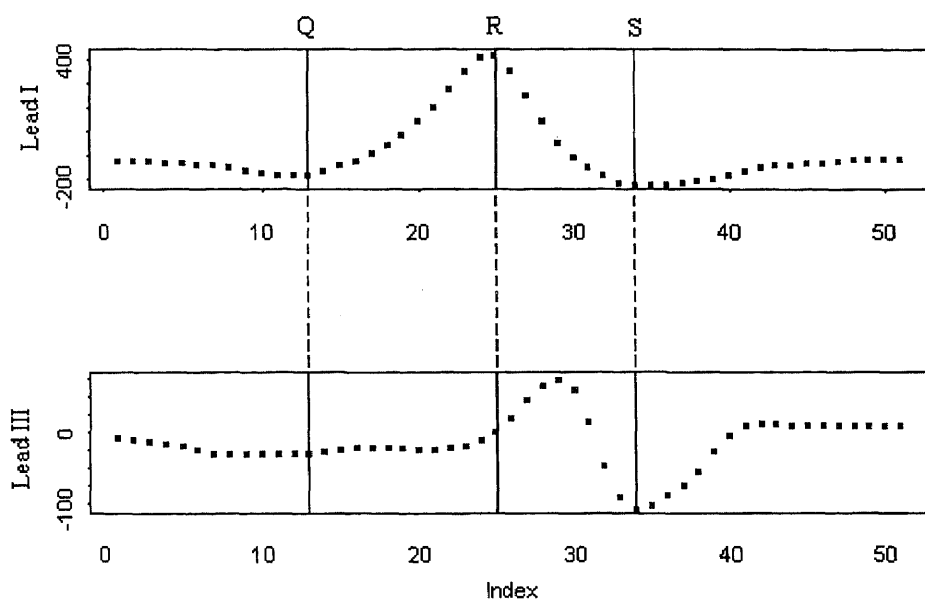


Figure 2.23 An Example of How the Times of the Q, R, and S-Waves from the Dominant Lead Were Used to Correspond to the Times of the Q, R, and S-Waves in the Non-Dominant Lead.

The main steps of the program are similar to the variable window, independent leads method except for two differences. One difference is that the Q, R, and S-waves from one lead are used as the Q, R, and S-waves in the other (as shown in Figure 2.23). To obtain these points, the program analyzes the dominant lead, which should be input first on the command line of the program. Once the areas for each QRS complex are

calculated, the values of the QRS complex areas are placed at the R-waves, which in this case, correspond to the same time. Therefore, the second difference is that the arctangent of the QRS complex areas are taken, and the arctangent values are then interpolated. In the other methods, the areas for each lead are first interpolated and then the arctangent is taken between the interpolated areas because the R-waves might not occur at the same time in each lead.

To detect the R-waves, the program relies on the HRV analysis to be done so the location of the R-waves in the dominant lead will already be detected. The values of the areas are then placed at the R-waves, which in this case, correspond to the same time. Therefore, the arctangent of the values is taken, and the arctangent values are then interpolated. The Q-wave and S-wave detection is the same for the variable QRS window, independent leads method. In addition, the inputs to the program and the name of the outputs are also the same as the variable QRS window, independent leads method.

2.7 Developed Methods That Were Unsuccessful

In addition to the four methods explained above, four other methods were developed to derive the respiration from the ECG. These methods are slight modifications of the methods explained above. They all try to estimate the change in angle of the mean cardiac vector during respiration from two orthogonal leads. They were not used to derive the respiration because all of them yielded poor results.

The first method is a slight modification that can be made to all three of the above methods which calculate the area under the QRS complex. This modification involves the

calculation of the baseline area. It was proposed that instead of taking the local minimum of each QRS complex, the minimum of all the QRS complexes is taken to compute one overall baseline area. When this was done, the accuracy of the derived respiration methods decreased dramatically. Therefore, the proper way to calculate the baseline area, is to calculate the baseline area of each individual QRS complex.

The second method developed but not used because it provided poor results is a modification of the method based on the amplitude modulation of the R-waves. In this method, no detrending was done at all, so as not to disturb the natural modulating waveform. As a result, the frequency of respiration was not as easily identifiable in the power spectrum compared to when detrending was done. Therefore, it is necessary to detrend the ECG before deriving the method based on the amplitude modulation of the R-waves. In addition, once the modulating waveform was obtained, it was detrended again to remove any low frequencies below 0.05 Hz which might dominate the power spectrum.

The last two methods developed but not used in this thesis, were developed to reduce the influence of the noise in the ECG. In the initial method, the area under the ECG was calculated from 0.2 seconds before each R-wave to 0.2 seconds before the following R wave. The time preceding each R-wave was necessary to include the appropriate P-wave for that cardiac cycle in the area calculation. In the development of this method it was realized that the respiration will be contained in this method in two ways, in both the amplitude and in the time between R-waves. The initial hope for this method relied on the fact that the ECG is being amplified, and that the amplitude of the P, Q, R, S, and T-waves of the ECG would provide more area than the difference in length

of time of the baseline of the ECG. After some investigation, the resulting respiration waveform had a very high correlation with the interpolated interbeat interval. Therefore, it was concluded that the main contributor to the derived respiration in this method was the change in time between beats, or the interbeat interval, which depends on the autonomic activity of the heart.

To remove the contribution of the interbeat interval in the previous method, the minimum interbeat interval was found, and the area under the ECG was then calculated from 0.2 seconds before each R-wave to a point which occurred at a time equal to the minimum interbeat interval away. Unfortunately, this method provided nothing that resembled a respiration waveform. This gives merit to the methods in Section 2.6, which try to estimate the mean cardiac vector for just a brief period in time of the QRS complex.

CHAPTER 3

RESULTS

The purpose of this chapter is to quantitatively display the results of the different methods developed to derive the respiration waveform from the ECG. To begin the chapter, a basic description of the two signal processing techniques used to analyze and compare the outputs of the derived respiration methods is given. These two techniques, cross-correlation and coherence, were used to compare the derived respiration signals to the measured respiration in both the time domain and frequency domain, respectively.

3.1 Theory of Cross-Correlation

The technique of cross-correlation was used in order to compare the derived respiration signals to the measured respiration signal in the time domain. The cross-correlation between two time signals measures the way the signals change with respect to one another. In other words, if $f(x)$ always increases and decreases as $g(x)$ increases and decreases, then $f(x)$ and $g(x)$ are positively correlated. If they tend to change in opposite directions then they are negatively correlated. The correlation of two continuous functions $f(x)$ and $g(x)$, denoted as $f(x) \circ g(x)$, is defined by the following equation[27]

$$f(x) \circ g(x) = \int_{-\infty}^{\infty} f(x)^* g(x + \lambda) dx \quad (3.1)$$

where $*$ is the complex conjugate. For this study, the signals were not complex. Therefore, to calculate the cross-correlation, the function $g(x)$ is shifted, by different

values of λ , over the length of $f(x)$, the signals are multiplied, and the area under the product of the two signals is computed. Figure 3.1 illustrates the process to perform the calculation. In Figure 3.1 (a) and (b), the two continuous signals $f(x)$ and $g(x)$ are shown as a square and rectangle function, respectively. Figure 3.1 (c) illustrates the meaning of the shift λ , in $g(x + \lambda)$. Figure 3.1 (d) represents $g(x + \lambda)$ being shifted for values of λ between -1 and 0, while (e) illustrates $g(x + \lambda)$ for values of λ between 0 and 1. The shaded areas of (d) and (e) indicates regions where the product of $f(x)$ and $g(x + \lambda)$ are not zero. The result is the cross-correlation function shown in (f). From this example, one can see that the cross-correlation of two continuous signals is also continuous. If the cross-correlation function is normalized by the product of the square root of the auto cross-correlation of each function, then the normalized cross correlation will have a range from 0 to 1. For two signals that are the same, the cross-correlation at zero lag (when $\lambda=0$) is equal to 1. The closer the cross-correlation value is to 1, the more similar the waveforms are to one another.

It should be pointed out that the signals in this study are not continuous, but discrete. Therefore, to compute the discrete cross-correlation, the following equation was used[28]

$$C_{fg}(\lambda) = \frac{\frac{1}{N-1} \sum_{n=1}^N (f(n) - \bar{f})(g(n+\lambda) - \bar{g})}{\sqrt{\frac{1}{N-1} \sum_{n=1}^N (f(n) - \bar{f})^2 \frac{1}{N-1} \sum_{n=1}^N (g(n) - \bar{g})^2}} \quad (3.2)$$

where N is the number of points in the signal. To compute the cross-correlations for this thesis, a program was written in S-Plus and is listed in Appendix K.

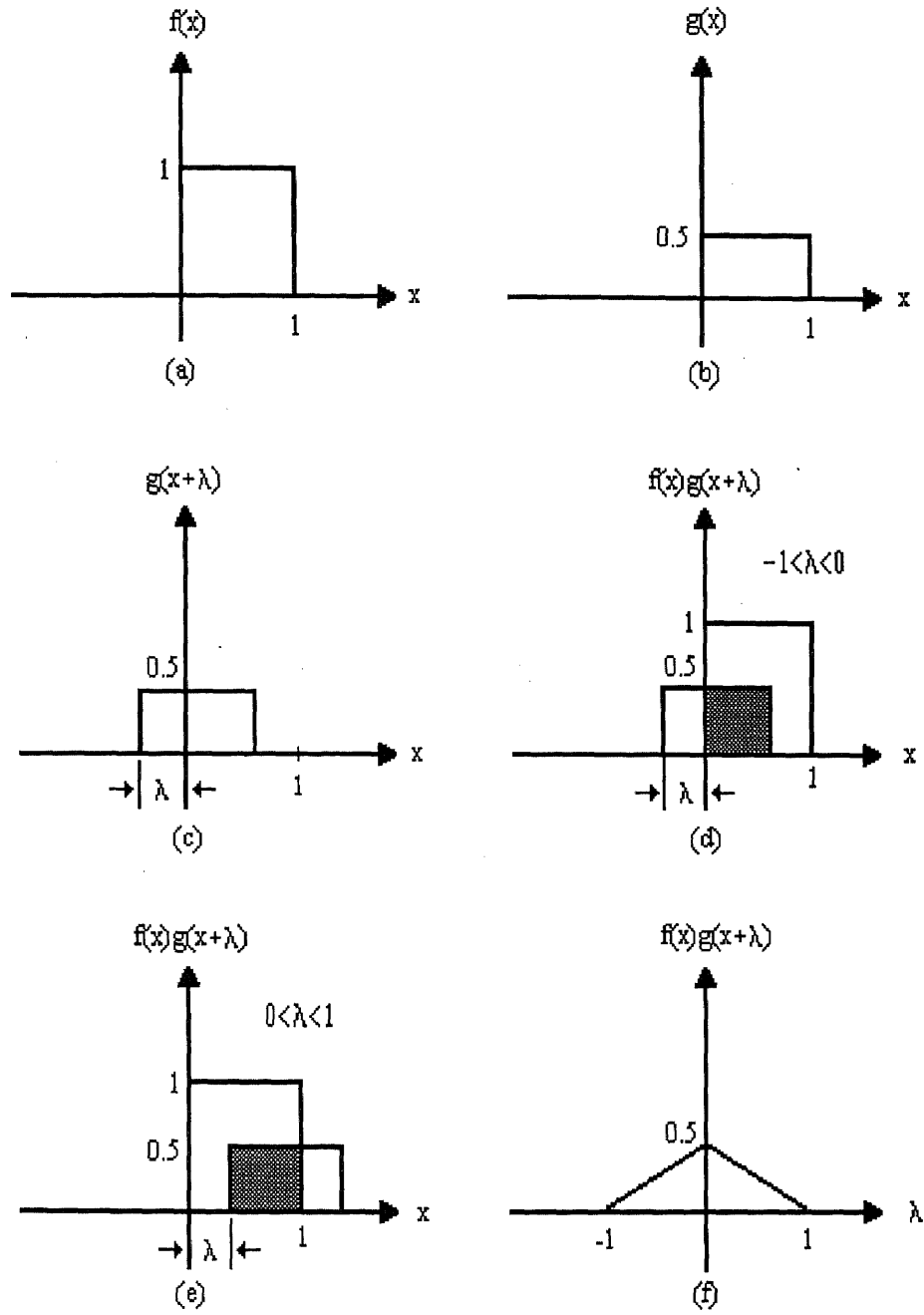


Figure 3.1 Illustration of the Cross-Correlation Calculation.

3.1.1 Understanding the Cross-Correlation Function

In order to get a firm understanding on the meaning of cross-correlation, the cross-correlation was calculated for six different examples. The examples were chosen to understand how the amplitude, frequency, phase, dc offset, and waveshape affect the cross-correlation results. In all the following plots, (a) and (b) are the signals of interest and (c) is the cross-correlation. Note that the cross correlation signal is twice as long as the original signals. Thus, the cross-correlation point indicating when the signals have no shift between them (zero lag) is the center of the cross-correlation wave.

The two signals of interest in the first example are two sine waves of the same frequency and in phase. However, the amplitude of one wave is three times the amplitude of the other. The signals and the cross-correlation of them are shown in Figure 3.2. This example demonstrates that cross-correlation at zero lag is 1.0 when the two signals are in phase. Note that the relative amplitude of the waves did not affect the results. The reason the cross-correlation is not equal to 1.0 at peaks other than at zero lag is because these signals are finite in length.

For the second example, the effect of the phase was examined by calculating the cross-correlation for two sine waves of the same amplitude and frequency, but 180 degrees out of phase. The result is that at zero lag, the cross-correlation is -1.0. This result indicates that cross-correlation at zero lag is sensitive to changes in phase. The negative sign indicates that the signals are negatively related. For example, when one wave is increasing, the other wave is decreasing.

The next example investigates whether or not the DC value of the signals affects the cross-correlation. The signals used to test this situation were two sine waves with the same frequency, amplitude, and in phase. However, one sine wave had a DC offset equal to 1. The results are shown in Figure 3.3. If the DC offset has no effect on the outcome, then the cross-correlation at zero-lag should be equal to 1. However, with a DC offset, the cross-correlation at zero lag is equal to 0.6. Therefore, the DC components do affect the cross-correlation. To understand why this is, the cross correlation involving a signal with a DC offset is computed as follows:

$$\begin{aligned}
 f(x) \circ [1 + g(x)] &= \int_{-\infty}^{\infty} f(x)[1 + g(x + \lambda)] dx \\
 &= \int_{-\infty}^{\infty} [f(x) + f(x)g(x + \lambda)] dx \\
 &= \int_{-\infty}^{\infty} f(x)g(x + \lambda) dx + \int_{-\infty}^{\infty} f(x) dx
 \end{aligned} \tag{3.3}$$

When equation (3.3) is compared to equation (3.1), it is apparent that there is an extra term in equation (3.3). The extra term ($\int_{-\infty}^{\infty} f(x) dx$) results from the mathematics and does indeed change the results. Therefore, it is necessary to remove the DC component of the signals before performing the cross-correlation.

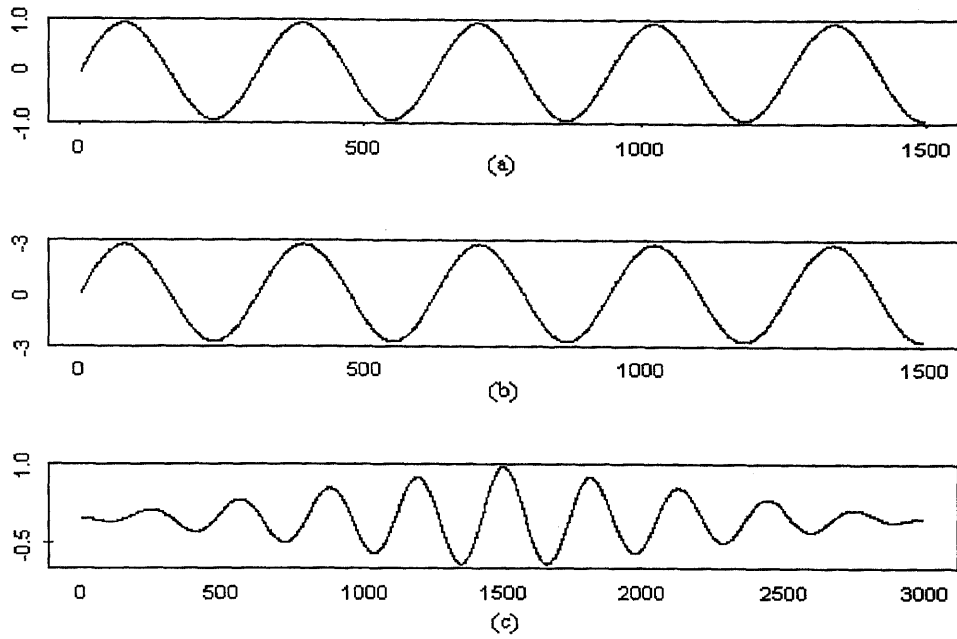


Figure 3.2 Cross Correlation of Two Sine Waves with the Same Frequency, in Phase, and with Different Amplitudes. (a) $\sin[\omega_1 t]$; (b) $3\sin[\omega_2 t]$; (c) $\sin[\omega_1 t] \circ \sin[\omega_2 t]$ ($\omega_1 = \omega_2$)

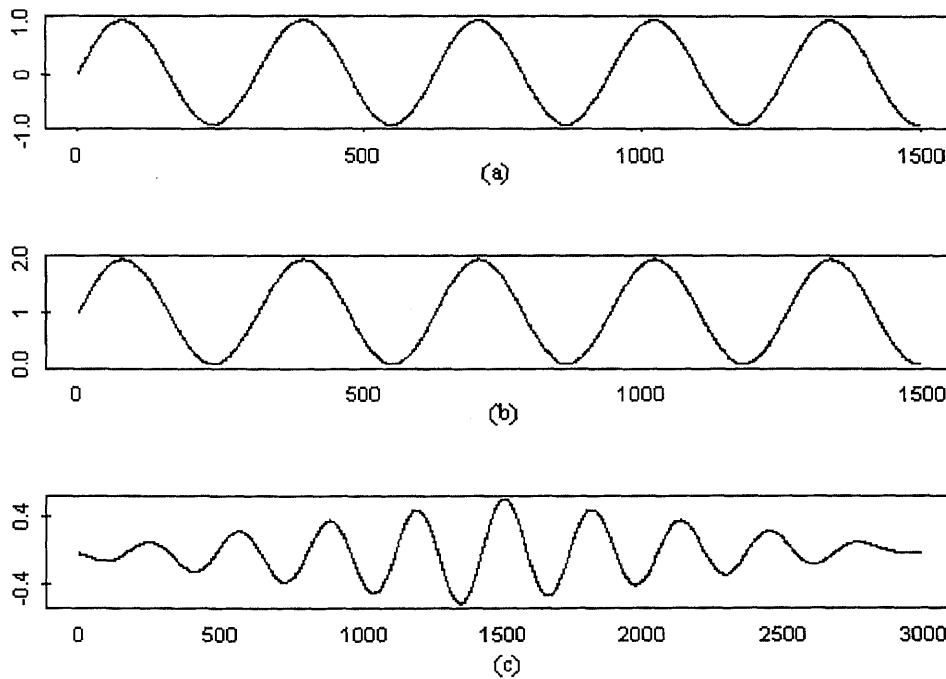


Figure 3.3 Cross Correlation Between Two Sine Waves, One Which Contains a DC Component. (a) $\sin[\omega t]$; (b) $(1 + \sin[\omega t])$; (c) $\sin[\omega t] \circ (1 + \sin[\omega t])$

For the fourth example, the cross-correlation between two signals with different frequencies is shown in Figure 3.4. At zero lag, the cross-correlation is 0.0047. Note that with either a slightly positive or negative phase shift, the cross-correlation increases to 0.023. Thus, there is more correlation at these shifts; however, the value is still significantly below the normalized value of 1, and therefore, it is safe to say there is no similarity between these signals.

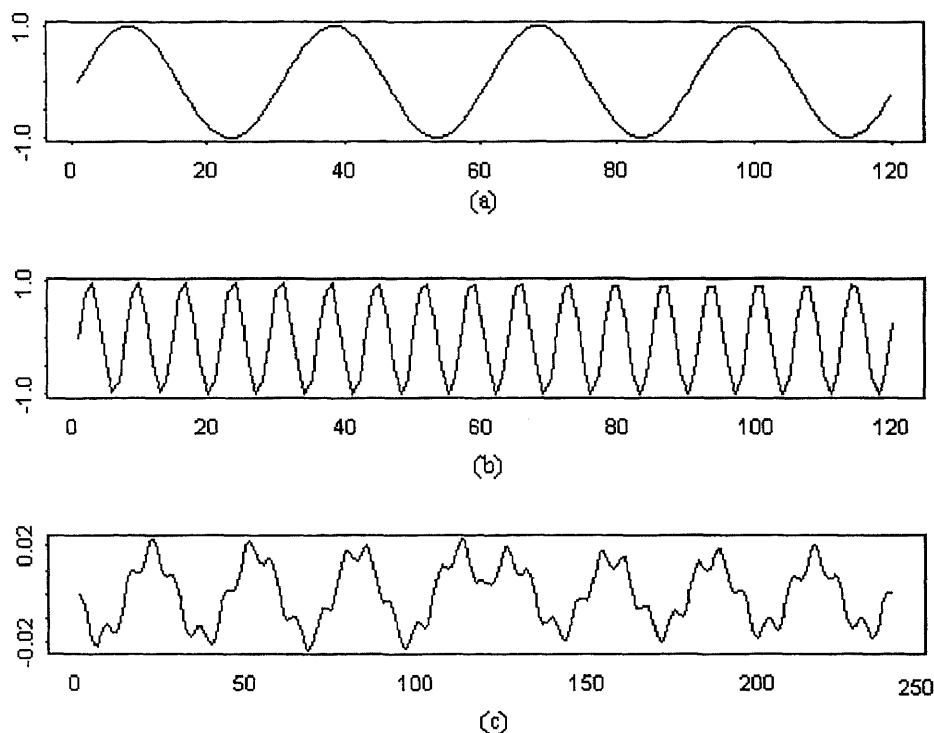


Figure 3.4 Cross Correlation of Two Sine Waves with Different Frequencies.
 (a) $\sin[\omega_1 t]$; (b) $\sin[\omega_2 t]$; (c) $\sin[\omega_1 t] \circ \sin[\omega_2 t]$ ($\omega_1 \neq \omega_2$)

In the next example, the cross-correlation is computed for two signals that have a common frequency component. In other words, the frequency of one signal is included in

the waveform of the other. This is illustrated in Figure 3.5. From this example, it is clear that there is some correlation between the two signals; however at zero lag the cross-correlation is not equal to 1, but is 0.71. After further investigation, it was found that if the amplitude of the higher frequency component of the signal in (b) was decreased, then the cross-correlation approached unity. This case would be an example of a signal which contains a high frequency noise. Also, if the frequency of the noise is increased, the cross correlation also approaches unity.

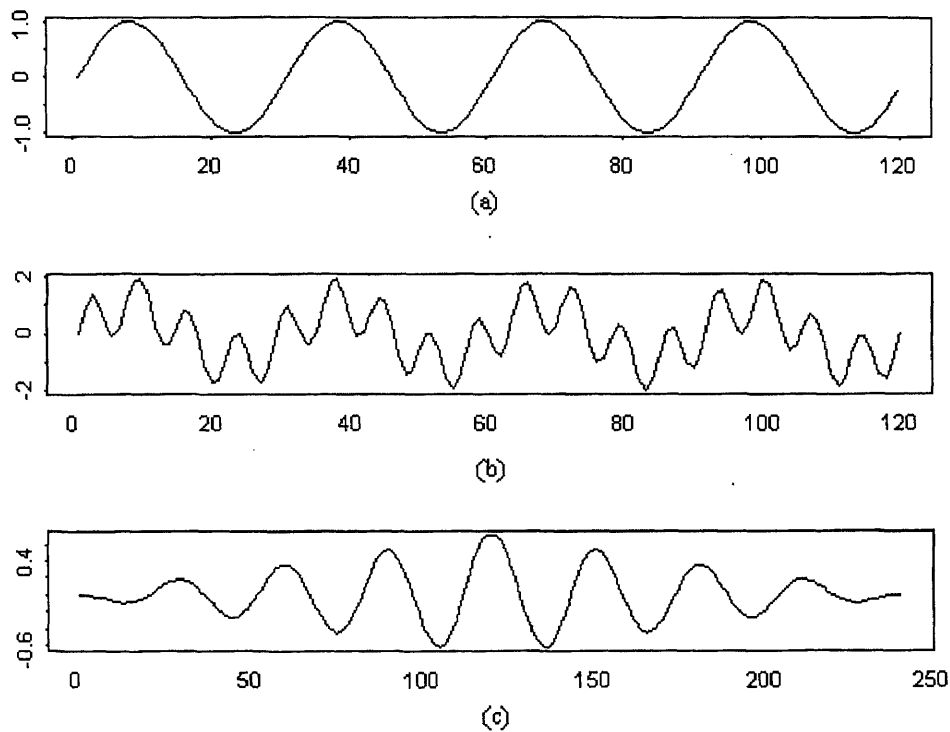


Figure 3.5 Cross Correlation Between Two Sine Waves, One Which Contains a Frequency Component of the Other. (a) $\sin[\omega_1 t]$; (b) $(\sin[\omega_2 t] + \sin[\omega_1 t])$; (c) $\sin[\omega_1 t] \circ (\sin[\omega_2 t] + \sin[\omega_1 t])$; ($\omega_1 \neq \omega_2$)

In the final example, the shape of the waveforms is investigated to see if they have any effect on the cross-correlation. The signal in Figure 3.6 (a) is a triangle waveform and the signal in (b) has an exponential characteristic. The frequency of the waveforms are exactly the same, and the DC component of each has been removed. Figure 3.6 (c) shows the cross-correlation function. The cross-correlation at zero shift is 0.69. Therefore, the waveshape does have a profound effect on the cross-correlation.

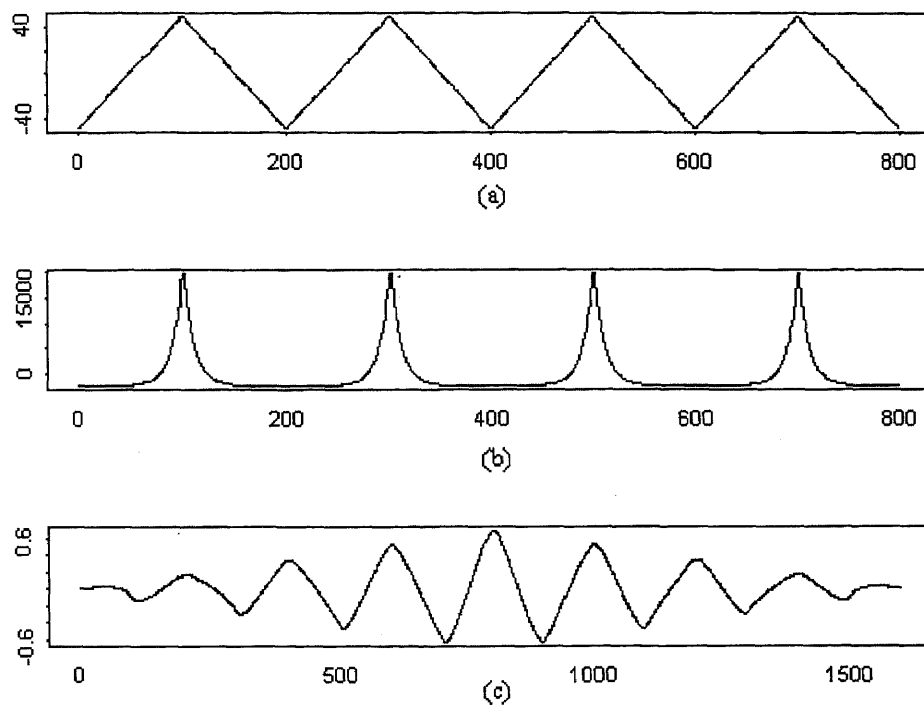


Figure 3.6 Cross-Correlation of Two Signals with the Same Frequency, but Different Waveshapes.

3.2 Theory of Coherence

The coherence function is a technique to measure the similarity between two signals in the frequency domain. Coherence can be referred to as a correlation coefficient in the

frequency domain which yields values as a function of frequency. The coherence function is normalized to yield values between zero and unity. The function in its basic form is complex and is defined as[29]

$$C_{xy}(\omega) = \frac{P_{xy}(\omega)}{\sqrt{P_{xx}(\omega)P_{yy}(\omega)}} \quad (3.4)$$

where $P_{xy}(\omega)$ is the cross-power spectrum between signals $x(t)$ and $y(t)$, and $P_{xx}(\omega)$ and $P_{yy}(\omega)$ are the power spectra of $x(t)$ and $y(t)$ respectively. More commonly used is the magnitude-squared coherence (MSC) function, defined as[29]

$$MSC = |C_{xy}(\omega)|^2 = \frac{|P_{xy}(\omega)|^2}{P_{xx}(\omega)P_{yy}(\omega)} \quad (3.5)$$

Using complex mathematics, one might notice that if the spectra $P_{xy}(\omega)$, $P_{xx}(\omega)$, and $P_{yy}(\omega)$ are estimated with complex functions, which they are, and substituted in equation (3.5), that the result is $MSC=1$, for any two signals $x(t)$ and $y(t)$.

Therefore, there is obviously an important step involved when computing the coherence that is left unsaid in equation (3.5). The important step is to compute the coherence by means of averaged estimates based on segments of the original signals. In other words, the signals $x(t)$ and $y(t)$ are broken up into N segments of equal length and the power spectra(P_{xx} and P_{yy}) and cross spectrum(P_{xy}) are estimated on the basis of averages taken from the individual spectra of the segments. To increase the number of individual spectra, which increases the accuracy, the segments may overlap. In addition, care must be taken to assure that the segments are long enough to obtain an accurate spectrum. Therefore, there is a compromise required in the choice of the segment length;

it must be long enough to obtain accurate frequency resolution, but short enough to allow a sufficient number of segments in the average. In addition, each segment must be extracted using a time-domain window to control the sidelobes in the frequency domain. To make things more complicated, if too many segments are taken then the accuracy declines due to a greater correlation between segments.

To perform coherence calculations for this study, a program was written, called “cohere”, which executes in S-Plus and is listed in Appendix L. The signals of interest in this study were 120 seconds long. To determine the optimum window length and overlap, several trials were done with signals from different sections of the experimental protocol. Based on the outputs from these trials, it was determined that a 700 point window with a 350 point overlap was the best choice. This means that the windows are 35 seconds long and the overlap is 17.5 seconds. For a 120 second long signal, this provides 12 segments to be averaged.

3.3 Visual Comparison

Figure A.1 in Appendix A is a graphical comparison between the measured respiration and the ECG derived respiration for each of the four methods described in Chapter 2 and for each section of the experimental protocol performed by subject #7. In the figure, the time domain signal of the measured respiration and the four derived respirations are shown, as well as their respective spectra. Each page represents one section of the experimental protocol. On each page, the left column contains the time domain signal and the right column contains the spectrum of the corresponding time signal. Each row represents a

different measure of respiration: the top row is the original respiration measured with the RESPI, the second row is the respiration derived from the amplitude modulation of the R-waves, the third row is the respiration derived using the fixed window, independent leads method, the fourth row is the respiration from the variable QRS window, independent leads method, and the last row is the respiration derived by the variable QRS window, dependent leads method.

When the measured respiration is visually compared to the derived respirations in the time domain, it is observed that the fundamental frequency of the measured respiration is the fundamental frequency in the derived respiration signals. However, for some of the derived respiration methods, the fundamental frequency is not as obvious as in the RESPI. For example, in Figure A.1 (b), it can be observed that the subject was pace breathing at 8 bpm from any of the derived respiration waveforms, but the waveforms possess some high frequency content that is not in the RESPI recording. In addition, in the frequency domain, the frequency of respiration peak that is dominant in the spectrum of the RESPI recording is also dominant in the power spectrum of all the derived respiration methods.

Because an important aspect of this study is to be able to derive the respiration from the ECG when there is a lot of upper and lower body motion, the signals and spectra in Figure A.1 (e) and (f) should be examined closely. Figure A.1 (e) and (f) represent sections of the experimental protocol when the subject was exercising on the treadmill at 3.5 mph with no incline and 3.5 mph at 5% incline. Notice that the method based on the amplitude modulation of the R-waves does not produce a respiration signal in the time domain that resembles the measured respiration. In addition, note that in the power

spectra, the frequency of respiration is present; however, significant power exists at other frequencies other than the frequency of respiration. If the power spectrum of the measured respiration was not available, the frequency of respiration in the derived spectrum would not be identified easily for this method. However, when the time signal of the measured signal is compared to the respiration signals derived from the other three methods, the fundamental frequency is noticeable, and consequently, is the dominant peak in the power spectra. Therefore, one can conclude that the area operation does indeed contain more information about the mean cardiac vector than just the amplitude.

Another important point to be noticed is that the respiration signal derived with the variable QRS window, dependent leads method in the time domain is the most similar to the measured respiration in all cases except in Figure A.1(d). In this particular case, the method based on the amplitude modulation of the R-waves produced superior results compared to the other three methods. This leads to the conclusion that the method based on the amplitude modulation of the R-waves is inconsistent.

When the fundamental frequency is present in the measured and derived spectra, it is interesting to note that sometimes the peak of the frequency of respiration of the derived signals has a wider bandwidth than the respiration measured with the RESPI. In addition, some spectral components that are not present in the spectrum of the RESPI are present in the spectra of the derived respiration. Therefore, to determine the best method quantitatively, the cross-correlation and coherence between the measured respiration and of each of the derived respiration signals for each section of the protocol was computed.

3.4 Cross-Correlation of the ECG Derived Respiration with the Measured Respiration

Based on the cross-correlation method presented in Section 3.1, the cross-correlation coefficient between the ECG derived respiration and the measured respiration was calculated for each subject, during each section of the experimental protocol, and for each of the four methods developed for this study. Table 3.1 tabulates the cross-correlation coefficients of the measured respiration and the fixed QRS window, independent leads method. Tables 3.2, 3.3, and 3.4 display the cross-correlation coefficients between the measured respiration and the method based on the amplitude modulation of the R-waves, the variable window, independent leads method, and the variable window, dependent leads method, respectively. It should be noted that the tables display the maximum absolute value of the cross-correlation function. In addition, although each program produces three signals representing the respiration, the signal that estimates the change in the mean cardiac vector (the arctangent of the other two signals) is the derived respiration waveform of interest. In all the following results, the ECG of subject #3 during the last section of the experimental protocol was corrupted by a large DC offset. Therefore, no analysis was done for that subject for that section.

An example of the cross-correlation between an ECG derived respiration signal and the measured respiration is shown in Figure 3.7. For this particular example, the maximum of the cross-correlation function is 0.725. This indicates that a cross-correlation coefficient of 0.7 is still acceptable because the derived respiration shown in Figure 3.7 is a good estimate of the actual respiration by visual observation. In fact, from experience, a cross-correlation coefficient higher than 0.6 indicates a high degree of similarity between

the respiration signals. The cross-correlation is lower than 1 because the signals have different waveshapes, a different change in relative amplitude from peak-to-peak, and perhaps a very slight difference in instantaneous frequency.

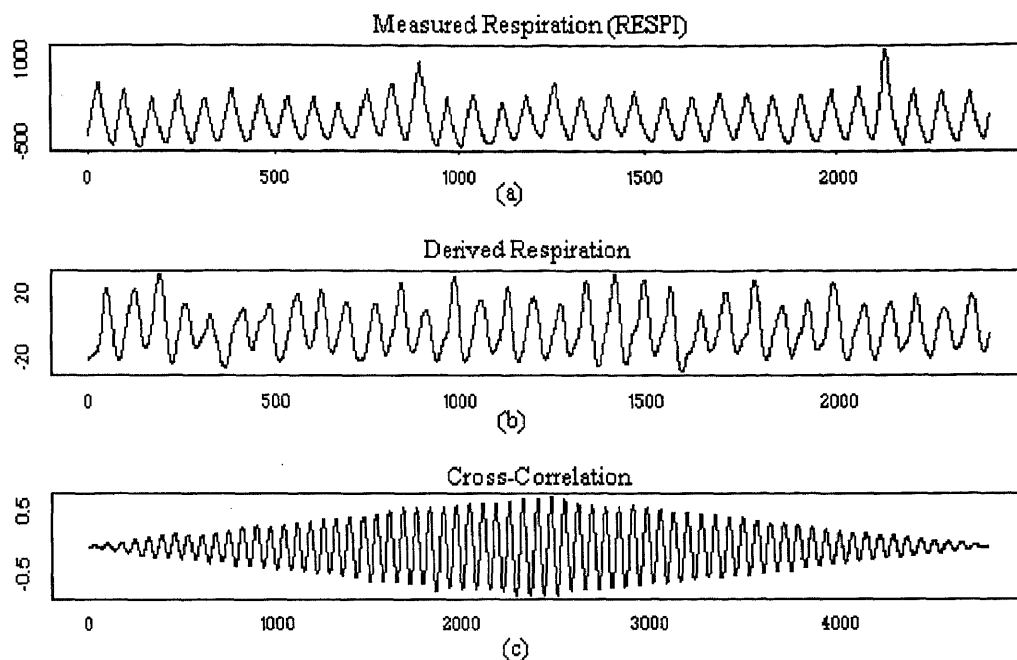


Figure 3.7 Cross-Correlation of the ECG Derived Respiration with the Measured Respiration. (a) Measured Respiration. (b) ECG Derived Respiration. (c) The Cross-Correlation of the Original Respiration and the ECG Derived Respiration

Table 3.1 Cross-Correlation Between the Derived Respiration and the Measured Respiration for the Fixed QRS Window, Independent Leads Method

Subject #	Rest	Paced at 8 bpm	Paced at 12 bpm	Paced at 16 bpm	3.5 mph	3.5 mph, 5% incline
1	0.532	0.864	0.845	0.725	0.523	0.441
2	0.189	0.690	0.600	0.662	0.659	0.484
3	0.551	0.555	0.625	0.613	0.143	*
4	0.577	0.917	0.865	0.711	0.579	0.408
5	0.537	0.760	0.661	0.686	0.434	0.491
6	0.544	0.840	0.793	0.616	0.432	0.485
7	0.487	0.661	0.516	0.516	0.500	0.665
8	0.438	0.620	0.737	0.684	0.221	0.211
9	0.359	0.550	0.523	0.256	0.200	0.222

When one looks at these tables and compares them to determine which method produces the best respiration method in the time domain, there appears to be no consistency. As expected, the derived respiration methods have a higher correlation coefficient for the sections of the protocol when the subject was pace breathing. It is also interesting to point out that the cross-correlation coefficients decrease as the frequency of respiration increases. In order to determine which method is more accurate, the average of the correlation coefficients for each method and the standard deviation from the average were computed for each section of the experimental protocol. The results are shown in Table 3.5.

In table 3.5, the variable QRS window, dependent leads method has a slightly higher average cross-correlation than the other three methods. In addition, the overall average of the standard deviation for every section of the protocol for the variable QRS Window, dependent leads method is the same or smaller than the overall average standard deviation of the other three methods as shown in Table 3.6. To get a better understanding of the distribution of the means from subject to subject within each section of the experimental protocol, box plots were generated and are displayed in Figure A.2(a) in Appendix A.

A box plot displays the distribution of data about the median. In a box plot, the upper and lower quartiles of the data are portrayed by the top and bottom of a rectangle, and the median is portrayed by a horizontal line segment within the rectangle. The median, which is not the same as the mean, shows the center of the distribution. The spread of the central 50% of the data is located within the rectangle. The lengths of the

dashed lines relative to the box show how stretched the distribution is. The values that are located outside the box, can be investigated to see if they are outliers. The box plot also is capable of assessing the symmetry of a distribution. If the distribution is symmetric, then the box plot is symmetric about the median.

In the box plots shown in Figure A.2(a), there appears to be no consistency of the distribution of the cross-correlations for each method within each section of the experimental protocol. For example, in Figure A.2(a), the box plot of the cross-correlations for the section of the experimental protocol where the subject is resting, the variable QRS window, dependent leads method has the smallest range of the central 50% of the distribution when compared to the other three leads. However, in the other box plots corresponding to the other sections of the experimental protocol, the central 50% of the distribution of the cross-correlation coefficients for the variable QRS window, dependent leads method does not have the smallest range. In addition, there is no consistency of the medians within each section of the experimental protocol, for each method.

Table 3.2 Cross-Correlation Between the Derived Respiration and the Measured Respiration for the Method Based on the Amplitude Modulation of the R-waves

Subject #	Rest	Paced at 8 bpm	Paced at 12 bpm	Paced at 16 bpm	3.5 mph	3.5 mph, 5% incline
1	0.524	0.875	0.853	0.755	0.593	0.461
2	0.352	0.582	0.646	0.780	0.635	0.408
3	0.593	0.628	0.652	0.599	0.229	*
4	0.554	0.921	0.866	0.565	0.627	0.425
5	0.463	0.698	0.609	0.627	0.504	0.593
6	0.461	0.687	0.688	0.659	0.541	0.544
7	0.492	0.686	0.692	0.727	0.305	0.339
8	0.399	0.618	0.755	0.623	0.167	0.214
9	0.548	0.820	0.662	0.267	0.261	0.195

Table 3.3 Cross-Correlation Between the Derived Respiration and the Measured Respiration for the Variable QRS Window, Independent Leads Method

Subject #	Rest	Paced at 8 bpm	Paced at 12 bpm	Paced at 16 bpm	3.5 mph	3.5 mph, 5% incline
1	0.531	0.865	0.836	0.691	0.520	0.411
2	0.260	0.692	0.600	0.702	0.682	0.478
3	0.603	0.611	0.594	0.620	0.303	*
4	0.573	0.918	0.865	0.502	0.581	0.409
5	0.613	0.765	0.661	0.641	0.436	0.517
6	0.554	0.828	0.817	0.656	0.346	0.490
7	0.584	0.720	0.668	0.539	0.487	0.629
8	0.440	0.639	0.750	0.684	0.238	0.226
9	0.532	0.729	0.565	0.244	0.282	0.216

Table 3.4 Cross-Correlation Between the Derived Respiration and the Measured Respiration for the Variable QRS Window, Dependent Leads Method

Subject #	Rest	Paced at 8 bpm	Paced at 12 bpm	Paced at 16 bpm	3.5 mph	3.5 mph, 5% incline
1	0.537	0.866	0.845	0.731	0.542	0.408
2	0.279	0.649	0.630	0.780	0.598	0.459
3	0.639	0.621	0.700	0.580	0.275	*
4	0.564	0.917	0.850	0.525	0.592	0.411
5	0.588	0.748	0.657	0.641	0.446	0.516
6	0.550	0.837	0.828	0.680	0.410	0.510
7	0.551	0.840	0.769	0.759	0.559	0.644
8	0.445	0.619	0.758	0.679	0.235	0.253
9	0.549	0.706	0.537	0.260	0.253	0.262

Assuming that the methods are not subject dependent, then it is safe to assume that the derived respiration waveforms produced by the variable QRS window, dependent leads method correlate slightly better in time with the measured respiration. This is because the overall mean of the cross-correlation between the derived respiration and the measured respiration for every patient, throughout the entire experiment is higher for this method than the other three as shown in Table 3.6. To verify this qualitatively, one can

see that in Figure A.1 (a), (b), (c), (e), and (f), the variable QRS, dependent leads method does resemble the measured respiration more closely than the other methods, as mentioned in the previous section. In Figure A.1 (d), the respiration signal derived with the method based on the amplitude modulation of the R-waves corresponds better with the RESPI recording. Table 3.6 shows the average cross-correlation coefficient for each method, regardless of the different sections of the experimental protocol. Notice that there is no significant difference among the correlation coefficients of the other three methods.

Table 3.5 Average Correlation Coefficient and Standard Deviation Between the Derived Respiration and the Measured Respiration for the Four Methods, for Each Section of the Experimental Protocol

Method	Rest	Paced at 8 bpm	Paced at 12 bpm	Paced at 16 bpm	3.5 mph	3.5 mph, 5% incline
Fixed QRS Window Independent Leads	0.468 ± 0.125	0.717 ± 0.135	0.685 ± 0.132	0.608 ± 0.146	0.410 ± 0.182	0.426 ± 0.150
Amplitude Modulation of the R-Waves	0.487 ± 0.078	0.724 ± 0.120	0.714 ± 0.092	0.622 ± 0.152	0.429 ± 0.187	0.397 ± 0.143
Variable QRS Window Independent Leads	0.521 ± 0.111	0.671 ± 0.103	0.706 ± 0.114	0.587 ± 0.146	0.399 ± 0.150	0.422 ± 0.142
Variable QRS Window Dependent Leads	0.522 ± 0.105	0.756 ± 0.113	0.730 ± 0.108	0.626 ± 0.160	0.434 ± 0.149	0.433 ± 0.131

Table 3.6 Average Cross-Correlation Coefficients for Each Method

Method	Average
Fixed QRS Window Independent Leads	0.552 ± 0.145
Amplitude Modulation of the R-waves	0.562 ± 0.128
Variable QRS Window Independent Leads	0.551 ± 0.127
Variable QRS Window Dependent Leads	0.584 ± 0.128

3.5 Coherence Between the ECG Derived Respiration and the Measured Respiration

To get another quantitative measure on how well the four derived respiration waveforms compare to the measured respiration, the coherence between the four different derived respiration waveforms and the measured respiration was computed. Because coherence is a function of frequency, the coherence was recorded only at the peak of the main frequency of respiration. Table 3.7 tabulates the coherence between the measured respiration and the respiration derived by the fixed QRS window, independent leads method at the frequency of respiration. Tables 3.8, 3.9, and 3.10 display the coherence at the main frequency of respiration between the measured respiration and the respiration derived by the method based on the amplitude modulation of the R-waves, the variable window, independent leads method, and the variable window, dependent leads method, respectively.

An example of the coherence between two signals is shown in Figure 3.8. The signals used to create Figure 3.8 were a derived respiration waveform and the directly measured respiration for the protocol when the subject is pace breathing at 12 breaths per minute. Twelve breaths per minute corresponds to a frequency of 0.2 Hz. Therefore, the signals, if they are similar, will have a high coherence at 0.2 Hz. For this example the coherence at 0.2 Hz was 0.990, indicating that the signals both contained the frequency component of 0.2 Hz.

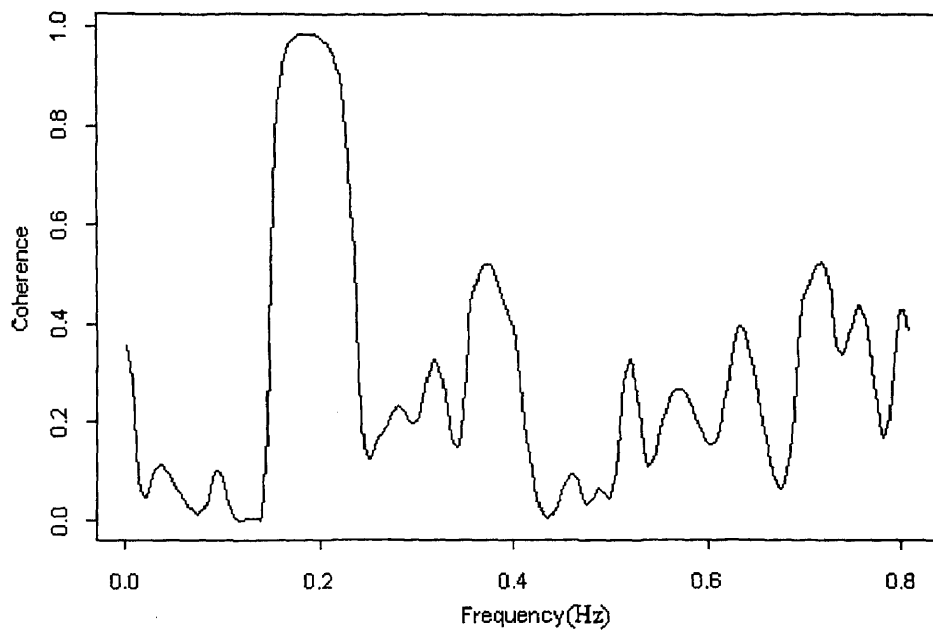


Figure 3.8 Example of Coherence Between the Measured Respiration and the ECG Derived Respiration

Table 3.7 Coherence Between the Derived Respiration and the Measured Respiration for the Fixed QRS Window, Independent Leads Method

Subject #	Rest	Paced at 8 bpm	Paced at 12 bpm	Paced at 16 bpm	3.5 mph	3.5 mph, 5% incline
1	0.769	0.930	0.914	0.917	0.343	0.556
2	0.563	0.866	0.928	0.875	0.696	0.852
3	0.747	0.955	0.954	0.860	0.631	*
4	0.699	0.990	0.981	0.799	0.505	0.499
5	0.649	0.949	0.891	0.903	0.600	0.562
6	0.534	0.983	0.952	0.855	0.392	0.745
7	0.428	0.950	0.915	0.811	0.687	0.766
8	0.392	0.899	0.874	0.963	0.426	0.647
9	0.575	0.952	0.974	0.869	0.508	0.315

Table 3.8 Coherence Between the Derived Respiration and the Measured Respiration for the Method Based on the Amplitude Modulation of the R-waves

Subject #	Rest	Paced at 8 bpm	Paced at 12 bpm	Paced at 16 bpm	3.5 mph	3.5 mph, 5% incline
1	0.639	0.952	0.936	0.963	0.418	0.444
2	0.544	0.853	0.978	0.885	0.744	0.756
3	0.822	0.932	0.863	0.753	0.623	*
4	0.664	0.989	0.987	0.801	0.504	0.493
5	0.663	0.864	0.883	0.878	0.453	0.571
6	0.553	0.915	0.896	0.945	0.243	0.727
7	0.369	0.958	0.932	0.814	0.880	0.909
8	0.351	0.906	0.898	0.938	0.636	0.506
9	0.462	0.952	0.978	0.550	0.649	0.589

Table 3.9 Coherence Between the Derived Respiration and the Measured Respiration for the Variable QRS Window, Independent Leads Method

Subject #	Rest	Paced at 8 bpm	Paced at 12 bpm	Paced at 16 bpm	3.5 mph	3.5 mph, 5% incline
1	0.771	0.930	0.946	0.944	0.342	0.504
2	0.342	0.873	0.928	0.880	0.622	0.847
3	0.785	0.914	0.954	0.850	0.662	*
4	0.698	0.991	0.982	0.818	0.711	0.505
5	0.595	0.957	0.873	0.904	0.546	0.514
6	0.527	0.988	0.927	0.884	0.282	0.626
7	0.678	0.928	0.901	0.667	0.659	0.908
8	0.382	0.904	0.860	0.955	0.362	0.401
9	0.546	0.919	0.938	0.820	0.387	0.483

Table 3.10 Coherence Between the Derived Respiration and the Measured Respiration for the Variable QRS Window, Dependent Leads Method

Subject #	Rest	Paced at 8 bpm	Paced at 12 bpm	Paced at 16 bpm	3.5 mph	3.5 mph, 5% incline
1	0.798	0.932	0.952	0.950	0.372	0.516
2	0.658	0.879	0.909	0.879	0.546	0.819
3	0.836	0.962	0.930	0.741	0.649	*
4	0.640	0.990	0.934	0.794	0.542	0.511
5	0.629	0.935	0.881	0.909	0.405	0.488
6	0.509	0.986	0.953	0.918	0.362	0.751
7	0.313	0.943	0.946	0.701	0.553	0.863
8	0.383	0.897	0.870	0.947	0.386	0.453
9	0.571	0.910	0.946	0.654	0.410	0.392

When one examines these tables and compares the coherence values between them to determine which method produces the best respiration signal in the frequency domain, it is noticed that, in general, all the coherence values are relatively high. However, there appears to be no consistency as far as one method being better than another. As expected, the derived respiration methods have a higher coherence for the sections of the protocol when the subject was pace breathing. In fact, values of coherence greater than 0.9 are very common. In order to determine which method is more accurate, the average of the coherence and standard deviation for each method were computed for each section of the experimental protocol. The results are shown in Table 3.11. In addition, box plots of the distribution of the means from subject to subject within each section of the experimental protocol, are displayed in Figure A.2 (b) in Appendix A.

From Table 3.11, it is clear that there is no one method that is consistently better than the others. In addition, the range of the coherence within the sections of the protocol is very small. For example, for the part of the protocol when the subject is pace breathing at 12 bpm, the difference between the maximum average coherence and minimum average coherence is 0.008. This can also be seen in the box plot in Figure A.2(b). In the entire table, for each section of the experimental protocol, the range of the average coherence varies from 0.008 to 0.103. In fact, the second highest range is 0.039. As expected, the coherence for the paced breathing sections of the experimental protocol are much higher than at rest or during exercise.

Table 3.11 Average Coherence at the Frequency of Respiration Between the Derived Respiration and the Measured Respiration for the Four Methods, for Each Section of the Experimental Protocol

Method	Rest	Paced at 8 bpm	Paced at 12 bpm	Paced at 16 bpm	3.5 mph	3.5 mph, 5% incline
Fixed QRS Window Independent Leads	0.595 ± 0.133	0.942 ± 0.039	0.931 ± 0.037	0.872 ± 0.051	0.532 ± 0.129	0.618 ± 0.172
Amplitude Modulation of the R-Waves	0.563 ± 0.153	0.925 ± 0.045	0.928 ± 0.046	0.836 ± 0.129	0.572 ± 0.190	0.624 ± 0.159
Variable QRS Window Independent Leads	0.592 ± 0.158	0.934 ± 0.039	0.923 ± 0.039	0.858 ± 0.086	0.508 ± 0.165	0.599 ± 0.183
Variable QRS Window Dependent Leads	0.593 ± 0.173	0.937 ± 0.038	0.925 ± 0.031	0.833 ± 0.113	0.469 ± 0.104	0.599 ± 0.182

3.6 Cross-Correlation of the Spectra

Ideally, if the derived respiration is the same as the measured respiration, unity values for the cross-correlation and coherence functions will be obtained. Although the ideal measures to satisfy the goal of deriving the respiration consistently for all experimental conditions have not been obtained, the values obtained for cross-correlation and coherence are still excellent. To stress this point, it should be mentioned that the resultant spectra from all the derived respiration methods contain the main frequency of respiration which is present in the spectrum of the measured respiration. In addition, the signal processing techniques of cross-correlation and coherence are extremely sensitive and, in reality, values of unity would be almost impossible to obtain. For example, Figure 3.7 shows a case where the ECG derived respiration and the measured respiration look very similar; however, the cross-correlation is only 0.725. Therefore, in order to indicate the similarities of the spectra between the different ECG derived respiration waveforms and

the measured waveforms, the cross-correlation of the spectra has been calculated. This will indicate how similar the shape of the spectra are to one another. The results are listed in Tables 3.12 through 3.15. Figure 3.9 illustrates an example of the cross-correlation between two spectra.

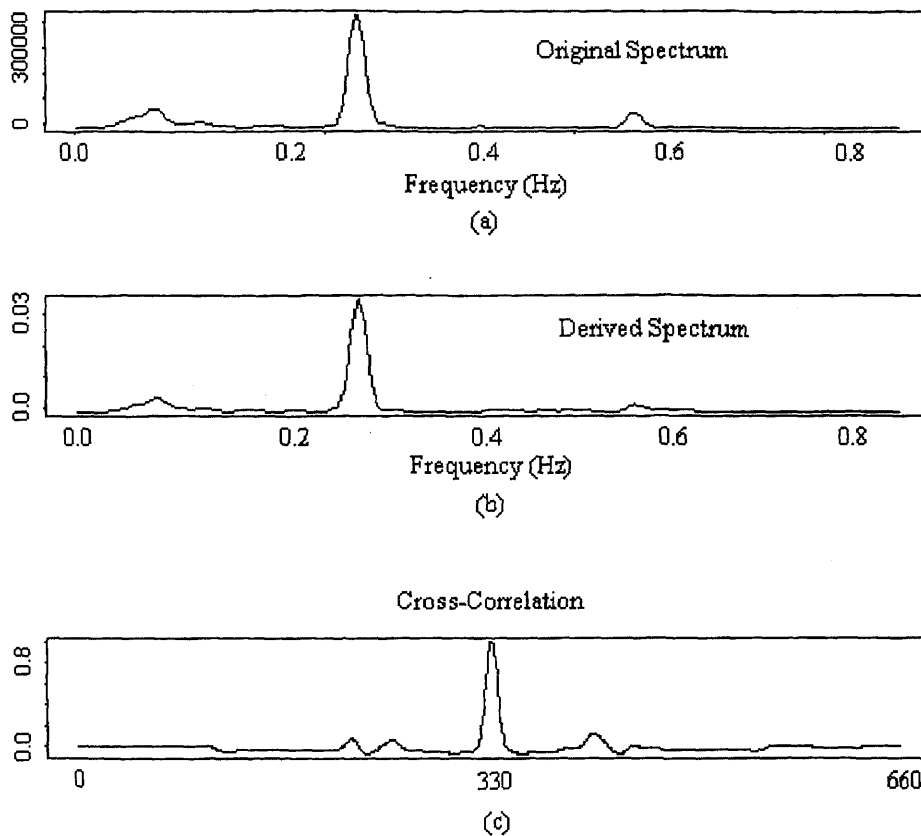


Figure 3.9 Cross-Correlation Between Two Spectra. (a) The Spectrum of the Measured Respiration. (b) The Spectrum of the ECG Derived Respiration. (c) The Cross-Correlation of the Spectrum of the Measured Respiration with the spectrum of the ECG Derived Respiration

As with the cross-correlation and coherence, when one looks at the tabulated values in Tables 3.12 to 3.15 to determine which method produces a spectrum which is

more similar to the spectrum of the RESPI, it is very hard to decipher. Therefore, Table 3.16 displays the averages and standard deviations for each section of the experimental protocol for each method. Again, it appears that the variable QRS window, dependent leads method has a slightly better correlation of the spectra than the other three methods. It should also be pointed out that the relative values of cross-correlation between the spectra are very high. This indicates that the spectrum have a very similar shape. When this point is considered, it is important to remember that the waveshape of the two signals in the cross-correlation has a profound affect on the output. Therefore, one can conclude the spectra for the derived respiration methods closely resembles the spectrum from the measured respiration. The last point of interest noticeable in Table 3.15, is that the method based on the amplitude modulation of the R-waves has the worst coherence at the frequency of respiration in 5 of the six cases.

Table 3.12 Cross-Correlation Between the Spectra of the Derived Respiration and the Measured Respiration for the Fixed QRS Window, Independent Leads Method

Subject #	Rest	Paced at 8 bpm	Paced at 12 bpm	Paced at 16 bpm	3.5 mph	3.5 mph, 5% incline
1	0.952	0.997	0.998	0.990	0.846	0.871
2	0.537	0.985	0.974	0.978	0.924	0.944
3	0.959	0.913	0.984	0.985	0.599	*
4	0.973	0.999	0.999	0.993	0.855	0.747
5	0.801	0.995	0.993	0.982	0.810	0.777
6	0.841	0.998	0.996	0.985	0.791	0.771
7	0.881	0.975	0.965	0.943	0.901	0.977
8	0.487	0.984	0.996	0.988	0.553	0.633
9	0.756	0.950	0.915	0.823	0.661	0.685

Table 3.13 Cross-Correlation Between the Spectra of the Derived Respiration and the Measured Respiration for the Method Based on the Amplitude Modulation of the R-waves

Subject #	Rest	Paced at 8 bpm	Paced at 12 bpm	Paced at 16 bpm	3.5 mph	3.5 mph, 5% incline
1	0.949	0.997	0.999	0.988	0.831	0.870
2	0.839	0.754	0.964	0.984	0.871	0.614
3	0.961	0.909	0.974	0.986	0.673	*
4	0.963	0.999	0.999	0.957	0.885	0.775
5	0.640	0.990	0.942	0.981	0.900	0.802
6	0.771	0.983	0.978	0.978	0.911	0.782
7	0.865	0.987	0.988	0.998	0.596	0.525
8	0.513	0.979	0.997	0.986	0.547	0.694
9	0.914	0.994	0.971	0.962	0.526	0.719

Table 3.14 Cross-Correlation Between the Spectra of the Derived Respiration and the Measured Respiration for the Variable QRS Window, Independent Leads Method

Subject #	Rest	Paced at 8 bpm	Paced at 12 bpm	Paced at 16 bpm	3.5 mph	3.5 mph, 5% incline
1	0.955	0.997	0.998	0.990	0.857	0.892
2	0.803	0.956	0.984	0.981	0.907	0.910
3	0.973	0.889	0.985	0.982	0.750	*
4	0.973	0.999	0.990	0.927	0.852	0.749
5	0.920	0.994	0.968	0.993	0.847	0.756
6	0.856	0.997	0.997	0.994	0.745	0.799
7	0.917	0.996	0.987	0.890	0.925	0.978
8	0.529	0.983	0.996	0.987	0.557	0.536
9	0.936	0.988	0.954	0.949	0.634	0.653

Table 3.15 Cross-Correlation Between the Spectra of the Derived Respiration and the Measured Respiration for the Variable QRS Window, Dependent Leads Method

Subject #	Rest	Paced at 8 bpm	Paced at 12 bpm	Paced at 16 bpm	3.5 mph	3.5 mph, 5% incline
1	0.952	0.997	0.997	0.986	0.846	0.877
2	0.787	0.982	0.974	0.985	0.926	0.939
3	0.973	0.896	0.974	0.988	0.699	*
4	0.973	0.999	0.999	0.898	0.859	0.744
5	0.898	0.995	0.969	0.993	0.849	0.816
6	0.857	0.997	0.997	0.991	0.641	0.760
7	0.914	0.986	0.979	0.933	0.899	0.982
8	0.491	0.979	0.997	0.988	0.552	0.602
9	0.957	0.994	0.972	0.900	0.739	0.488

Table 3.16 Average Cross-Correlation of the spectra of the Derived Respiration and the Measured Respiration for the Four Methods, for Each Section of the Experimental Protocol

Method	Rest	Paced at 8 bpm	Paced at 12 bpm	Paced at 16 bpm	3.5 mph	3.5 mph, 5% incline	overall
Fixed QRS Window Independent Leads	0.799 ± 0.179	0.977 ± 0.029	0.980 ± 0.027	0.963 ± 0.055	0.771 ± 0.184	0.801 ± 0.121	0.882 ± 0.091
Amplitude Modulation of the R-Waves	0.824 ± 0.157	0.955 ± 0.080	0.979 ± 0.019	0.980 ± 0.013	0.749 ± 0.162	0.723 ± 0.142	0.868 ± 0.090
Variable QRS Window Independent Leads	0.874 ± 0.141	0.978 ± 0.036	0.984 ± 0.015	0.966 ± 0.036	0.786 ± 0.125	0.784 ± 0.144	0.888 ± 0.083
Variable QRS Window Dependent Leads	0.867 ± 0.154	0.981 ± 0.033	0.985 ± 0.013	0.962 ± 0.040	0.779 ± 0.125	0.776 ± 0.167	0.892 ± 0.089

3.7 Comparison of the Standard Method to Compute Parasympathetic Activity to a More Theoretical Method

As mentioned in Section 1.6.3, the best defined peak in the power spectrum of heart rate variability is the high frequency peak which normally occurs between 0.15 and 0.4 Hz. The high frequency peak reflects changes in the interbeat interval, which cycles up and down at the same frequency as respiration[10]. This rhythmical fluctuation in heart periods is defined as the respiratory sinus arrhythmia and is considered purely parasympathetic in origin[11]. Therefore, to calculate parasympathetic activity, the frequency of respiration must be known.

Despite this fact, the standard way to calculate the parasympathetic activity that is universally accepted is to find the area in the HRV power spectrum under the high frequency band from 0.15 to 0.4 Hz. If this does not change, then there is really no need to be able to derive the respiration from the ECG, because the frequency of respiration is not used in the analysis. The frequencies 0.15 and 0.4 Hz correspond to 9 and 24 breaths per minute, respectively.

There are times when the frequency of respiration falls outside this range of 9 to 24 breaths per minute. For instance, at rest it is possible for people to breathe slower than 9 breaths per minute. In fact, in this experiment, the subjects were asked to breathe at 8 breaths per minute in the second portion of the protocol. In addition, two of the nine subjects breathed faster than 24 breaths per minute during exercise. Therefore, to solve this problem one might just assume to extend the range of frequencies for different parts of the protocol, and therefore, the respiration need not be recorded. However, this does not always work either because the range would have to be very large, and the direction of increased range must be known. For instance, in this study, one subject's breathing rate became very regular during exercise at approximately 0.15 Hz, which is the opposite of what is expected to happen. Normally, a person breathes faster during exercise than at rest; however, this subject was a well trained athlete and practices proper breathing techniques during exercise on a regular basis.. Despite the fact that the subject was exercising, the subject's breathing rate during exercise was slower than at rest. Therefore, the investigator can not make any assumptions on the frequency of respiration because it is unique for each subject.

Theoretically, if the respiration was recorded, the best way to calculate the parasympathetic activity would be to compute the coherence between the respiration signal and the interpolated interbeat interval. Then the area under the HRV power spectrum would be calculated for the range of frequencies whose coherence is greater than a pre-determined threshold.

Table 3.17 Values Indicating the Parasympathetic Activity Computed by the Traditional Method (top number) and by Coherence (bottom number)

Subject #	Rest	Paced at 8 bpm	Paced at 12 bpm	Paced at 16 bpm	3.5 mph	3.5 mph, 5% incline
1	42.82	123.09	45.92	34.72	20.44	1.00
	39.54	113.03	39.10	26.36	19.75	0.42
2	11.52	1112.61	78.36	28.35	52.87	7.85
	9.43	871.28	75.59	26.38	184.50	17.39
3	143.14	202.31	125.17	49.33	32.28	*
	135.30	187.16	118.15	42.29	33.58	
4	41.18	130.84	94.48	41.37	1.02*	0.77*
	38.50	108.31	82.64	37.35	0.64	0.29
5	141.46	926.10	384.43	96.67	33.93	1.59
	190.17	902.25	362.92	80.64	34.36	1.74
6	33.79	235.40	73.36	33.05	35.21	2.75
	33.81	227.52	68.31	25.81	40.66	2.65
7	150.71	644.43	233.57	21.20	61.83*	19.64*
	146.71	532.08	218.17	12.67	53.74	17.15
8	211.17	861.39	797.75	370.86	10.11	2.43
	153.27	821.40	751.01	311.30	5.19	0.45
9	87.84	269.27	85.71	97.32	3.17	0.47
	86.08	254.30	99.07	79.93	3.43	0.29

* frequency range of 0.15 to 0.6 Hz

For this study, the standard method of computing the parasympathetic activity was compared to the more theoretical approach. To do this, the coherence between the interpolated interbeat interval and the respiration recorded using the RESPI was computed using segments that were 700 points long, with 350 points of overlap. The frequencies corresponding to parasympathetic activity were found from the coherence plot above a threshold level of 0.35. The threshold of 0.35 was chosen because during rest and exercise, the coherence between the respiration signal and the interpolated interbeat interval becomes smaller. With a threshold of 0.35, the coherence between the respiration and the interpolated interbeat interval results in a frequency band which appears to contain

the frequency of respiration consistently. Obviously for paced breathing a much higher threshold could have been used; however, the threshold was kept consistent for all sections of the experimental protocol. Table 3.17 lists the power of the HRV spectrum representing the parasympathetic activity calculated by the traditional method and the theoretical method. For the section of the experimental protocol where the subject was pace breathing at 8 bpm, the high frequency area was calculated between 0.1 and 0.4 Hz. During exercise, two subjects breathed faster than 24 breaths per minute; they are noted with an asterisk indicating the frequency range for which the high frequency area was calculated.

Upon examining Table 3.17, there appears to be no significant difference between calculating the parasympathetic activity by either method. In some cases for the theoretical method, the bandwidth of the high frequency peak was extremely small; however, the difference in parasympathetic activity was negligible. For example, the high frequency peak in the HRV power spectrum and the spectrum of respiration had a coherence above 0.35 for the frequencies between 0.112 to 0.169 Hz (as opposed to 0.15 to 0.4 Hz) for subject #6 pace breathing at 8 bpm. The difference in the parasympathetic activity calculated by the two methods changed from 235.40 to 227.52.

However, upon further examination of the table, one point of interest becomes apparent. This point involves the values that are in bold italics. Note that in all these cases, the coherent method of computing the parasympathetic activity gives a greater value than the traditional method. In other words, when the breathing rate is paced, there is only one case out of 27 that the vagal tone is higher for the coherent method. In

conclusion, the parasympathetic activity does not necessarily need a frequency of respiration to be computed properly when the subject is paced breathing because of two reasons. One reason is because the frequency of respiration is known and the other reason is because the band of respiration is relatively small and contains the majority of the power representing vagal tone. However, during the rest and exercise sections of the experimental protocol, there were more cases in which the coherent method indicated more parasympathetic activity than the traditional method. Because these sections of the protocol might not have high parasympathetic activity to begin with, it makes no sense to disregard any of it. Therefore, the application of the coherent method is more critical to the rest and the exercise sections of the protocol than it is to the paced breathing sections.

CHAPTER 4

DISCUSSION AND CONCLUSIONS

The purpose of this chapter is to explain the progress of research in extracting the respiration waveform from the electrocardiogram. The actual results were presented in Chapter 3. The following is the summary of the meaning of these results. In addition, suggestions are given for the next steps that should be done in order to advance the research.

4.1 General Summary of the Work in This Thesis

As mentioned in Section 1.7.2, there has been previous research done to derive the respiration waveform from the ECG. In the previous methods, a quality respiration waveform could not be derived on a consistent basis. Therefore, the goal of this thesis was to attempt to extract the respiration from the ECG on a consistent basis. This would require determining the optimum signal processing algorithm for such a task. Therefore, in this study, four different algorithms were developed and compared to determine if there was an advantage of one over the others.

More specifically, this thesis is a continuation of research previously done by Zhao[22]. The initial program written by Zhao is the basis for the programs written in this thesis. However, as explained in Section 2.6.1.2, four errors in the signal processing in his program were found. These errors were corrected, resulting in the fixed QRS window, independent leads method. Although Zhao's program was not used as a basis for

comparison in this thesis, the author maintains that the fixed QRS window, independent leads program provides superior results when compared to the original program written by Zhao. To emphasize the point, all four methods developed in this thesis derive the respiration from two leads by estimating the angle of the mean cardiac vector. When using the program written by Zhao, it is usually only possible to derive the respiration from one lead of ECG, rather than two. In addition, the power spectra of respiration during exercise for three of the four methods developed for this study contain a more dominant frequency peak than the spectra derived by Zhao's program. An example is shown in Figure 4.1

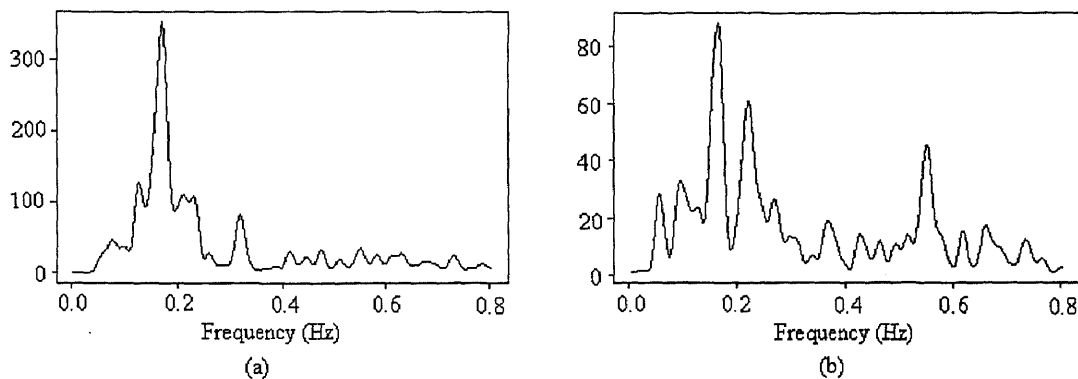


Figure 4.1 Comparison of the Spectra for the Respiration Derived from the (a) Fixed QRS Window, Independent Leads Method to the (b) Respiration Derived Using Zhao's Program.

In addition to the software development, the data acquisition procedure was also improved. To reduce the quantization error during playback of the Holter cassette, a two channel amplifier was designed and utilized during this study. Also, the optimum sampling

frequency to accurately locate the time of occurrence of the peak of the R-waves was determined to be 500 Hz, as explained in Section 2.4.2.1.

Finally, it should be mentioned that the derived respiration waveforms were compared to the measured respiration in a more scientific manner in this thesis than in Zhao's. To compare the derived respirations to the measured respirations, Zhao used the concept of central frequency. Figure 4.2 shows how Zhao calculated the central frequency. The amplitude of the spectral peak indicating respiration was first detected. Then the frequency values corresponding to 30% of the amplitude of the spectral peak were located on each side of the peak. These frequencies are referred to as f_l and f_h . The central frequency was calculated in such a way that the area A_l under the spectral peak between the frequencies f_l and f_c was equal to the area A_h under the spectral peak between the frequencies f_c and f_h . To compare the derived respiration to the measured respiration, Zhao simply compared the central frequency of each. However, this method of central frequency is a poor measure of the similarities between two signals in both the time domain and the frequency domain. Therefore, in this study, software was developed to compare the respiration waveforms in both the time domain and the frequency domain using the techniques of cross-correlation and coherence, respectively.

4.2 Comparison of the Different Methods Developed to Derive the Respiration

As mentioned previously, the goal of this thesis was to extract the respiration from the ECG accurately and consistently. This goal was attempted by developing four different software algorithms which derived the respiration by estimating the change in the angle of

the mean cardiac electrical vector during the QRS complex. At the conclusion of this study, three of the four methods can consistently and reliably derive the respiration from the ECG.

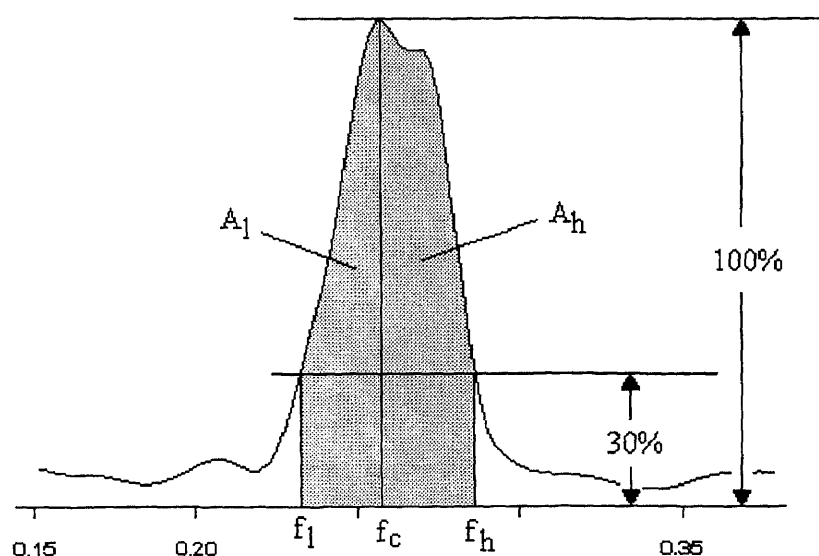


Figure 4.2 Illustration of the Central Frequency Calculation

From a qualitative standpoint, the goal was accomplished because the frequency of respiration is the dominant frequency of the derived respiration spectrum. Not only is it the dominant frequency, the majority of the time it is the only significant frequency present in the spectrum. This was true for all sections of the experimental protocol, regardless of whether the patient was resting, pace breathing, or exercising.

The quantitative basis to measure whether or not the goal was obtained relied on the cross-correlation and coherence calculations explained in Sections 3.1 and 3.2 respectively. The average values of cross-correlation for each method ranges from 0.551

to 0.584. As shown in Chapter 3, a value close to unity for cross-correlation is extremely hard to obtain and a cross-correlation above approximately 0.6 is an acceptable cross-correlation coefficient. Therefore, the author wishes to stress a few important points about the quantitative analysis of these methods. First, heavy emphasis is to be placed on the fact that in most, if not all, of the spectra of the derived respiration, the main frequency of respiration is clearly evident. In addition, not only is it evident, but it is mostly the dominant peak, if not the only peak in the power spectrum. This is because the power in the frequency band of respiration is so much greater than the power at other frequencies, that the power of the other frequencies can not be seen in the spectrum. Although this power at the other frequencies is not seen in the power spectrum, it is still present in the time signal, which therefore can cause a lower cross-correlation. In addition, one possible reason the cross-correlations were low, even during the paced breathing, is because the RESPI output usually has a waveform that contains an exponential characteristic. Most of the derived respiration waveforms do not have an exponential characteristic. Thus, the cross-correlation of two different waveshapes with the same frequency does not necessarily yield a high cross-correlation coefficient, as was shown in Section 3.1 and the example in Figure 3.6. The reason the cross-correlations are low for the exercise sections of the experimental protocol is because the RESPI recording always contains some amount of noise from the subject's body movement. Figure 4.3 shows an example of a good RESPI recording during exercise and a bad RESPI recording for exercise obtained in this thesis.

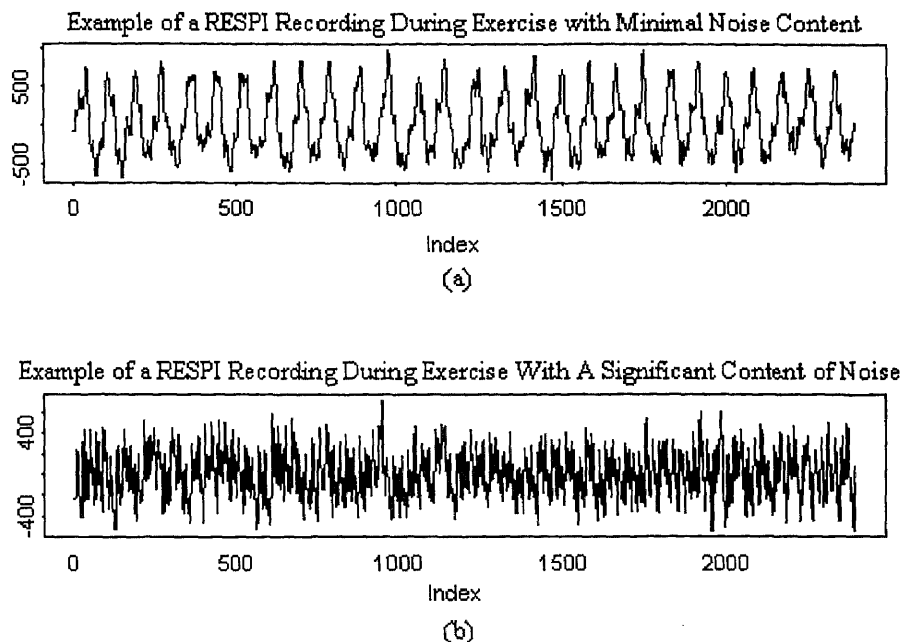


Figure 4.3 Examples of the RESPI Recording During Exercise. (a) A Good RESPI Recording for Exercise Containing Minimal Noise. (b) A RESPI Recording Containing Noise.

In addition, when the cross-correlation was calculated between the spectra for the four different methods, the smallest overall average of the correlations for the different sections of the protocol was 0.868. To the author, this is considered to be an extremely high result which expresses the merit of this thesis. This method of analyzing the analysis predicts better results because if the power spectra are dominated by the main peak of the frequency of respiration, the smaller frequencies are not apparent. From this, one can conclude that the derived respiration spectrum can predict the frequency of respiration as well as the spectrum of a RESPI recording. As an example, see Figure A.1 in Appendix A. Except for the spectra during the exercise section of the protocol representing the method based on the amplitude modulation of the R-waves, the frequency of respiration is the dominant frequency of respiration in all the spectra.

It should be noted that the best cross-correlation coefficients and coherence were measured for the sections of the experimental protocol when the subjects were paced breathing. This is because paced breathing is a controlled breathing pattern where the respiration frequency consists essentially of one frequency component. In addition, during the experiment when the subject is paced breathing, there is virtually no body movement. It is interesting to point out that the cross-correlation coefficients and coherence for the paced breathing sections of the experimental protocol decrease with increasing breathing frequency. A logical explanation of this fact might be because as the frequency of respiration increases, tidal volume decreases, thus decreasing the movement of the heart in the thoracic cavity.

It should also be pointed out that the variable QRS window, dependent leads method had a slightly higher average cross-correlation coefficient than the other methods. However, in the frequency domain, there is no distinct difference among the coherence between the methods. In addition, the variable QRS window, dependent leads method had a higher cross-correlation of its spectra with the spectra obtained with the RESPI when compared to the other methods. Therefore, based on these quantitative measures, the best method to derive the respiration from the ECG is the variable QRS window, dependent leads method.

One last point to be stressed is that the method based on the amplitude modulation of the R-waves is inconsistent and appears to be subject dependent. In some cases, this method provides better results when compared to the other methods, and in some cases

the results are worse. Therefore, it is recommended that this method should not be used to derive the respiration.

4.3 Factors Affecting the ECG Derived Respiration Results

As mentioned in Section 2.4.1, the measure of respiration by impedance pneumography is an indirect method. Similarly, estimating the change in the angle of the mean cardiac vector in the frontal plane is also an indirect measure of respiration. A direct measure of respiration would detect the rate and volume of air flow in and out of the lungs. Perhaps one reason why the cross-correlation and the coherence weren't as high as expected is because the comparison is between two indirect methods.

Despite that fact, it is also important to point out that the change in angle of the mean cardiac vector is subject dependent. In other words, the change in the angle of the mean cardiac vector might depend on the anatomic structure of the individual, the tidal volume of breathing, and the type of breathing (abdominal vs. thoracic). For instance, when the subject breathes, if most of the expansion in his lungs is towards his abdominal cavity, then perhaps the heart will not move during inspiration and expiration as much as when the subject breathes thoracically.

Another major factor affecting the outcome of this thesis, is the quality of the ECG during different sections of the experimental protocol. As mentioned before, during paced breathing there is relatively no movement of the subject, producing a clean ECG signal. However, during exercise, the ECG contains noise due to the body movement. One source of the noise is from the electrical activity of the surrounding muscles called EMG.

Also, during exercise, the skin-electrode interface produces noise from movement of the skin on the body and from the leads hanging from the electrodes.

4.4 Comparison of the Parasympathetic Activity When Calculated by the Traditional Method and With a More Theoretical Method

The results of Section 3.7, which compares the traditional method of computing the parasympathetic activity to a more theoretical approach, may at first appear to provide no difference between the two methods. This is because the results appear to indicate that if the frequency of respiration is taken into account when computing the vagal tone, that the results are very similar to the vagal tone computed for the standard frequency range of 0.15 to 0.4 Hz. However, this is only true for sections of the experimental protocol when the subject was pace breathing. During the resting sections and exercise sections of the experimental protocol when the level of parasympathetic activity might be low, the vagal tone was often more when computed by the theoretical method over the traditional method. This supports the fact that the frequency of respiration is needed during ambulatory studies to accurately determine the parasympathetic activity.

4.5 Future Work

In the future, if more methods and techniques are developed to derive the respiration from the electrocardiogram, better measures of the actual respiration waveform are needed for comparison purposes. As mentioned previously, a direct measure of respiration will measure the flow rate and volume of air entering and exiting the lungs. Such a device is

unknown to the author. In existence is an instrument called a spirometer that measures the air flow only on expiration. Therefore, other methods must be developed which produce a noise free respiration waveform under all experimental conditions.

In the future, a device consisting of a thick elastic band and a strain gauge should be developed. This device is called a band impedance meter in the literature. The theory behind its operation is that when a subject breathes, the thoracic cavity expands and contracts during inspiration and expiration respectively. The strain gauge measures the change in the circumference of the band, and outputs a voltage proportional to this change. One important point to be investigated with this method is the placement of the band. The placement of the band might be affected by whether or not the subject breathes with his abdomen, thoracic cavity, or both. Another factor which might affect the output is the affect of muscle contractions during exercise.

Another possible method to measure the actual respiration utilizes a nasal thermistor mounted in the opening in a mask that is placed over the nose and mouth. This method works by measuring the change in temperature of the air entering and leaving the mask. Typically, the air entering from outside the body during inspiration is cooler than the air exiting the body during expiration. Thus, a waveform proportional to the temperature is obtained.

In the literature, two recent articles were published which were written by the same authors discussing the topic of improving the signal-to-motion artifact ratio in an impedance pneumograph recording[30,31]. In these papers, the authors discuss using two different frequencies that are not harmonically related to obtain a noise free respiration

waveform during excessive body motion. In addition, they investigate the difference in frequencies used to obtain the respiration waveform. In one of the papers, they conclude that it is better to use higher frequencies than the ones commonly used. An additional technique they developed to improve the signal-to-motion artifact ratio was accomplished utilizing an adaptive filtering technique to the raw output of the impedance pneumograph.

Once an accurate representation of the actual respiration is obtained, several other techniques to derive the respiration from the electrocardiograph should be researched. One such technique is to examine how the mean cardiac vector moves in three-dimensional space. The methods developed in this study are based on measuring the change in angle of the mean cardiac vector in the frontal plane defined by the two orthogonal leads. However, if one more lead is acquired which is perpendicular to the two leads which define the frontal plane, it might be possible to obtain a more detailed indication of the movement of the heart within the chest. At the present time, the Holter monitor is only capable of recording two channels of ECG. If the ability of being able to acquire a third channel of ECG is developed, this method seems like the next logical step.

To better perform the analysis of the ECG, a software package that contains built in libraries of different signal processing algorithms should be utilized. It has been rather difficult to perform the signal processing techniques in S-Plus because it is a statistical analysis based software. A good program which performs signal processing is MATLAB. An example of why better software is necessary is explained by the example of how the ECG is detrended in S-Plus. The IIBI is detrended in the analysis of HRV to reduce any extremely low frequency component which might dominate the power spectrum. In S-

Plus, this is done with a locally weighted robust algorithm which has no engineering analogy. For example, what is the frequency response of this function? How does this algorithm affect the frequencies of interest in the HRV power spectrum? Instead, with a good signal processing software, the IIBI can be high pass filtered with a filter which has a known frequency response, reassuring the user that the output is properly computed. Some times, there are some extremely low frequencies present in the HRV power spectrum that technically should not exist after the detrending.

Once an adequate software package is obtained and utilized, the noise that exists in the ECG during body movement can be ascertained. If possible, filtering might be performed which could improve the results of the ECG derived respiration methods. In addition, the methods in this thesis should be reprogrammed using the proper engineering techniques. It is not at all impossible that the detrending algorithm used is the only factor separating the goal of this thesis with the ideal outcome.

To better understand the comparison of the derived respiration methods with the measured respiration, more specific experiments should be conducted than those conducted in this experiment. For example, a section of a protocol might call for a person to inhale for as long as possible, hold his breath for as long as possible, and then exhale. Another experiment might determine the affect of tidal volume on the derived respiration method. One interesting result of this study that should be investigated is how the frequency of respiration affects the derived respiration. It is proposed that the decrease in the cross-correlation and in the coherence which was accompanied by an increase in the frequency of respiration is related to the tidal volume of respiration. Therefore, specific

experiments which control and measure the subjects tidal volume should be done.

Finally, the last suggestion for future work involves the application of the frequency of respiration to the HRV power spectrum. In this study, the coherence between the interpolated interbeat interval and the respiration signal was calculated to determine the parasympathetic activity from a different viewpoint. For this part of the study, the minimum coherence value indicating similar frequency content between the signals was chosen to be 0.35. In order to obtain more accurate results, the coherence threshold should be increased. A higher coherence value was not used in this study partly due to the inexperience of the author with coherence. The coherence function is sensitive to changes in the number of point FFT, segment length, overlap, and type of window used. Therefore, these parameters can be optimized to provide a more detailed coherence function, and therefore, a more accurate investigation of coherence can be done than was done for this study.

APPENDIX A

SOME FIGURES FOR CHAPTER 3

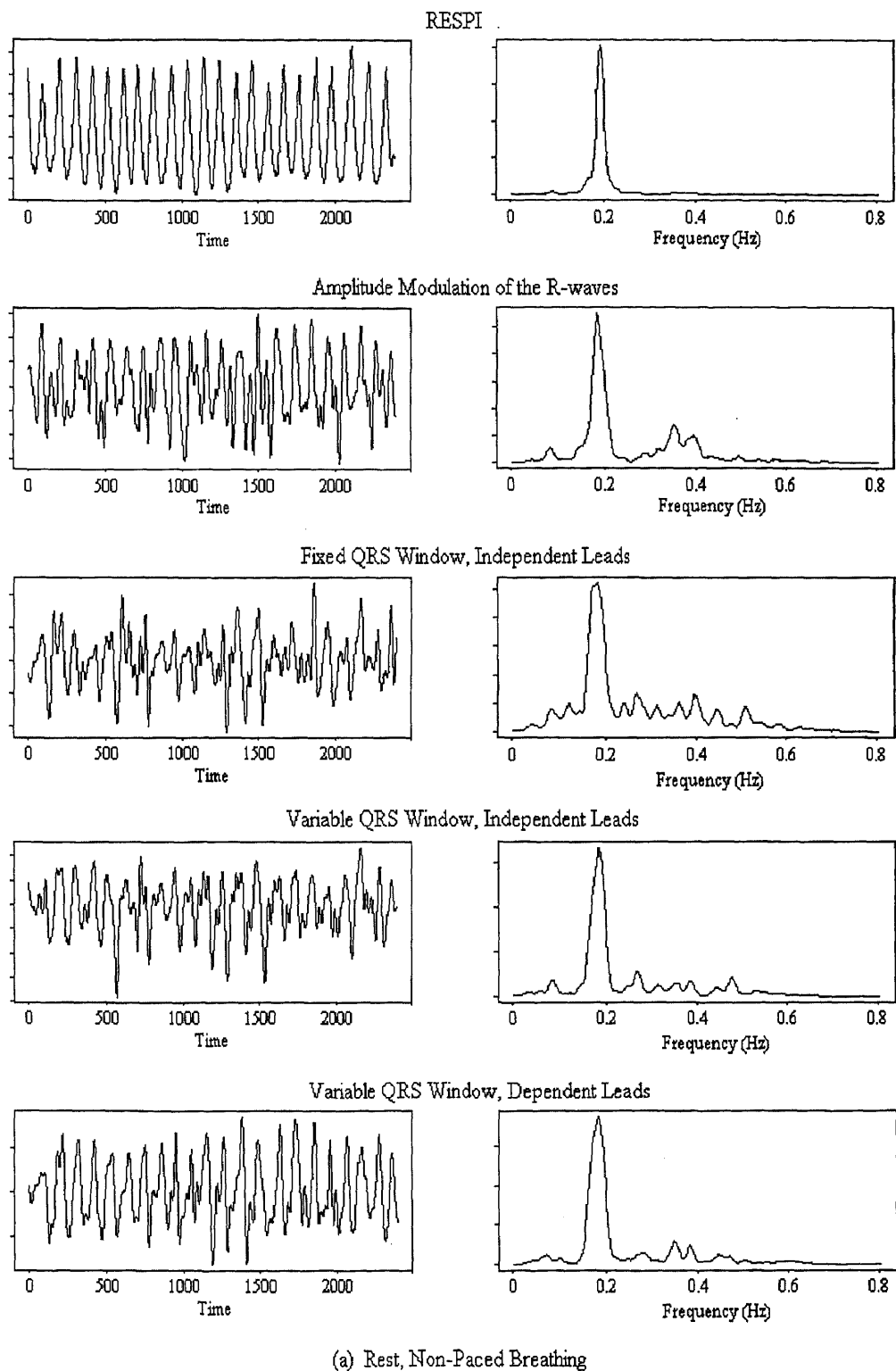
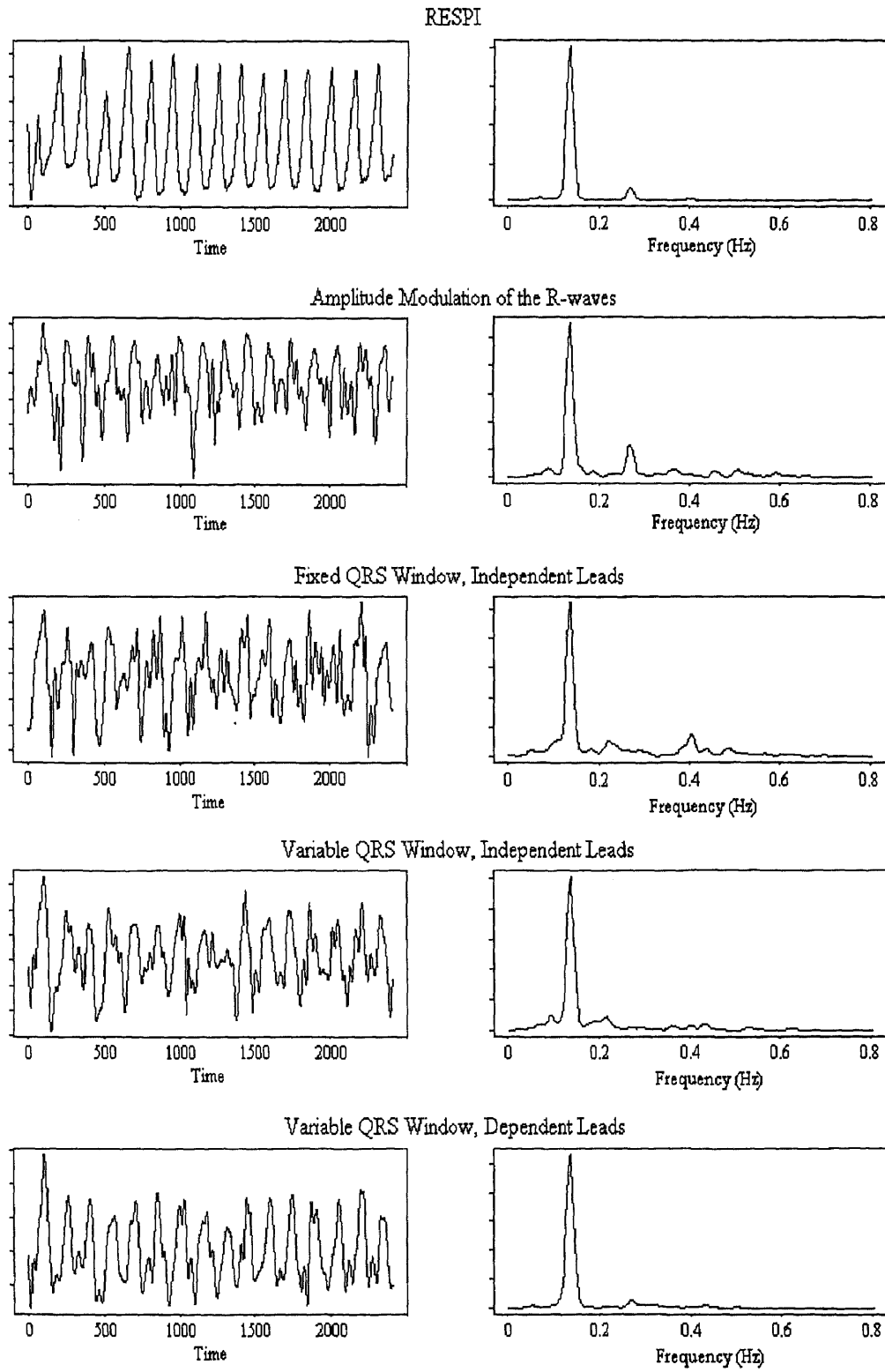


Figure A.1 Comparison of the Measured Respiration with the ECG Derived Respiration from All Four Methods For Each Section of the Experimental Protocol (continued on the next page)



(b) Paced Breathing at 8 bpm

Figure A.1 (continued on next page)

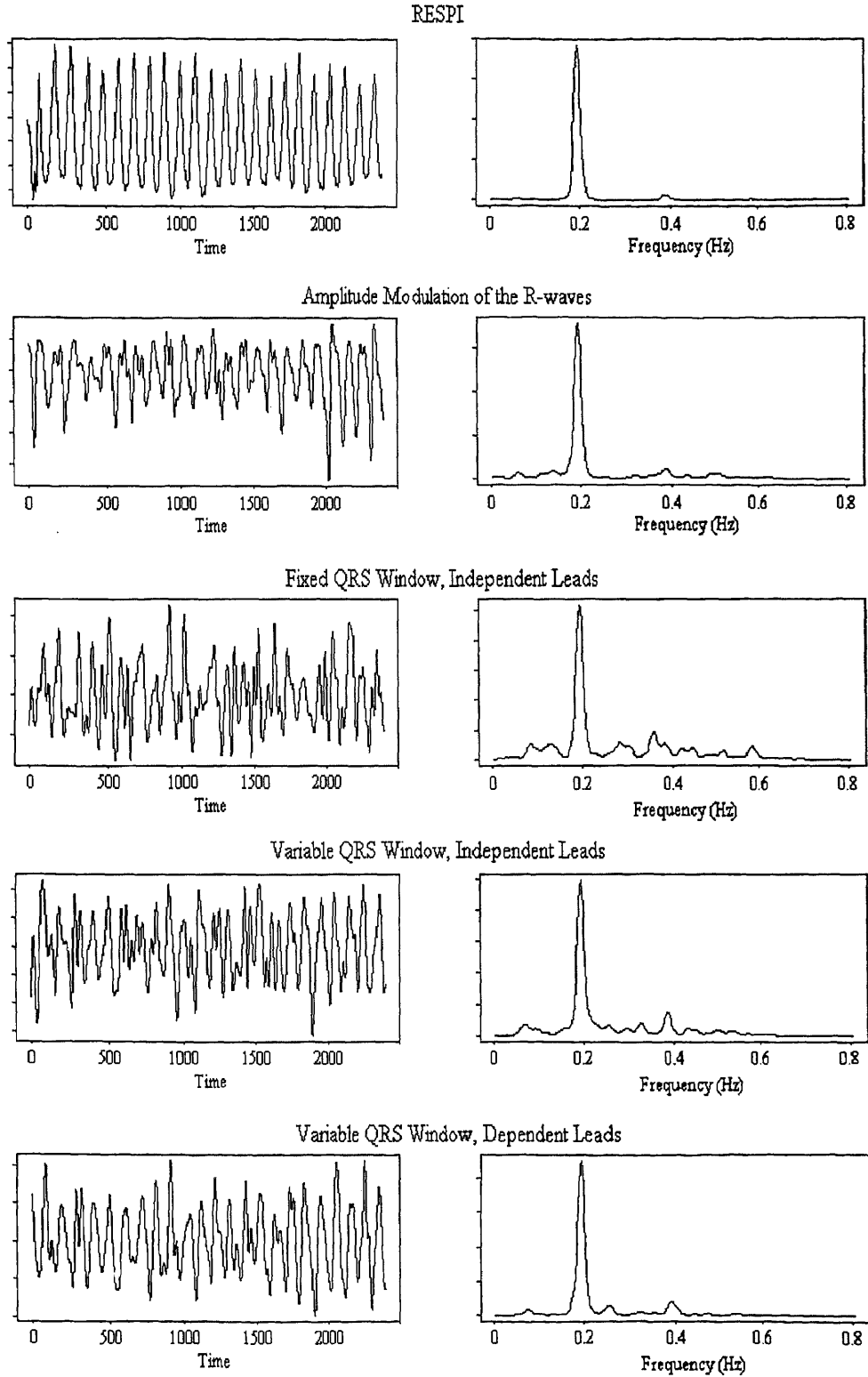
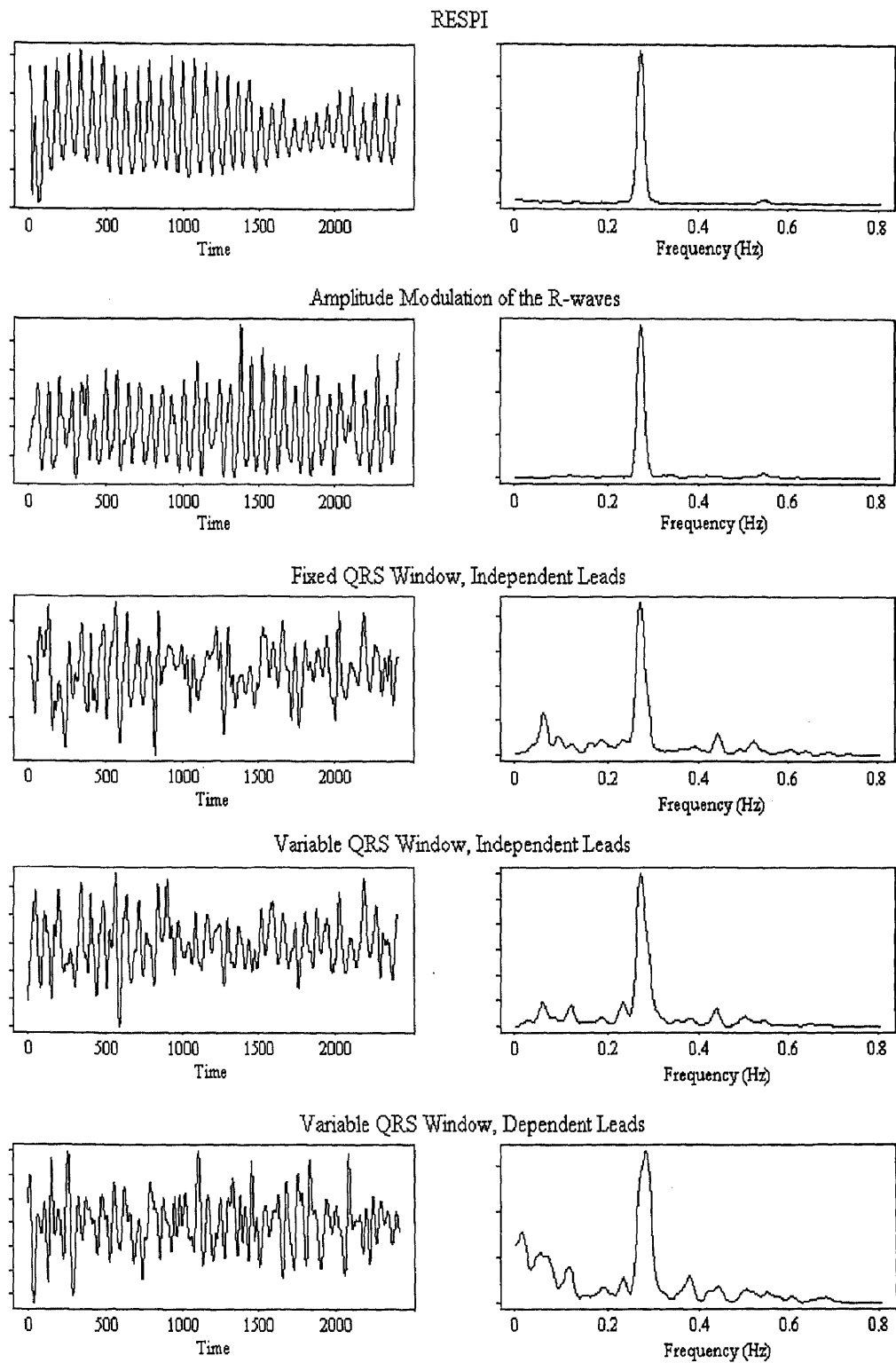
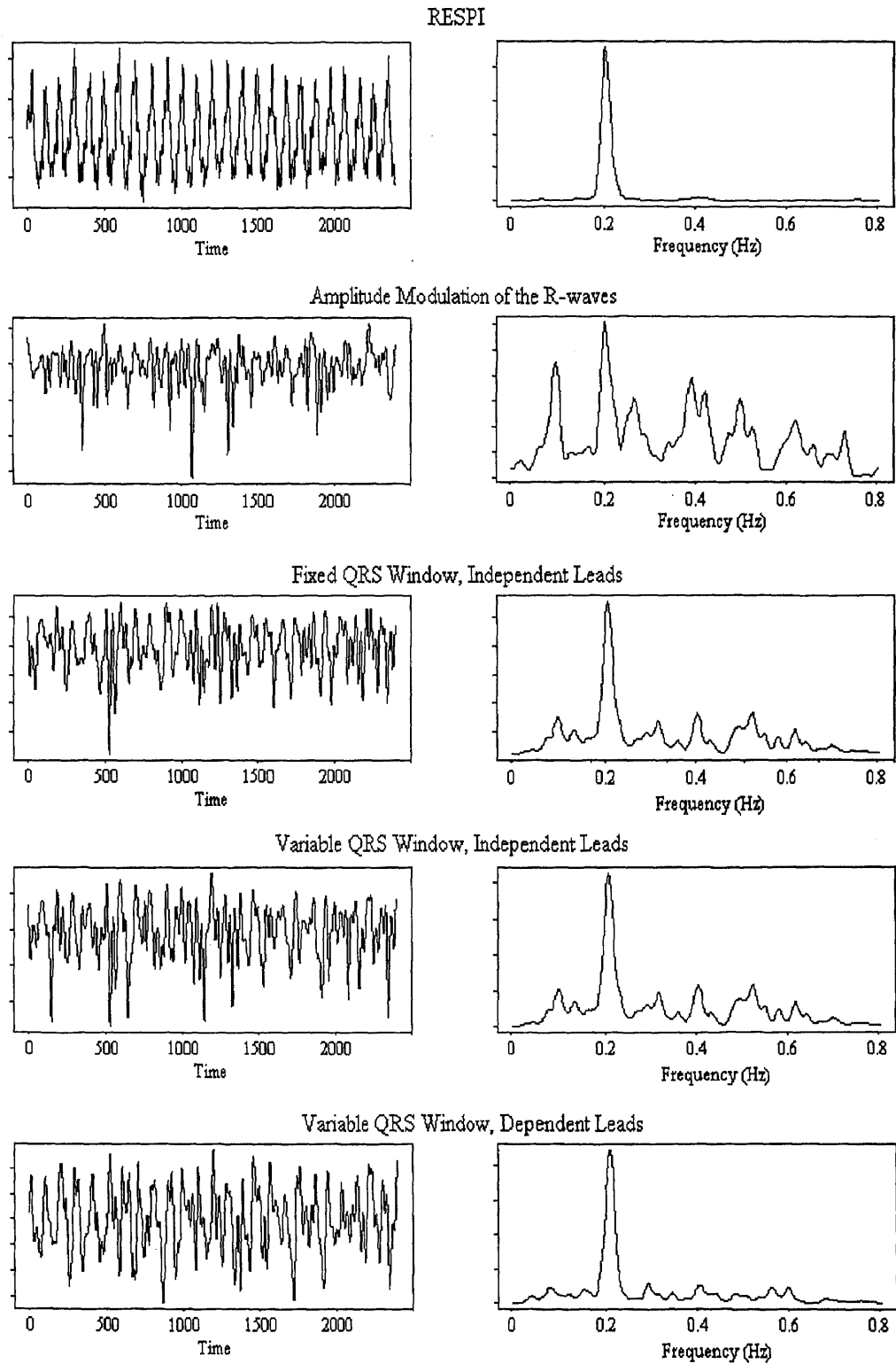


Figure A.1 (continued on next page)



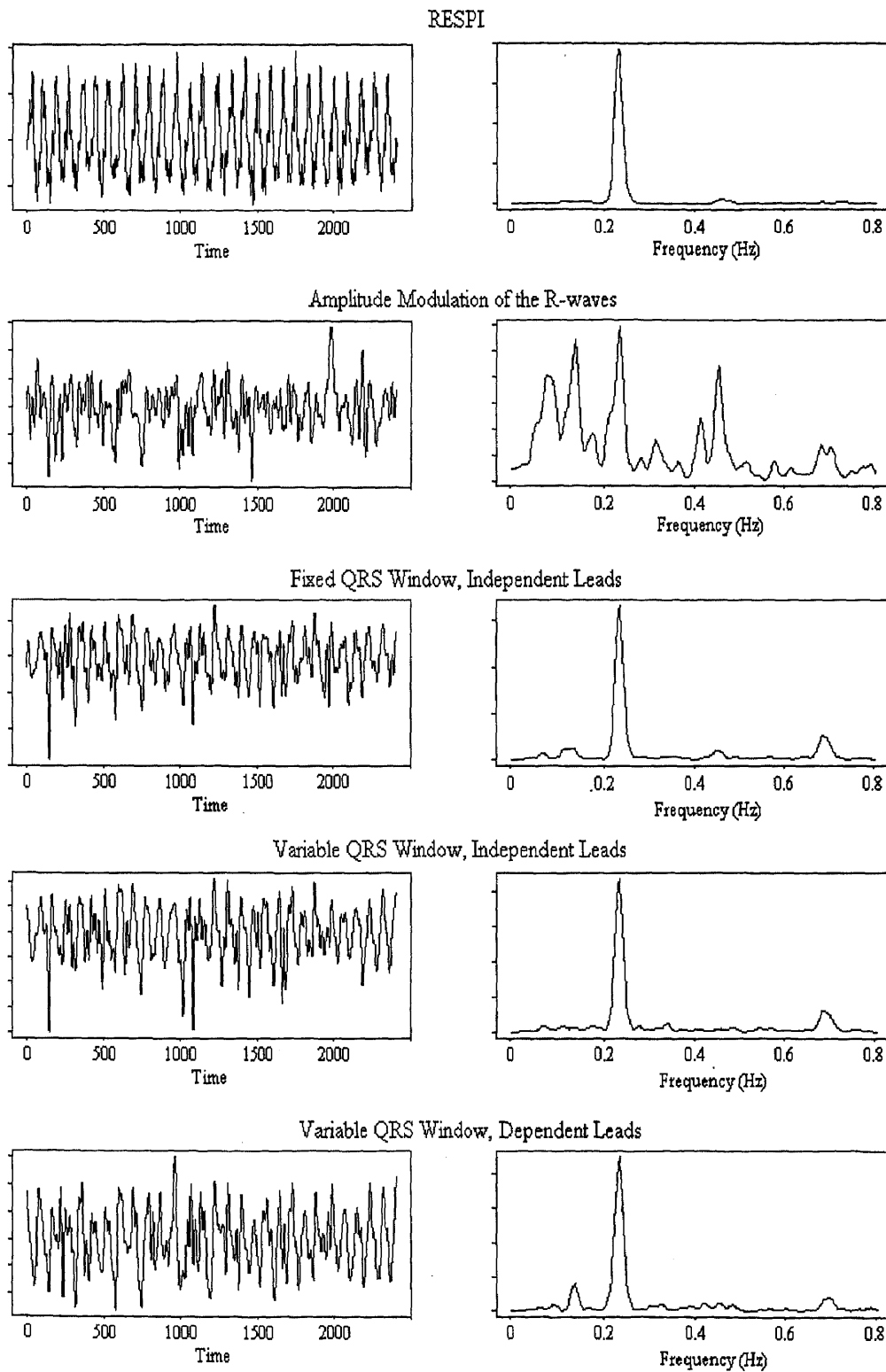
(d) Paced Breathing at 16 bpm

Figure A.1 (continued on next page)



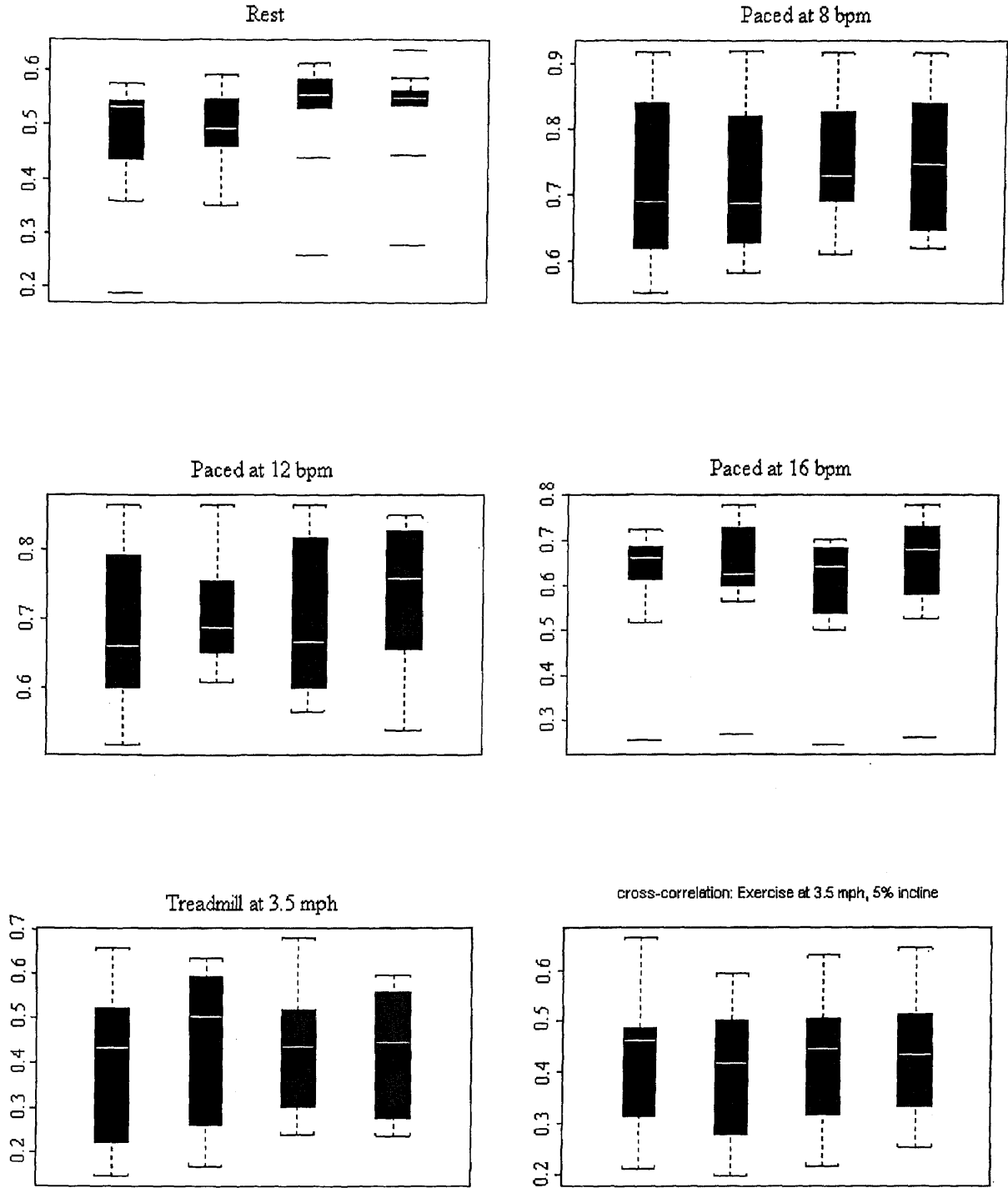
(e) Treadmill at 3.5 mph, No Incline

Figure A.1 (continued on next page)



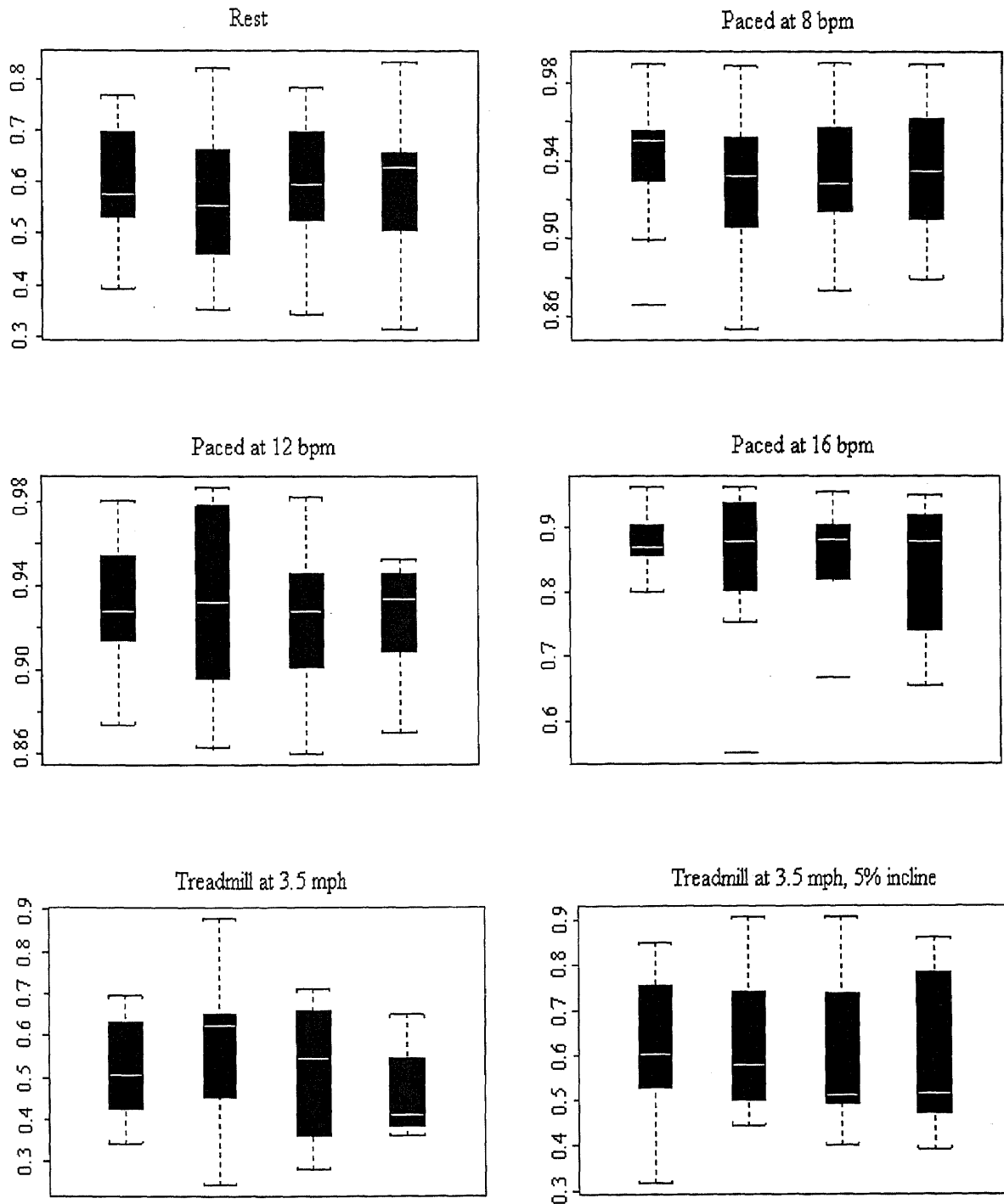
(f) Treadmill at 3.5 mph, 5% Incline

Figure A.1 (continued from previous page)



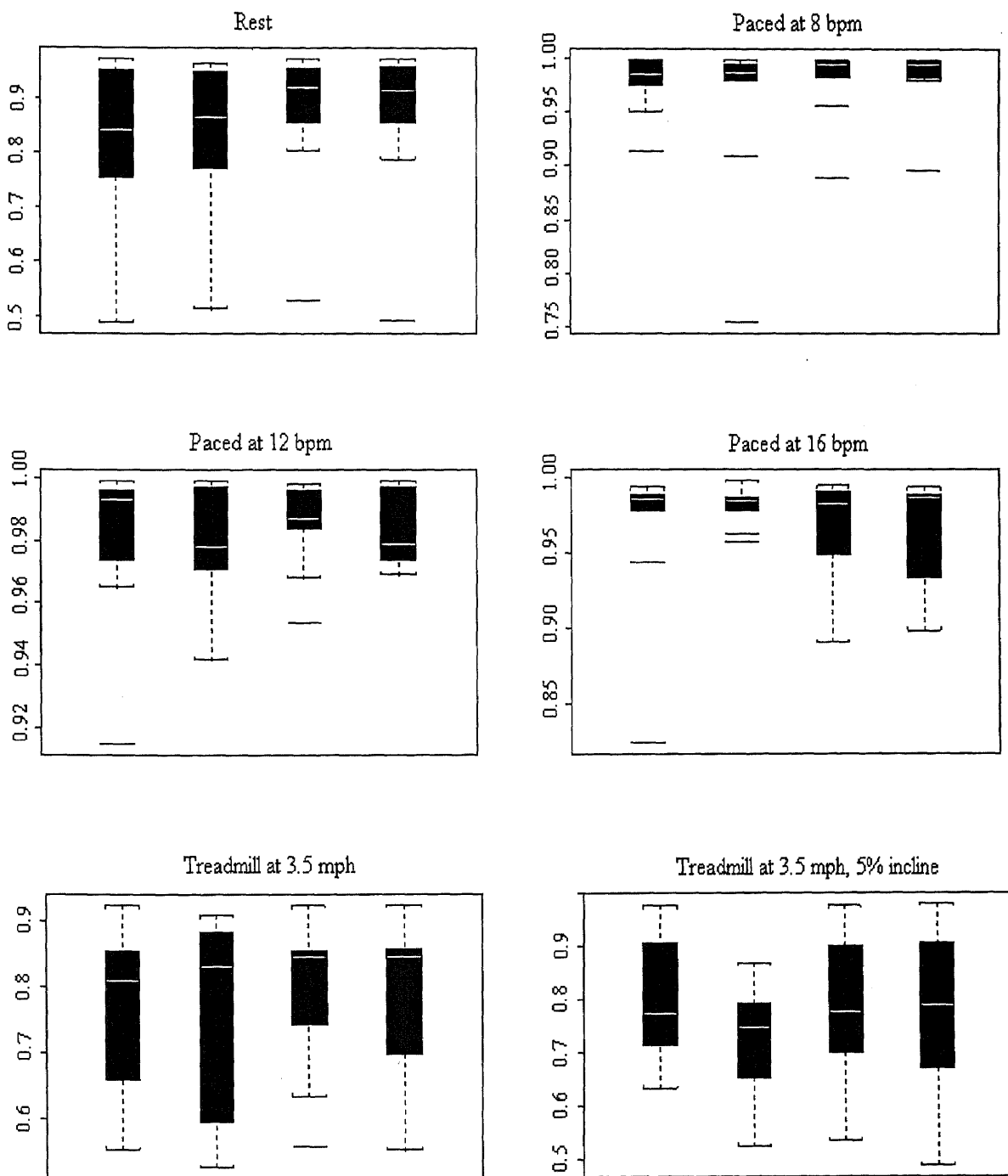
(a) Box Plots for Cross-Correlation Between Time Domain Signals

Figure A.2 Boxplots for Data in Chapter 3. In Each Plot, the Boxes, from Left to Right, Represent the Fixed QRS Window, Independent Leads Method, the Method Based on the Amplitude Modulation of the R-Waves, the Variable QRS Window, Independent Leads Method, and the Variable QRS Window, Dependent Leads Method. (continued on the next page)



(b) Box Plots for Coherence

Figure A.2 Boxplots of Data in Chapter 3. (continued)



(c) Box Plots for Cross-Correlation Between Spectra

Figure A.2 Boxplots of Data in Chapter 3.

APPENDIX B

**A COPY OF THE IRB PROPOSAL TO CONDUCT AN EXPLORATORY
STUDY INVOLVING HUMAN SUBJECTS**

KESSLER

INSTITUTE FOR REHABILITATION, INC.

Dedicated to the care of the physically disabled, Kessler is an accredited nonprofit hospital affiliated with the University of Medicine and Dentistry of New Jersey.

APPLICATION TO CONDUCT AN EXPLORATORY STUDY INVOLVING HUMAN SUBJECTS

TITLE OF PROPOSED RESEARCH: ECG Derived Respiration

INVESTIGATORS AND DEPARTMENTS:

Principal Investigator: David J. Caggiano

Mailing Address: (not relevant to thesis)

Telephone No: (not relevant to thesis)

Ext: _____

Co-Investigators: Dr. Stanley Reisman

Dept.: _____

Dept.: _____

Dept.: _____

THIS PROTOCOL IS TO BE CONSIDERED FOR (*Check only one box*):

EXPEDITED REVIEW (Indicate paragraph of Federal Guidelines to certify expedited review [see appendix B]).
Section 46.110, paragraph 3,7

FULL IRB REVIEW

PURPOSE OF DEFINITIVE STUDY:

When doing HRV studies, it is necessary to acquire a respiratory waveform to accurately determine the parasympathetic activity. During ambulatory (Holter) recording, respiration information is not acquired. Therefore, the purpose of this study is to develop a method which derives the respiration waveform from the ECG. As a result, the parasympathetic activity can be obtained for ambulatory studies.

BRIEF BACKGROUND:

In 1985 Mark and Moody proposed a method that derives the respiration from multileads of ECG. In 1994, Lingeng Zhao presented a thesis to the committee of biomedical engineering at NJIT that utilized the methods presented by Mark and Moody. The results of Lingeng's thesis showed that the method was not reliable under numerous circumstances. In addition, nobody has tried any other methods or techniques other than that proposed by Mark and Moody to extract the respiratory information from the ECG.

ROLE OF EXPLORATORY STUDY:

The role of this study is to determine the best technique to extract the respiratory waveform from the ECG. Many software methods have been developed which derive the respiration from the ECG. An experiment needs to be conducted to acquire two ECG leads and a directly measured respiratory signal. Upon analysis, each technique will be compared to determine which technique is the most accurate and consistent. In addition, it may shed some new light as to why certain methods do not work, and what can be done in the future to improve the methods in this area of research.

DESCRIPTION OF PROTOCOL:

The patients will be connected to two instruments, one which records ECG (holter monitor) and one which records the patient's respiration waveform (RESPI impedance pneumography). The ECG will be used to derive the patient's respiration waveform and then will be compared to the respiration waveform recorded with the RESPI. During the experiment, the patient will be asked to rest for 4 min, pace breath at 8,12, and 16 breaths per minute for 4 minutes each, walk on the treadmill at 3.5 mph for 4 minutes, and the last 4 min the patient will be asked to walk on the treadmill at 3.5 mph with a 5% incline. This is a one time only experiment and no follow up experiment is required by the patient. Also, there will be no medications delivered during the experiment, and no specimens will be taken.

SAFETY

There are some physical risks when walking on a treadmill that are related to the stress caused by the exercise.

Start date of exploratory study: October 27th, 1995

Estimated end date of exploratory study: November 27th, 1995

Please attach an appropriate consent form that indicates that the proposed research will be exploratory in nature and designed to assist the researcher in determining if further investigation is feasible

Approved: _____

John DeLuca, Ph.D.
Chair, IRB

_____ Date

**CODE OF FEDERAL REGULATIONS
TITLE 35: PUBLIC WELFARE
PART 46: PROTECTION OF HUMAN SUBJECTS**

APPENDIX B: EXPEDITED ACTIVITIES

§ 46.110

Research activities involving no more than minimal risk *and* in which the only involvement of human subjects will be in one or more of the following categories (carried out through standard methods) may be reviewed by the Institutional Review Board through the expedited review procedure.

(1) Collection of: hair and nail clippings in a nondisfiguring manner; deciduous teeth; and permanent teeth if patient care indicates a need for extraction.

(2) Collection of excreta and external secretions including sweat, uncannulated saliva, placenta removed at delivery, and amniotic fluid at the time of rupture of membrane prior to or during labor.

(3) Recording of data from subjects 18 years of age or older using noninvasive procedures routinely employed in clinical practice. This includes the use of physical sensors that are applied either to the surface of the body or at a distance and do not involve input of matter or significant amounts of energy into the subject or an invasion of the subject's privacy. It also includes such procedures as weighing, testing sensory acuity, electrocardiography, electroencephalography, thermography, detection of naturally occurring radioactivity, diagnostic echography, and electroretinography. It does not include exposure to electromagnetic

radiation outside the visible range (for example, x-rays, microwaves).

(4) Collection of blood samples by venipuncture, in amounts not exceeding 450 milliliters in an eight-week period and no more often than two times per week, from subjects 18 years of age or older and who are in good health and not pregnant.

(5) Collection of both supra- and subgingival dental plaque and calculus provided the procedure is not more invasive than routine prophylactic scaling of the teeth and the process is accomplished in accordance with accepted prophylactic techniques.

(6) Voice recordings made for research purposes such as investigations of speech defects.

(7) Moderate exercise by healthy volunteers.

(8) The study of existing data, documents, records, pathological specimens, or diagnostic specimens.

(9) Research on individual or group behavior or characteristics of individuals, such as studies of perception, cognition, game theory, or test development, where the investigator does not manipulate subjects' behavior and the research will not involve stress to the subjects.

(10) Research on drugs or devices for which an investigational new drug exemption or an investigational device exemption is not required.

KESSLER

INSTITUTE FOR REHABILITATION, INC.

Dedicated to the care of the physically disabled, Kessler is an accredited nonprofit hospital affiliated with the University of Medicine and Dentistry of New Jersey

APPLICATION TO UNDERTAKE A RESEARCH PROJECT INVOLVING HUMAN SUBJECTS

Part B (Informed Consent)

The informed consent form is the document that will be presented to each subject of a research activity for review and signature. It must be written in prose style and content so that it can be understood by the proposed subjects of the study. It must be attached to Part A for detailed review and approval by the IRB. If the investigator wishes to raise any issues concerning the informed consent form with the IRB (e.g., preference for obtaining oral rather than written informed consent, omission of a particular portion of the form or deviation from the usual format), this must be done in a separate communication accompanying the protocol.

A model informed consent format is attached. This should be used in preparing your informed consent form as appropriate. Each of the following points must be covered in the informed consent form:

1. It must be stated that the study involves research.
2. The purpose of the study must be clearly stated.
3. The procedure(s) that will be employed must be clearly described.
4. For each procedure to be used, particularly if it would not be used as part of the medical care of the subject, anticipated risks and the degree of likelihood of their occurrence must be stated.
5. If a drug is to be administered, particularly if it would not be administered as part of the medical care of the subject, this must be clearly stated and the nature and timing of the drug must be explained. Anticipated risks and side effects of the drug and the degree of likelihood of their occurrence must be described.
6. If a test is to be performed, particularly if it would not be performed as part of the medical care of the subject, this must be clearly stated and the nature of the test must be described. Anticipated risks of the test and the degree of likelihood of their occurrence must be described.
7. If the subject may be used as a control, this must be clearly stated and the specific benefits and risks, including the degree of likelihood of their occurrence must be described.
8. A statement must be included as to whether participation of the subject in the research activity may or may not provide specific benefits to that subject; if benefits are anticipated, their nature and degree of likelihood of occurrence must be stated.

9. A statement must be included that a subject may choose not to participate in the proposed study or may withdraw from the study at any time upon notification to the investigator, without any penalty, change in available medical care, or other loss of benefits to which the subject is otherwise entitled.
10. A statement must be included describing measures which will be taken to protect the confidentiality of the results of the study and the subjects' right to privacy.
11. A statement must be included listing any special signs or symptoms during the course of the study to which the subject has been or is to be alerted.

§ 46.116

General Requirements for Informed Consent

Except as provided elsewhere in this or other subparts, no investigator may involve a human being as a subject in research covered by these regulations unless the investigator has obtained the legally effective informed consent of the subject or the subject's legally authorized representative. An investigator shall seek such consent only under circumstances that provide the prospective subject or the representative sufficient opportunity to consider whether or not to participate and that minimize the possibility of coercion or undue influence. The information that is given to the subject or the representative shall be in language understandable to the subject or the representative. No informed consent, whether oral or written, may include any exculpatory language through which the subject or the representative is made to waive or appear to waive any of the subject's legal rights, or releases or appears to release the investigator, the sponsor, the institution or its agents from liability for negligence.

(a) **Basic elements of informed consent.** Except as provided in paragraph (c) or (d) of this section, in seeking informed consent the following information shall be provided to each subject:

(1) A statement that the study involves research, an

explanation of the purposes of the research and the expected duration of the subject's participation, a description of the procedures to be followed, and identification of any procedures which are experimental;

(2) A description of any reasonably foreseeable risks or discomforts to the subject;

(3) A description of any benefits to the subject or to others which may reasonably be expected from the research;

(4) A disclosure of appropriate alternative procedures or courses of treatment, if any, that might be advantageous to the subject;

(5) A statement describing the extent, if any, to which confidentiality of records identifying the subject will be maintained;

(6) For research involving more than minimal risk, an explanation as to whether any compensation and an explanation as to whether any medical treatments are available if injury occurs and, if so, what they consist of, or where further information may be obtained;

(7) An explanation of whom to contact for answers to pertinent questions about the research and research subject's rights, and whom to contact in the event of a research-related injury to the subject; and

(8) A statement that participation is voluntary, refusal to participate will involve no penalty or loss of benefits to which the subject is otherwise

entitled; and the subject may discontinue participation at any time without penalty or loss of benefits to which the subject is otherwise entitled.

(b) **Additional elements of informed consent.** When appropriate, one or more of the following elements of information shall also be provided to each subject:

(1) A statement that the particular treatment or procedure may involve risks to the subject (or to the embryo or fetus, if the subject is or may become pregnant) which are currently unforeseeable;

(2) Anticipated circumstances under which the subject's participation may be terminated by the investigator without regard to the subject's consent;

(3) Any additional costs to the subject that may result from participation in the research;

(4) The consequences of a subject's decision to withdraw from the research and procedures for orderly termination of participation by the subject;

(5) A statement that significant new findings developed during the course of the research which may relate to the subject's willingness to continue participation will be provided to the subject; and

(6) The approximate number of subjects involved in the study.

(c) An IRB may approve a consent procedure which does

not include, or which alters, some or all of the elements of informed consent set forth above, or waive the requirement to obtain informed consent provided the IRB finds and documents that:

(1) the research or demonstration project is to be conducted by or subject to the approval of state or local government officials and is designed to study, evaluate, or otherwise examine: (i) public benefit or service programs; (ii) procedures for obtaining benefits or services under those programs; (iii) possible changes in or alternatives to those programs or procedures; or (iv) possible changes in methods or levels of payment for benefits or services under those programs; and

(2) the research could not practicably be carried out without the waiver or alteration.

(d) An IRB may approve a consent procedure which does not include, or which alters, some or all of the elements of informed consent set forth in this section, or waive the requirements to obtain informed consent provided the IRB finds and documents that:

(1) the research involves no more than minimal risk to the subjects;
 (2) the waiver or alteration will not adversely affect the rights and welfare of the subjects;
 (3) the research could not practicably be carried out without the waiver or alteration; and
 (4) whenever appropriate, the subjects will be provided with

additional pertinent information after participation.

(e) The informed consent requirements in this policy are not intended to preempt any applicable Federal, State, or local laws which require additional information to be disclosed in order for informed consent to be legally effective

(f) Nothing in this policy is intended to limit the authority of a physician to provide emergency medical care, to the extent the physician is permitted to do so under applicable Federal, State, or local law. (Approved by the Office of Management and Budget under Control Number 9999-0020.)

§ 46.117

Documentation of Informed Consent

(a) Except as provided in paragraph (c) of this section, informed consent shall be documented by the use of a written consent form approved by the IRB and signed by the subject or the subject's legally authorized representative. A copy shall be given to the person signing the form.

(b) Except as provided in paragraph (c) of this section, the consent form may be either of the following:

(1) A written consent document that embodies the elements of informed consent required by Paragraph 46.116. This form may be read to the subject or the subject's legally authorized representative, but in any event, the investigator shall give either the subject or the representative adequate opportunity to read it before it is signed; or

(2) A short form written consent document stating that the elements of informed consent required by Paragraph 46.116 have been presented orally to the subject or the subject's legally authorized representative. When this method is used, there shall be a witness to the oral presentation. Also, the IRB shall approve a written summary of what is to be said to the subject or the representative. Only the short form itself is to be signed by the subject or the representative. However, the witness shall sign both the short form and a copy of the summary. A copy of the summary shall be given to the subject or the representative, in addition to a copy of the short form.

(c) The IRB may waive the requirement for the investigator to obtain a signed consent form for some or all subjects if it finds either:

(1) That the only record linking the subject and the research would be the consent document and the principal risk would be potential harm resulting from a breach of confidentiality. Each subject will be asked whether the subject wants documentation linking the subject with the research, and the subject's wishes will govern; or

(2) That the research presents no more than minimal risk of harm to subjects and involves no procedures for which written consent is normally required outside of the research context.

In cases in which the documentation requirement is waived, the IRB may require the investigator to provide subjects with a written statement regarding the research.

(Approved by the Office of Management and Budget under Control Number 9999-0020.)

KESSLER

INSTITUTE FOR REHABILITATION, INC.

Dedicated to the care of the physically disabled, Kessler is an accredited nonprofit hospital affiliated with the University of Medicine and Dentistry of New Jersey

CONSENT TO PARTICIPATE IN A RESEARCH STUDY

TITLE OF STUDY:

ECG Derived Respiration

RESEARCH STUDY:

I, _____, have been asked to participate in a research study under the direction of Dr Stanley Reisman and David Caggiano. Other professional persons who work with them as study staff may assist or act for them. All research projects carried out in this hospital are covered by the rules of both the Federal Government and Kessler Institute.

PURPOSE:

By participating in this research experiment, I will be contributing information that can be used to help devise the best method to determine a person's breathing rate from the electrocardiogram (ECG). It is important to be able to derive the breathing rate from the ECG since it is a key factor in accurately determining the relationship between a person's central nervous system and their variation in their heart rate.

DURATION:

My participation in this study will last for about 1 hour.

PROCEDURES:

I have been told that, during the course of this study, the following will occur:

I will be connected to two instruments, one which records my ECG and one which records my respiration (breathing). The ECG will be used to derive my respiration waveform which will then be compared to the respiration waveform recorded with the second instrument. During the experiment, I will be asked to rest for 4 min and then breathe at the rates of 8, 12, and 16 breaths per minute for 4 minutes each. I will then walk on the treadmill at 3.5 mph for 4 minutes, and 3.5 mph at 5% incline for another 4 minutes. I understand that this is a one time only experiment and that no follow up is required. Also, there will be no medications delivered during the experiment, and no specimens will be taken.

SUBJECTS:

I will be one of about 10 subjects to participate in this trial.

Subjects will be older than 18 yrs of age and younger than 40 yrs. Subjects may be of either sex. The subject's heritage, ethnicity, and background does not matter. The subjects should be able to read and understand the English language. Subjects excluded from the study include pregnant women and anyone with breathing disorders.

EXCLUSIONS:

I will inform the researcher if any of the following apply to me:

- (a) If I am pregnant
- (b) If I suffer from any breathing disorders.
- (c) If I am younger than 18 yrs old or older than 40 yrs old.

RISKS/DISCOMFORTS:

I have been told that the study described above may involve the following risks and/or discomforts:

I may become faint or dizzy when exercising on the treadmill. In the unlikely event that this should happen, the treadmill will be stopped immediately and I will be allowed to rest and be closely monitored until I am feeling better.

There also may be risks and discomforts that are not yet known.

BENEFITS:

I have been told that I will receive no direct benefit from my participation in this study, but it may help the researchers to better understand how to determine a person's breathing pattern from an ECG. As a result, future studies can be done that will accurately measure the activity of a patient's nervous system as it controls heart rate and breathing.

ALTERNATIVES:

The following alternative procedures or treatments are available if I choose not to participate in this study:

There are no alternatives.

NEW FINDINGS:

During the course of the study, I will be told about any new information that may affect my willingness to remain in the study.

CONFIDENTIALITY:

Every effort will be made to maintain the confidentiality of my study records. Officials of the Kessler Institute for Rehabilitation will be allowed to inspect sections of my medical and research records related to this study. If the findings from the study are published, I will not be identified by name. My identity will remain confidential unless disclosure is required by law.

FINANCIAL COSTS TO THE SUBJECTS:

I understand that my participation in this study may incur the following (increased/decreased) costs to me. Some of these costs may be covered by my health insurance provider.

I understand there will be no additional cost to me for my participation in this study.

PAYMENT FOR PARTICIPATION:

I have been told that I will receive no money for my participation in this study.

MEDICAL THERAPY FOR INJURY:

Medical therapy will be arranged for me by Kessler Institute for Rehabilitation for any physical injuries sustained as a direct consequence of my participation in this research. My health insurance carrier or other third party payer will be billed for the cost of this medical therapy. All claims should be made to the researcher who will arrange for review in accordance with Kessler Institute for Rehabilitation policy. No other compensation is available.

RIGHT TO REFUSE OR WITHDRAW:

I understand that my participation is voluntary and I may refuse to participate, or may discontinue my participation at any time, without penalty or loss of benefits to which I am otherwise entitled. I also understand that the investigator has the right to withdraw me from the study at any time.

INDIVIDUAL(S) TO CONTACT:

If I have any questions about my treatment or the research procedures, I can contact:

Dr. Stanley Reisman (201)-731-3600 Kessler Inst. for Rehab. West Orange

If I have concerns only regarding my rights as a research subject, I may contact Judy Macêdo, the administrator of the Institutional Review Board, at 800-248-3221, extension 6073.

I will receive a copy of this consent form if I agree to participate in this research study.

_____ Subject's Initials

SIGNATURE OF SUBJECT

I have read this entire form, or it has been read to me, and I understand it completely. All of my questions regarding this form or this study have been answered to my complete satisfaction. I agree to participate in this research study.

Subject: Name: _____ Signature: _____

Date: _____

SIGNATURE OF INVESTIGATOR OR RESPONSIBLE INDIVIDUAL

To the best of my knowledge, the subject, _____, (or his /her parent/legal guardian) has understood the entire content of the above consent form, and comprehends the study and its risks well. The subject's questions and those of his/her parent/legal guardian have been accurately answered to his/her/their complete satisfaction.

Investigator's Name: _____ Signature: _____

Date: _____

SIGNATURE OF WITNESS

I further attest that I was present as a witness throughout the above mentioned oral presentation, including the answering of any and all questions raised by the subject (or his/her parent/legal guardian).

Witness Name: _____ Signature: _____

Date: _____

APPENDIX C

PROCEDURE FOR A/D CONVERSION OF A HOLTER CASSETTE

- 1: Two stereo systems are needed to perform the analog to digital conversion. One stereo system is the JVC TD-W10 consumer cassette player, which does not have speakers. The type of the other system does not matter, but it must have speakers. Also needed is a two channel amplifier.
- 2: Connect the left channel output of the JVC TD-W10 to channel one of the amplifier and the right channel output of the JVC TD-W10 to channel two of the amplifier. Then connect the outputs of channel 1 and 2 of the amplifier to the cable adapter's channel 1 and 2 for the A/D acquisition board. Make sure the power to the amplifier is on.
- 3: Connect a two channel oscilloscope to each of the channels to monitor the ECGs during playback.
- 4: Playback the holter cassette on the stereo with speakers to verify the correct number of event markers for the experimental protocol.
- 5: For each section of the experimental protocol, a data file needs to be created. To do this, type the following command at the DOS prompt on the acquisition computer:

c:\mkfile l120795a.dat 240 [enter]

where:

l - represents the first letter of the patient's last name

120795 - represents the date of the experiment (e.g. December 7th, 1995)

a - represents the letter corresponding to each section of the protocol

240 - represents the file size in Kilobytes

to calculate the file size, use the following formula:

$$\text{file size} = 2 * T * C * f_s$$

where:

2 - necessary because the DAS16 uses two bytes per sample

T - the time of the experiment in seconds

C - the number of channels being collected

f_s - the sampling frequency (samples/second/channel)

Remember that the holter playback is 48.35 times faster than which it was recorded. Therefore, either multiply the original sampling frequency by 48.35 or divide T by 48.35 to get the correct playback time in seconds.

6. To check the connections between the JVC TD-W10 and the data acquisition board do the following to check the signal on the screen:
c:\plot [enter] [enter]
set "channel to monitor:" equal to 1
[f4] to centralize the data
play holter tape on JVC TD-W10, check for signal, stop tape
[f5] to change channels
set "channel to monitor" equal to 2
[f4] to centralize the data
play holter tape on JVC TD-W10, check for signal, stop tape
note: sometimes when performing this step, the primplot signal on the screen does not move. If this is the case, the ECG signal might have a small amplitude. Therefore, increase the amplification with the amplifier.
7. Setup the acquisition software using the following command:
c:\streamer das16
 set the following parameters:
 Drive c:
 Data File\1120795a.dat (change this line each time before step 8)
 Log file
 Sample rate = sampling frequency per channel * # of channels*48.35
 set first channel equal to 1
 set last channel equal to 2
 put cursor on Drive c:
8. Position the holter cassette at the proper event marker by listening to the holter cassette using the stereo with speakers. As soon as you hear the proper event marker, stop the tape! Using your finger, rewind the tape by about one half of a turn. Now, put the tape in the JVC TD-W10's B cassette deck. Press play. Adjust the gain on the amplifier so as to get a signal that is as close to 5 volts for the entire test section, but be sure that it never exceeds five volts. Stop the tape and find the proper marker again using the procedure mentioned above and the stereo with speakers. Using your finger, rewind the tape by about one half of a turn. Now, put the tape in the JVC TD-W10's B cassette deck. Press play. As soon as the signal appears on the oscilloscope, press [f1] to acquire the data. Repeat steps 7 and 8 for each section of the experiment, giving the data file a different name for each section.

- 9: To transfer the data over the network from the data acquisition computer to the data analysis computers, type the following at the DOS prompt:

```
c:\transfer
```

```
s:
```

```
cd users\davidc
```

```
c:
```

```
cd..
```

```
copy all data files to s:
```

APPENDIX D

ANALYSIS PROCEDURES TO OBTAIN POWER SPECTRUM OF HRV

In the following example, we are going to use a sample data file “filename.dat” to explain the syntax of the programs used to calculate the HRV power spectrum. Let’s assume the file contains two channels of ECG data, two minutes long, and sampled at 500 Hz.

- 1 Begin the analysis by unpacking the data file in DOS. This converts each sample of data from binary format to ASCII format separated by commas.

```
unpack filename.dat,filename.asc,0-119999/b/das16
```

- 2 Attach to the user directory where the filename.asc file is stored. The rest of the commands from here on are performed in S-Plus.

```
attach(“c:\users\dauidc\_data”,pos=1)
```

- 3 Create a matrix of data in S-Plus consisting of the values of the samples taken. Each column of the matrix corresponds to a single channel of data.

```
filename_matrix(scan(“c:\users\dauidc\_data\filename.asc”,sep=“,”,skip=1),ncol=2,byrow=T)
```

Now check to make sure the matrix is the proper size.

```
dim(filename)
```

- 4 Create a graphics window.

```
win.graph()
```

- 5 Plot a section of the file to check the integrity of the data

```
plot(filename[1:15000,1],type=“l”)
```

- 6 If needed, a file may be cut into smaller subfiles of data.

```
filename.c_filename[1:###]
```

- 7 Generate the interbeat interval signal.

```
filename.l_hlws(filename[,1]) or [,2] - depending on which lead is dominant (for the remainder of this example, lets assume channel 1 was dominant [,1]).
```

To increase the threshold level for R-wave detection, you can increase the parameter called qhg. The default is qhg=0.25.

filename.l_htlws(filename[,1],qh=0.1)

Examine the output plot that is automatically generated with this command. It is a plot of the interbeat interval. If there are improper detections, you can delete a QRS complex using the command `dqrs` and you can identify a QRS complex by using the command `mqrs`.

- 8 If there is a low outlier in the plot, this may mean that an extra erroneous detection(s) occurred. In this case, delete the erroneous detection(s). To identify the outliers, position the cross hairs on the outlier and click the left mouse button. Once all the low outliers are identified, click the right mouse button to zoom in on each individual outlier. If it is confirmed to be an extra erroneous detection, click the erroneous detection where it crosses the ECG signal several times with the left mouse button, then press the right mouse button to move on to the next low outlier previously identified.

filename.d_dqrs(filename[,1],filename.l\$pk)

Then examine the interbeat interval to make sure it was deleted. If not, do the above command again.

plot(diff(filename.d))

- 9 If there is a high outlier in the interbeat interval plot, it may mean that an R-wave was not detected. In this case, manually detect the R-wave. To identify the outliers, position the cross hairs on the high outliers and click the left mouse button. Once all the high outliers are identified, click the right mouse button to zoom in on each individual section of ECG. If it is confirmed to be a mis-detection, click on both sides of the R-wave to with the left mouse button and then click the right mouse button to identify it.

(a) If changes were made with `dqrs`

filename.m_mqrs(filename[,1],filename.d,pout(diff(filename.d)))

(b) If no changes were made in `dqrs`

filename.m_mqrs(filename[,1],filename.l\$pk,pout(diff(filename.l\$pk)))

Then examine the interbeat interval, it should be properly detected now.

plot(diff(filename.m))

- 10 Make sure the R-waves are properly detected by using `correcth`. This program will detect the R-waves exactly to the point if the initial detection is within `w` points of the R-wave peak. The default number of points `w` is 7.

(a) If no changes were made with `dqrs` or `mqrs`

filename.h_correcth(filename,filename.l\$pk,w)

(b) If changes were made with `dqrs` and `mqrs`, or just `mqrs`

filename.h_correcth(filename,filename.m,w)

(c) If changes were made in `dqrs` only

filename.h_correcth(filename,filename.d,w)

- 11 Calculate the power spectrum and make the final file.
filename.fin_fworkb(filename,filename.h\$pk)

APPENDIX E

ANALYSIS PROCEDURES AND PROGRAM TO ANALYZE THE ORIGINAL RESPIRATION WAVEFORM

In the following example, we are going to use a sample data file "filename.dat" to explain the syntax of the programs used to analyze the original respiration.

1 Begin the analysis by unpacking the data file in DOS using kunpack1. This converts each sample of data from binary format to ASCII format.

```
kunpack1 filename.dat,filename.asc,0-23999/b/das16
```

2 Perform the following few commands in Matlab. These commands filter and decimate the respiration waveform and then write it to an ASCII format. To begin, load the ASCII file into Matlab.

```
load filename.asc
```

3 Then change the background for the plotting area from black to white.

```
whitebg
```

4 Plot the signal. You will notice that the first point is equal to one (representing the channel #).

```
plot (filename)
```

5 Cut this point off.

```
filename = filename(2:24001);
```

6 Now filter and decimate the file with the decimate command from the signal processing toolbox.

```
decfile=decimate(filename,10);
```

7 Check the decimated signal.

```
plot(dec.file)
```

8 Write the decimated signal to an ASCII format which can be analyzed in S-Plus.

```
save newfile.asc decfile -ascii
```

9 Perform the following commands in S-Plus. First, attach to the user directory where the filename.asc file is stored.

```
attach("c:\\users\\davidc\\_data",pos=1)
```

- 10 Create a matrix of data in S-Plus consisting of the values of the samples taken.
**newfile_matrix(scan("c:\\users\\davidc_data\\newfile.asc",sep="," ,skip=1),n
col=1,byrow=T)**
- 11 Use the program "respspect" to calculate the detrended respiration and the spectrum of the respiration. These are saved to the filename given at the time of execution.
respfile_respspect(newfile)

```
function(r, title = "", nt = 8192, ns = 6, sr = 20, taper = 0.2)
{
  r.l <- lowess(1:length(r), r, f = 0.3, iter = 2, delta = ceiling((length(r) * 0.3)/8))$y
  r.d <- r - r.l
  if(any(is.na(r.d)))
    stop("NA's not allowed")
  if(taper < 0 | taper > 1)
    stop("taper must be between 0 & 1")
  r.dumb <- r.d
  if(nt < length(r.dumb))
    r.dumb <- r.dumb[1:nt]
  r.dumb <- r.dumb - mean(r.dumb)
  r.dumb <- spec.taper(r.dumb, taper)
  print(paste("Windowing length per side is ", nt * taper, sep = ""))
  if(nt > length(r.dumb))
    r.dumb <- c(r.dumb, rep(0, nt - length(r.dumb)))
  r.spect <- (Mod(fft(r.dumb))^2/(2 * pi * nt))[1:(nt %/% 2 + 1)]
  if(ns > 0) {
    r.spect <- spec.smo(r.spect, span = 7)
    r.spect <- rev(r.spect)
    r.spect <- spec.smo(r.spect, span = 7)
    r.spect <- rev(r.spect)
  }
  xf <- ((1:330) - 1)/nt * sr
  par(mfrow = c(1, 1), mar = c(6.1, 6.1, 4.1, 4.5))
  plot(xf, r.spect[1:330], type = "l", xlab = "Frequency", ylab = "Resp
    Power (RespI)", main = title)
  z <- list(rsp = r.d, spect = r.spect)
  return(z)
}
```

APPENDIX F

PROGRAM "CORRECTH" TO CORRECT R-WAVE DETECTION

```
function(ecg, pkx, w = 7, wait = T)
{
  pkxnew <- vector("numeric", 0)
  for(i in 1:length(pkx)) {
    xofrmax <- ((pkx[i] - w):(pkx[i] + w))[ecg[(pkx[i] - w):(pkx[i] + w)]
      > ecg[pkx[i]]]
    if(length(xofrmax) > 0) {
      print(paste("improper detection!!!! - being corrected"))
      print(paste("pkx=", pkx[i]))
      plot((pkx[i] - w):(pkx[i] + w), ecg[(pkx[i] - w):(pkx[i] + w)])
      abline(v = pkx[i])
      xofmax <- ((pkx[i] - w):(pkx[i] + w))[ecg[(pkx[i] - w):
        (pkx[i] + w)] == max(ecg[(pkx[i] - w):(pkx[i] + w)])]
      if(length(xofmax) > 1) {
        xofmax <- xofmax[1]
      }
      print(paste("xofmax=", xofmax))
      abline(v = xofmax, col = 2)
      if(wait)
        scan()
    }
    else {
      print(paste("xofmax = pkx"))
      xofmax <- pkx[i]
    }
    pkxnew <- c(pkxnew, xofmax)
  }
  z <- list(pk = pkxnew)
  z
}
```

APPENDIX G

“IMPQRSCA” PROGRAM LISTING

```
function(ecg1, ecg2, fin, w = 18, rq = 17, nfft = 8192, sr = 500, decim=25,
        wait = T, title = "")
{
  par(mfrow = c(1, 1), mar = c(6.1, 6.1, 4.1, 4.5))
  print(paste("creating necessary vectors"))
  xofr1 <- vector("numeric", 0)
  xofr2 <- vector("numeric", 0)
  xofq1 <- vector("numeric", 0)
  xofq2 <- vector("numeric", 0)
  qrscal <- vector("numeric", 0)
  minqrs1 <- vector("numeric", 0)
  qrscal2 <- vector("numeric", 0)
  minqrs2 <- vector("numeric", 0)
  pkx <- fin$pk
  if(pkx[1] < (2 * w)) {
    pkx <- pkx[2:length(pkx)]
  }
  if(length(ecg1) < (pkx[length(pkx)] + 2 * w)) {
    pkx <- pkx[1:(length(pkx) - 1)]
  }
  print(paste("sampling rate of ecgs = ",sr))
  print(paste("decim = ",decim))
  sr2 <- sr/decim
  print(paste("sr2 = ",sr2))
  print(paste("detrending ecgs"))
  lwf1 <- lowess(1:length(ecg1), ecg1, f = 45/length(
    ecg1), iter = 2, delta = 0.1)$y
  ecg1 <- ecg1 - lwf1
  lwf2 <- lowess(1:length(ecg2), ecg2, f = 45/length(
    ecg2), iter = 2, delta = 0.1)$y
  ecg2 <- ecg2 - lwf2
  print(paste("shifting ecgs"))
  minecg1 <- min(ecg1)
  minecg2 <- min(ecg2)
  if(minecg1 < 0) {
    ecg1 <- ecg1 + 1.1 * abs(minecg1)
  }
}
```

```

if(minecg2 < 0) {
  ecg2 <- ecg2 + 1.1 * abs(minecg2)
}
print(paste("detecting R-waves and Q-waves; PLEASE be patient"))
# the following performs R-wave and Q-wave detection for ecg1 and ecg2
for(i in 1:length(pkx)) {
# R-wave detection for ecg1
  xofrmax1 <- ((pkx[i] - w):(pkx[i] + w))[ecg1[(pkx[i] - w):(pkx[i] + w)] >
    ecg1[pkx[i]]]
  if(length(xofrmax1) > 0) {
    xofmax1 <- ((pkx[i] - w):(pkx[i] + w))[ecg1[(pkx[i] - w):(pkx[
      i] + w)] == max(ecg1[(pkx[i] - w):(pkx[i] + w))]]
    if(length(xofmax1) > 1) {
      xofmax <- xofmax[1]
    }
  }
  else {
    xofmax1 <- pkx[i]
  }
  xofr1 <- c(xofr1, xofmax1)
# R-wave detection for ecg2
  xofrmax2 <- ((pkx[i] - (2 * w):(pkx[i] + w))[ecg2[(pkx[i] - (2 *
    w):(pkx[i] + w)] > ecg2[pkx[i]]]
  if(length(xofrmax2) > 0) {
    xofmax2 <- ((pkx[i] - (2 * w):(pkx[i] + w))[ecg2[(pkx[i] - (
      2 * w):(pkx[i] + w)] == max(ecg2[(pkx[i] - (2 * w
        )):(pkx[i] + w))]]
    if(length(xofmax2) > 1) {
      xofmax2 <- xofmax2[1]
    }
  }
  else {
    xofmax2 <- pkx[i]
  }
  xofr2 <- c(xofr2, xofmax2)
# q wave detection for lead I and lead III
  minq1 <- ((xofr1[i] - rq):(xofr1[i]))[(ecg1[(xofr1[i] - rq):(xofr1[i])]] <=
    min(ecg1[(xofr1[i] - rq):(xofr1[i])]))]
  if(length(minq1) > 1) {
    minq1 <- minq1[length(minq1)]
  }
  xofq1 <- c(xofq1, minq1)
  minq2 <- ((xofr2[i] - rq):(xofr2[i]))[( ecg2[(xofr2[i] - rq):(xofr2[i])]] <=
    min(ecg2[(xofr2[i] - rq):(xofr2[i])]))]
  if(length(minq2) > 1) {

```

```

        minq2 <- minq2[length(minq2)]
    }
    xofq2 <- c(xofq2, minq2)
}
window1 <- round(mean(xofr1 - xofq1) * 2)
window2 <- round(mean(xofr2 - xofq2) * 2)
if(length(pkx) != length(xofq1)) {
    print(paste("Number of Q's is not equal to that of R's (lead 1)"))
    print(paste("Q's:", length(xofq1)))
    print(paste("R's:", length(xofr1)))
    stop( )
}
if(length(pkx) != length(xofq2)) {
    print(paste("Number of Q's is not equal to that of R's (lead 3)"))
    print(paste("Q's:", length(xofq2)))
    print(paste("R's:", length(xofr2)))
    stop( )
}
par(mfrow = c(2, 1), mar = c(6.1, 6.1, 4.1, 3.1))
for(i in 10:14) {
    plot((xofr1[i] - 100):(xofr1[i] + 100), ecg1[(xofr1[i] - 100):(xofr1[i] +
        100)], ylim = c(min(ecg1), max(ecg1)))
    abline(v = xofr1[i])
    abline(v = xofq1[i])
    abline(v = (xofq1[i] + window1), col = 2)
    plot((xofr1[i] - 100):(xofr1[i] + 100), ecg2[(xofr1[i] - 100):(xofr1[i] +
        100)], ylim = c(min(ecg2), max(ecg2)))
    abline(v = xofr2[i])
    abline(v = xofq2[i])
    abline(v = (xofq2[i] + window2), col = 2)
    if(wait)
        scan( )
}
print(paste("calculating areas"))
for(i in 1:length(pkx)) {
    cols1 <- ecg1[xofq1[i):(xofq1[i] + window1)]
    cols2 <- ecg2[xofq2[i):(xofq2[i] + window2)]
    area1 <- sum(cols1)
    area2 <- sum(cols2)
    base1 <- min(ecg1[xofq1[i):(xofq1[i] + window1)]) * window1
    base2 <- min(ecg2[xofq2[i):(xofq2[i] + window2)]) * window2
    a1 <- area1 - base1
    a2 <- area2 - base2
    qrscal <- c(qrscal, a1)
    qrscal <- c(qrscal, a2)
}

```



```

}
n <- length(ecg1) + 100
f1 <- 0.3
f2 <- 0.2
d <- 1
xf <- ((1:330) - 1)/nfft * sr2
iqrscal <- spline(xofr1, qrsca1, n)
iqrscal <- iqrscal$y
d.iqrscal <- iqrscal[seq(1, length(iqrscal), decim)]
par(mfrow = c(1, 1), mar = c(6.1, 6.1, 4.1, 4.5))
d.iqrscal1 <- lowess(1:length(d.iqrscal), d.iqrscal, f = f2, iter = 2, delta =
  ceiling((length(d.iqrscal) * 0.3)/8))$y
par(mfrow = c(1, 1), mar = c(6.1, 6.1, 4.1, 4.5))
plot((d.iqrscal - d.iqrscal1), type = "l", xlab = "Time", ylab =
  "ecg1 Deriv Resp (impQRSCA)", main = title)
if(wait)
  scan( )
d.iqrscal1s <- spect(d.iqrscal1 - d.iqrscal1, nt = nfft, ns = 6)
plot(xf, fin$isp[1:330], type = "l", xlab = "Frequency Number", ylab =
  "Power (ecg1)", main = title)
par(new = T)
plot(xf, d.iqrscal1s[1:330], type = "l", lty = 3, axes = F, xlab = "", ylab = "")
axis(4)
mtext("ecg1 Deriv Resp (impQRSCA) Power - - ", side = 4, line = 2)
if(wait)
  scan( )
iqrscal2 <- spline(xofr2, qrsca2, n)
iqrscal2 <- iqrscal2$y
d.iqrscal2 <- iqrscal2[seq(1, length(iqrscal2), decim)]
d.iqrscal2l <- lowess(1:length(d.iqrscal2), d.iqrscal2, f = f2, iter = 2, delta =
  ceiling((length(d.iqrscal2) * 0.3)/8))$y
plot((d.iqrscal2 - d.iqrscal2l), type = "l", xlab = "Time", ylab =
  "ecg2 Deriv Resp (impQRSCA)", main = title)
if(wait)
  scan( )
d.iqrscal2s <- spect(d.iqrscal2 - d.iqrscal2l, nt = nfft, ns = 6)
plot(xf, fin$isp[1:330], type = "l", xlab = "Frequency Number", ylab =
  "Power", main = title)
par(new = T)
plot(xf, d.iqrscal2s[1:330], type = "l", lty = 3, axes = F, xlab = "", ylab = "")
axis(4)
mtext("ecg2 Deriv Resp (impQRSCA) Power - - ", side = 4, line = 2)
if(wait)
  scan( )
d.iqrscal <- (atan(d.iqrscal2/d.iqrscal1) * 180)/pi

```

```

d.iqrscal <- lowess(1:length(d.iqrscas), d.iqrscas, f = f2, iter = 2, delta =
  ceiling((length(d.iqrscas) * 0.3)/8))$y
plot((d.iqrscas - d.iqrscal), type = "l", xlab = "Time", ylab =
  "Arctan (ecg2/ecg1) Deriv Resp (impQRSCA)", main = title)
if(wait)
  scan( )
d.iqrscas <- spect(d.iqrscas - d.iqrscal, nt = nfft, ns = 6)
par(mfrow = c(1, 1), mar = c(6.1, 6.1, 4.1, 4.5))
plot(xf, fin$isp[1:330], type = "l", xlab = "Frequency Number", ylab =
  "Power", main = title)
par(new = T)
plot(xf, d.iqrscas[1:330], type = "l", lty = 3, axes = F, xlab = "", ylab = "")
axis(4)
mtext("Arctan (ecg2/ecg1) Deriv Resp (impQRSCA) Power - - ",
  side = 4, line = 2)
if(wait)
  scan( )
plot(xf, d.iqrscas[1:330], type = "l", xlab = "frequency", ylab = "Power")
par(new = T)
plot(xf, d.iqrscas1s[1:330], type = "l", lty = 2, col = 2, axes = F)
par(new = T)
plot(xf, d.iqrscas2s[1:330], type = "l", lty = 3, col = 3, axes = F)
if(wait)
  scan( )
par(mfrow = c(3, 1), mar = c(6.1, 6.1, 4.1, 3.1))
plot((d.iqrscas2 - d.iqrscas1), type = "l", xlab = "Time", ylab = "ecg2",
  main = title)
plot((d.iqrscas1 - d.iqrscas1l), type = "l", xlab = "Time", ylab = "ecg1")
plot((d.iqrscas - d.iqrscal), type = "l", xlab = "Time", ylab = "Arctan (ecg2/ecg1)",
  sub = "Derived with impQRSCA")
if(wait)
  scan( )
par(mfrow = c(2, 1), mar = c(6.1, 6.1, 4.1, 4.5))
plot(d.iqrscas1[1:(length(d.iqrscas1)/2)], type = "l", main = title, xlab = "Time",
  ylab = "ecg1 (solid), ecg2 (dashed)", sub = "First Minute : Derived
  with impQRSCA")
par(new = T)
plot(d.iqrscas2[1:(length(d.iqrscas2)/2)], type = "l", xlab = "", axes = F, ylab = "",
  col = 2, lty = 2)
plot(((length(d.iqrscas1)/2):length(d.iqrscas1)), d.iqrscas1[(length(d.iqrscas1) / 2 )
  :length(d.iqrscas1)], type = "l", main = title, xlab = "Time", ylab =
  "ecg1 (solid), ecg2 (dashed)", sub = "Second Minute : Derived with
  impQRSCA")
par(new = T)

```

```
plot(((length(d.iqrsc2)/2):length(d.iqrsc2)), d.iqrsc2[(length(d.iqrsc2)/2)
  :length(d.iqrsc2)], type = "l", xlab = "", axes = F, ylab = "",
  col = 2, lty = 2)
z <- list(d.iqrsc1 = (d.iqrsc1 - d.iqrsc1l), d.iqrsc1s = d.iqrsc1s,
  d.iqrsc2 = (d.iqrsc2 - d.iqrsc2l), d.iqrsc2s = d.iqrsc2s,
  qrsc1 = qrsc1, qrsc2 = qrsc2)
z
}
```

APPENDIX H

“ADRESP” PROGRAM LISTING

```
function(ecg1, ecg2, fin, w = 17, sr = 500, decim = 25, nfft = 8192, wait = T, title = "")
{
  print(paste("creating necessary vectors"))
  pkx <- fin$pk
  rx1 <- vector("numeric", 0)
  rx2 <- vector("numeric", 0)
  ampmodx1 <- vector("numeric", 0)
  ampmody1 <- vector("numeric", 0)
  ampmodx2 <- vector("numeric", 0)
  ampmody2 <- vector("numeric", 0)
  print(paste("checking ecgs"))
  if(pkx[1] < 2 * w) {
    pkx <- pkx[2:length(pkx)]
  }
  if(length(ecg1) < (pkx[length(pkx)] + 2 * w)) {
    pkx <- pkx[1:(length(pkx) - 1)]
  }
  print(paste("sampling rate of ecgs = ", sr))
  print(paste("decim = ", decim))
  sr2 <- sr/decim
  print(paste("sr2 = ", sr2))
  print(paste("detrending ecgs"))
  lwf1 <- lowess(1:length(ecg1), ecg1, f = 110/length(ecg1), iter = 2, delta = 0.1)$y
  ecg1 <- ecg1 - lwf1
  lwf2 <- lowess(1:length(ecg2), ecg2, f = 110/length(ecg2), iter = 2, delta = 0.1)$y
  ecg2 <- ecg2 - lwf2
  print(paste("Detecting R-waves for ecg1"))
  # the following is for ecg1
  for (i in 1:length(pkx)) {
    xofrmax <- ((pkx[i] - w):(pkx[i] + w))[ecg1[(pkx[i] - w):(pkx[i] + w)]
      > ecg1[pkx[i]]]
    if (length(xofrmax) > 0) {
      xofmax <- ((pkx[i] - w):(pkx[i] + w))[ecg1[(pkx[i] - w):(pkx[i] +
        w)] == max(ecg1[(pkx[i] - w):(pkx[i] + w))]]
      if (length(xofmax) > 1) {
        xofmax <- xofmax[1]
      }
    }
  }
}
```

```

#           print(paste("pkx=", pkx[i]))
#           print(paste("xofrmax=", xofrmax))
#           plot((pkx[i] - w):(pkx[i] + w), ecg1[(pkx[i] - w):(pkx[i] + w)])
#           abline(v = pkx[i])
#           abline(v = xofrmax)
#           if(wait)
#               scan( )
        }
        else {
#           print(paste("xofrmax= pkx"))
            xofrmax <- pkx[i]
        }
        rx1 <- c(rx1, xofrmax)
    }
    print(paste("done detecting R-waves for ecg1"))
    n <- length(ecg1) + 100
    ampmod1 <- spline(rx1, ecg1[rx1], n)
    par(mfrow = c(1, 1), mar = c(6.1, 6.1, 4.1, 4.5))
    win <- 100
#   for(i in 10:15) {
#       plot((rx1[i] - win):(rx1[i] + win), ecg1[(rx1[i] - win):(rx1[i] + win)], ylim =
#           c(min(ecg1), max(ecg1)))
#       abline(v = rx1[i])
#       abline(v = pkx[i])
#       par(new = T)
#       plot(ampmod1$x[(rx1[i] - win):(rx1[i] + win)], ampmod1$y[(rx1[i] -
#           win):(rx1[i] + win)], type = "l", col = 2, axes = F, ylim =
#           c(min(ecg1), max(ecg1)))
#       if(wait)
#           scan( )
#   }
    ecg1 <- ecg1[rx1:rx1[length(rx1)]]
    ampmodx1 <- ampmod1$x
    ampmody1 <- ampmod1$y
    par(mfrow = c(2, 1), mar = c(6.1, 6.1, 4.1, 3.1))
    plot(ecg1[1:(length(ecg1)/2)], type = "l", ylim = c(min(ecg1), max(ecg1)), ylab =
        "ecg 1", main = title, sub = "First Minute")
    par(new = T)
    plot(ampmodx1[1:(length(ampmodx1)/2)], ampmody1[1:(length(ampmodx1)
        )/2]), type = "l", col = 2, axes = F, ylim = c(min(ecg1),
        max(ecg1)), ylab = "", xlab = "")
    plot(((length(ecg1)/2):length(ecg1), ecg1[((length(ecg1)/2):
        length(ecg1)]), type = "l", ylim = c(min(ecg1), max(ecg1)),
        ylab = "ecg1", sub = "Second Minute")
    par(new = T)

```

```

plot(ampmodx1[((length(ampmodx1)/2)):length(ampmodx1)], ampmodity1[((
  length(ampmodity1)/2)):length(ampmodity1)], type = "l", col =
  2, axes = F, ylim = c(min(ecg1), max(ecg1)), minx = c(((
  length(ampmodx1)/2)):length(ampmodx1)), ylab = "", xlab =
  "")
if(wait)
  scan( )
ampmodity11 <- lowess(1:length(ampmodity1), ampmodity1, f = 0.2, iter = 2,
  delta = ceiling((length(ampmodity1) * 0.3)/8))$y
ampmodity1 <- ampmodity1 - ampmodity11
ampmodity1 <- ampmodity1 + 1.5 * (abs(min(ampmodity1)))
par(mfrow = c(1, 1), mar = c(6.1, 6.1, 4.1, 4.5))
plot(ampmodity1, type = "l", ylab = "Amp Der. Resp (Lead I)", xlab = "time",
  main = title)
if(wait)
  scan( )
print(paste("starting spectrum calculation for ecg1"))
d.ampmod1 <- ampmodity1[seq(1, length(ampmodity1), decim)]
ampmod1.spec <- spect(d.ampmod1, nt = nfft, ns = 6)
print(paste("done with spectrum calculation for ecg1"))
xf <- ((1:330) - 1)/nfft * sr2
plot(xf, ampmod1.spec[1:330], type = "l", xlab = "frequency", ylab =
  "power (Amp Der Resp ecg1)", main = title)
if(wait)
  scan( )
# the following is for ecg2
print(paste("Detecting R-waves for ecg2"))
for(i in 1:length(pkx)) {
  xofrmax <- ((pkx[i] - (2 * w)):(pkx[i] + w))[ecg2[(pkx[i] - (
    2 * w)):(pkx[i] + w)] > ecg2[pkx[i]]]
  if(length(xofrmax) > 0) {
    xofmax <- ((pkx[i] - (2 * w)):(pkx[i] + w))[ecg2[(
      pkx[i] - (2 * w)):(pkx[i] + w)] == max(
        ecg2[(pkx[i] - (2 * w)):(pkx[i] + w))]]
    if(length(xofmax) > 1) {
      xofmax <- xofmax[1]
    }
  }
  print(paste("pkx=", pkx[i], "xofrmax=", xofmax))
  plot((pkx[i] - (2 * w)):(pkx[i] + w), ecg2[(pkx[i] - (2 * w)):(pkx[i] + w)])
  #
  abline(v = pkx[i], col = 2)
  #
  print(paste("xofmax=", xofmax))
  #
  abline(v = xofmax)
  #
  if(wait)
  #
  scan( )
}

```

```

else {
#       print(paste("xofmax= pkx"))
       xofmax <- pkx[i]
}
rx2 <- c(rx2, xofmax)
}
print(paste("done detecting R-waves for ecg2"))
ampmod2 <- spline(rx2, ecg2[rx2], n)
par(mfrow = c(1, 1), mar = c(6.1, 6.1, 4.1, 4.5))
# for(i in 10:15) {
#     plot((rx2[i] - win):(rx2[i] + win), ecg2[(rx2[i] - win):(rx2[i] + win)], ylim =
#         c(min(ecg2), max(ecg2)))
#     abline(v = rx2[i])
#     abline(v = pkx[i])
#     par(new = T)
#     plot(ampmod2$x[(rx2[i] - win):(rx2[i] + win)], ampmod2$y[(rx2[i] -
#         win):(rx2[i] + win)], type = "l", col = 2, axes = F, ylim =
#         c(min(ecg2), max(ecg2)))
#     if(wait)
#         scan( )
# }
ecg2 <- ecg2[rx2:rx2[length(rx2)]]
ampmodx2 <- ampmod2$x
ampmody2 <- ampmod2$y
par(mfrow = c(2, 1), mar = c(6.1, 6.1, 4.1, 3.1))
plot(ecg2[1:(length(ecg2)/2)], type = "l", ylim = c(min(ecg2), max(
    ecg2)), main = title, ylab = "ecg2", sub = "First Minute")
par(new = T)
plot(ampmodx2[1:(length(ampmodx2)/2)], ampmody2[1:(length(ampmodx2
    )/2)], type = "l", col = 2, axes = F, ylim = c(min(ecg2),
    max(ecg2)), ylab = "", xlab = "")
plot(((length(ecg2)/2)):length(ecg2), ecg2[((length(ecg2)/2)):
    length(ecg2)], type = "l", ylim = c(min(ecg2), max(ecg2)),
    ylab = "ecg2", sub = "Second Minute")
par(new = T)
plot(ampmodx2[((length(ampmodx2)/2)):length(ampmodx2)], ampmody2[((
    length(ampmody2)/2)):length(ampmody2)], type = "l", col =
    2, axes = F, ylim = c(min(ecg2), max(ecg2)), minx = c(((
    length(ampmodx2)/2)):length(ampmodx2)), ylab = "", xlab = "")
if(wait)
    scan( )
ampmody2l <- lowess(1:length(ampmody2), ampmody2, f = 0.2, iter = 2,
    delta = ceiling((length(ampmody2) * 0.3)/8))$y
ampmody2 <- ampmody2 - ampmody2l
ampmody2 <- ampmody2 + 1.5 * (abs(min(ampmody2)))

```

```

par(mfrow = c(1, 1), mar = c(6.1, 6.1, 4.1, 4.5))
plot(ampmody2, type = "l", ylab = "Amp Der. Resp (Lead III)", xlab =
      "time", main = title)
if(wait)
  scan( )
print(paste("starting spectrum calculation for ecg2"))
d.ampmod2 <- ampmody2[seq(1, length(ampmody2), decim)]
ampmod2.spec <- spect(d.ampmod2, nt = nfft, ns = 6)
print(paste("done with spectrum calculation for ecg2"))
plot(xf, ampmody2.spec[1:330], type = "l", xlab = "frequency", ylab =
      "power (Amp Der Resp ecg2)", main = title)
if(wait)
  scan( )
par(mfrow = c(2, 1), mar = c(6.1, 6.1, 4.1, 4.5))
plot(ampmodx1[1:(length(ampmodx1)/2)], ampmody1[1:(length(ampmody1)
  )/2]], type = "l", ylim = c(min(ampmody1), max(ampmody1)), sub =
  "ecg1: solid   ecg2: dashed", ylab = "", xlab = "", main = title)
par(new = T)
plot(ampmodx2[1:(length(ampmodx2)/2)], ampmody2[1:(length(ampmody2)
  )/2]], type = "l", ylim = c(min(ampmody2), max(ampmody2)),
  col = 2, ylab = "", xlab = "", axes = F, lty = 2)
plot(ampmodx1[(length(ampmodx1)/2):length(ampmodx1)], ampmody1[(
  length(ampmody1)/2):length(ampmody1)], type = "l", ylim =
  c(min(ampmody1), max(ampmody1)), sub = "ecg1: solid   ecg2: dashed",
  ylab = "", xlab = "")
par(new = T)
plot(ampmodx2[(length(ampmodx2)/2):length(ampmodx2)], ampmody2[(
  length(ampmody2)/2):length(ampmody2)], type = "l", ylim =
  c(min(ampmody2), max(ampmody2)), col = 2, ylab = "", xlab = "",
  axes = F, lty = 2)
if(wait)
  scan( )
ampmod <- vector("numeric", 0)
ampmod <- (atan(ampmody2/ampmody1) * 180)/pi
par(mfrow = c(3, 1), mar = c(6.1, 6.1, 4.1, 3.1))
plot(ampmody2[seq(1, length(ampmody2), 2)], type = "l", ylab =
  "Amp Der Resp (ecg2)", xlab = "time", main = title)
plot(ampmody1[seq(1, length(ampmody1), 2)], type = "l", ylab =
  "Amp Der Resp (ecg1)", xlab = "time")
plot(ampmod[seq(1, length(ampmod), 2)], type = "l", ylab =
  "Amp Der Resp (arctan(ecg2/ecg1)", xlab = "time")
if(wait)
  scan( )
ampmodl <- lowess(1:length(ampmod), ampmod, f = 0.2, iter = 2,
  delta = ceiling((length(ampmod) * 0.3)/8))$y

```



```

ampmod <- ampmod - ampmod1
par(mfrow = c(1, 1), mar = c(6.1, 6.1, 4.1, 4.5))
plot(ampmod[seq(1, length(ampmod), 2)], type = "l", ylab =
      "Amp Der. Resp (arctan(ecg2/ecg1)", xlab = "time", main = title)
if(wait)
  scan( )
print(paste("starting spectrum calculation for atan signal"))
d.ampmod <- ampmod[seq(1, length(ampmod), decim)]
ampmod.spec <- spect(d.ampmod, nt = nfft, ns = 6)
print(paste("done with spectrum calculation for atan signal"))
plot(xf, ampmod.spec[1:330], type = "l", xlab = "frequency", ylab =
      "power (Amp Der Resp (arctan ecg2/ecg1))", main = title)
print(paste("length of ampmod1=", length(d.ampmod1)))
print(paste("length of ampmod2=", length(d.ampmod2)))
print(paste("length of ampmod=", length(d.ampmod)))
z <- list(ampmod1 = d.ampmod1, ampmod1.spec = ampmod1.spec,
          ampmod2 = d.ampmod2, ampmod2.spec = ampmod2.spec,
          ampmod = d.ampmod, ampmod.spec = ampmod.spec)
z
}

```

APPENDIX I

“VQRSIND” PROGRAM LISTING

```
function(ecg1, ecg2, fin, w = 20, rq = 15, rs = 15, nfft = 8192, sr = 500,
        decim = 25, wait = T, title = "")
{
  print(paste("creating necessary vectors"))
  xofr1 <- vector("numeric", 0)
  xofr2 <- vector("numeric", 0)
  xofq1 <- vector("numeric", 0)
  xofq2 <- vector("numeric", 0)
  xofs1 <- vector("numeric", 0)
  xofs2 <- vector("numeric", 0)
  qrscal <- vector("numeric", 0)
  minqrs1 <- vector("numeric", 0)
  qrscal2 <- vector("numeric", 0)
  minqrs2 <- vector("numeric", 0)
  pkx <- fin$pk
  print(paste("checking ecgs"))
  if(pkx[1] < 2 * w) {
    pkx <- pkx[2:length(pkx)]
  }
  if(length(ecg1) < (pkx[length(pkx)] + 2 * rs)) {
    pkx <- pkx[1:(length(pkx) - 1)]
  }
  print(paste("sampling rate of ecgs = ", sr))
  print(paste("decim = ", decim))
  sr2 <- sr/decim
  print(paste("sr2 = ", sr2))
  print(paste("detrending ecgs"))
  lwf1 <- lowess(1:length(ecg1), ecg1, f = 110/length(ecg1), iter = 2, delta = 0.1)$y
  ecg1 <- ecg1 - lwf1
  lwf2 <- lowess(1:length(ecg2), ecg2, f = 110/length(ecg2), iter = 2, delta = 0.1)$y
  ecg2 <- ecg2 - lwf2
  print(paste("shifting ecgs"))
  minecg1 <- min(ecg1)
  minecg2 <- min(ecg2)
  if(minecg1 < 0) {
    ecg1 <- ecg1 + 1.1 * abs(minecg1)
  }
  if(minecg2 < 0) {
    ecg2 <- ecg2 + 1.1 * abs(minecg2)
  }
}
```

```

}
print(paste("checking R-waves for ecg1"))
for(i in 1:length(pkx)) {
# R wave detection for ecg1
  xofrmax1 <- ((pkx[i] - w):(pkx[i] + w))[ecg1[(pkx[i] - w):(pkx[i] + w)]
    > ecg1[pkx[i]]]
  if(length(xofrmax1) > 0) {
    xofmax1 <- ((pkx[i] - w):(pkx[i] + w))[ecg1[(pkx[i] - w):
      (pkx[i] + w)] == max(ecg1[(pkx[i] - w):(pkx[i] + w))]]
    if(xofmax1 > 1)
      xofmax1 <- xofmax1[1]
  }
  else {
    xofmax1 <- pkx[i]
  }
  xofr1 <- c(xofr1, xofmax1)
# R wave detection for ecg2
  xofrmax2 <- ((pkx[i] - (2 * w):(pkx[i] + w))[ecg2[(pkx[i] - (2 * w)):
    (pkx[i] + w)] > ecg2[pkx[i]]]
  if(length(xofrmax2) > 0) {
    xofmax2 <- ((pkx[i] - (2 * w):(pkx[i] + w))[ecg2[(pkx[i] -
      (2 * w):(pkx[i] + w)] == max(ecg2[(pkx[i] - (2 * w)):
      (pkx[i] + w))]]
    if(xofmax2 > 1)
      xofmax2 <- xofmax2[1]
  }
  else {
    xofmax2 <- pkx[i]
  }
  xofr2 <- c(xofr2, xofmax2)
# Q wave detection for ecg1 and ecg2
  minq1 <- ((xofr1[i] - rq):(xofr1[i]))[(ecg1[(xofr1[i] - rq):(xofr1[i]])]
    <= min(ecg1[(xofr1[i] - rq):(xofr1[i]])]]
  if(length(minq1) > 1) {
    minq1 <- minq1[length(minq1)]
  }
  xofq1 <- c(xofq1, minq1)
  minq2 <- ((xofr2[i] - rq):(xofr2[i]))[(ecg2[(xofr2[i] - rq):(xofr2[i]])]
    <= min(ecg2[(xofr2[i] - rq):(xofr2[i]])]]
  if(length(minq2) > 1) {
    minq2 <- minq2[length(minq2)]
  }
  xofq2 <- c(xofq2, minq2)
# S wave detection for ecg1 and ecg2
  mins1 <- (xofr1[i):(xofr1[i] + rs))[ecg1[xofr1[i):(xofr1[i] + rs)]]

```

```

        <= min(ecg1[xofr1[i):(xofr1[i] + rs)])]
if(length(mins1) > 1) {
  mins1 <- mins1[length(mins1)]
}
xofs1 <- c(xofs1, mins1)
mins2 <- (xofr2[i):(xofr2[i] + rs)][(ecg2[xofr2[i):(xofr2[i] + rs)])]
  <= min(ecg2[xofr2[i):(xofr2[i] + rs)])]
if(length(mins2) > 1) {
  mins2 <- mins2[length(mins2)]
}
xofs2 <- c(xofs2, mins2)
}
if(length(pkx) != length(xofq1)) {
  print(paste("Number of Q's is not equal to that of R's (ecg1)")
  print(paste("Q's:", length(xofq1)))
  print(paste("R's:", length(xofr1)))
  stop()
}
if(length(pkx) != length(xofs1)) {
  print(paste("Number of S's is not equal to that of R's (ecg1)")
  print(paste("S's:", length(xofs1)))
  print(paste("R's:", length(xofr1)))
  stop()
}
if(length(pkx) != length(xofq2)) {
  print(paste("Number of Q's is not equal to that of R's (ecg2)")
  print(paste("Q's:", length(xofq2)))
  print(paste("R's:", length(xofr2)))
  stop()
}
if(length(pkx) != length(xofs2)) {
  print(paste("Number of S's is not equal to that of R's (ecg2)")
  print(paste("S's:", length(xofs2)))
  print(paste("R's:", length(xofr2)))
  stop()
}
}
par(mfrow = c(2, 1), mar = c(6.1, 6.1, 4.1, 3.1))
for(i in 10:14) {
  plot((xofr1[i] - 25):(xofr1[i] + 25), ecg1[(xofr1[i] - 25):(xofr1[i] + 25)],
       ylim = c(min(ecg1), max(ecg1)))
  abline(v = xofr1[i])
  abline(v = xofq1[i])
  abline(v = xofs1[i])
  plot((xofr1[i] - 25):(xofr1[i] + 25), ecg2[(xofr1[i] - 25):(xofr1[i] + 25)],
       ylim = c(min(ecg2), max(ecg2)))

```

```

    abline(v = xofr2[i])
    abline(v = xofq2[i])
    abline(v = xofs2[i])
    if(wait)
        scan()
}
for(i in 1:length(pkx)) {
  cols1 <- ecg1[xofq1[i]:xofs1[i]]
  cols2 <- ecg2[xofq2[i]:xofs2[i]]
  area1 <- sum(cols1)
  area2 <- sum(cols2)
  if(ecg1[xofq1[i]] < ecg1[xofs1[i]]) {
    minqrs1[i] <- xofq1[i]
  }
  if(ecg1[xofs1[i]] < ecg1[xofq1[i]]) {
    minqrs1[i] <- xofs1[i]
  }
  if(ecg2[xofq2[i]] < ecg2[xofs2[i]]) {
    minqrs2[i] <- xofq2[i]
  }
  if(ecg2[xofs2[i]] < ecg2[xofq2[i]]) {
    minqrs2[i] <- xofs2[i]
  }
  window1 <- (xofs1[i] - xofq1[i])
  window2 <- (xofs2[i] - xofq2[i])
  base1 <- ecg1[minqrs1[i]] * window1
  base2 <- ecg2[minqrs2[i]] * window2
  a1 <- area1 - base1
  a2 <- area2 - base2
  qrsca1 <- c(qrsca1, a1)
  qrsca2 <- c(qrsca2, a2)
}
n <- length(ecg1) + 100
f1 <- 0.3
f2 <- 0.2
d <- 1
xf <- ((1:330) - 1)/nfft * sr2
iqrscal <- spline(xofr1, qrsca1, n)
iqrscal <- iqrscal$y
d.iqrscal <- iqrscal[seq(1, length(iqrscal), decim)]
par(mfrow = c(1, 1), mar = c(6.1, 6.1, 4.1, 4.5))
plot(d.iqrscal, type = "l", xlab = "Time", ylab = "ecg1 I Deriv Resp (vQRSind)",
     main = title)
if(wait)
  scan()

```

```

d.iqrscal1 <- lowess(1:length(d.iqrscal1), d.iqrscal1, f = f2, iter = 2, delta =
  ceiling((length(d.iqrscal1) * 0.3)/8))$y
d.iqrscal1s <- spect(d.iqrscal1 - d.iqrscal1, nt = nfft, ns = 6)
plot(xf, fin$isp[1:330], type = "l", xlab = "Frequency Number", ylab = "Power",
  main = title)
par(new = T)
plot(xf, d.iqrscal1s[1:330], type = "l", lty = 3, axes = F, xlab = "", ylab = "")
axis(4)
mtext("ecg1 Deriv Resp (vQRSind) Power - - ", side = 4, line
  = 3)
if(wait)
  scan()
iqrscal2 <- spline(xofr2, qrsca2, n)
iqrscal2 <- iqrscal2$y
d.iqrscal2 <- iqrscal2[seq(1, length(iqrscal2), decim)]
plot(d.iqrscal2, type = "l", xlab = "Time", ylab = "ecg2 Deriv Resp (vQRSind)",
  main = title)
if(wait)
  scan()
d.iqrscal2l <- lowess(1:length(d.iqrscal2), d.iqrscal2, f = f2, iter = 2, delta =
  ceiling((length(d.iqrscal2) * 0.3)/8))$y
d.iqrscal2s <- spect(d.iqrscal2 - d.iqrscal2l, nt = nfft, ns = 6)
plot(xf, fin$isp[1:330], type = "l", xlab = "Frequency Number", ylab = "Power",
  main = title)
par(new = T)
plot(xf, d.iqrscal2s[1:330], type = "l", lty = 3, axes = F, xlab = "", ylab = "")
axis(4)
mtext("ecg2 Deriv Resp (vQRSind) Power - - ", side = 4, line = 3)
if(wait)
  scan()
plot(d.iqrscal2/d.iqrscal1, type = "l", ylab = "interpolated ecg2/ interpolated ecg1",
  xlab = "Time", main = title)
if(wait)
  scan()
d.iqrscal <- atan(d.iqrscal2/d.iqrscal1)
plot(d.iqrscal, type = "l", xlab = "Time", ylab =
  "Arctan (ecg2/ecg1) Deriv Resp (vQRSind)", main = title)
if(wait)
  scan()
d.iqrscal <- lowess(1:length(d.iqrscal), d.iqrscal, f = f2, iter = 2, delta =
  ceiling((length(d.iqrscal) * 0.3)/8))$y
d.iqrscals <- spect(d.iqrscal - d.iqrscal, nt = nfft, ns = 6)
par(mfrow = c(1, 1), mar = c(6.1, 6.1, 4.1, 4.5))
plot(xf, fin$isp[1:330], type = "l", xlab = "Frequency Number", ylab = "Power",
  main = title)

```

```

par(new = T)
plot(xf, d.iqrscas[1:330], type = "l", lty = 3, axes = F, xlab = "", ylab = "")
axis(4)
mtext("Arctan (ecg2/ecg1) Deriv Resp (vQRSind) Power - - ", side = 4, line = 3)
if(wait)
  scan()
plot(xf, d.iqrscas[1:330], type = "l", xlab = "frequency", ylab = "Power")
par(new = T)
plot(xf, d.iqrscals[1:330], type = "l", lty = 2, col = 2, axes = F)
par(new = T)
plot(xf, d.iqrscas2s[1:330], type = "l", lty = 3, col = 3, axes = F)
if(wait)
  scan()
par(mfrow = c(3, 1), mar = c(6.1, 6.1, 4.1, 3.1))
plot(d.iqrscas2, type = "l", xlab = "Time", ylab = "ecg2", main = title)
plot(d.iqrscas1, type = "l", xlab = "Time", ylab = "ecg1")
plot(d.iqrscas, type = "l", xlab = "Time", ylab =
  "Arctan (ecg2/ecg1)", sub = "Derived with vQRSind")
if(wait)
  scan()
par(mfrow = c(2, 1), mar = c(6.1, 6.1, 4.1, 4.5))
plot(d.iqrscas1[1:(length(d.iqrscas1)/2)], type = "l", main = title, xlab = "Time",
  ylab = "ecg1 (solid), ecg2 (dashed)", sub = "First Minute : Derived with
  vQRSind")
par(new = T)
plot(d.iqrscas2[1:(length(d.iqrscas2)/2)], type = "l", xlab = "", axes = F, ylab = "",
  col = 2, lty = 2)
plot(((length(d.iqrscas1)/2):length(d.iqrscas1)), d.iqrscas1[(length(d.iqrscas1)/2):
  length(d.iqrscas1)], type = "l", main = title, xlab = "Time", ylab =
  "ecg1 (solid), ecg2 (dashed)", sub = "Second Minute : Derived with
  vQRSind")
par(new = T)
plot(((length(d.iqrscas2)/2):length(d.iqrscas2)), d.iqrscas2[(length(d.iqrscas2)/2):
  length(d.iqrscas2)], type = "l", xlab = "", axes = F, ylab = "", col = 2,
  lty = 2)
z <- list(d.iqrscas = (d.iqrscas - d.iqrscas1), d.iqrscas2 = d.iqrscas2, d.iqrscas1 =
  (d.iqrscas1 - d.iqrscas11), d.iqrscas1s = d.iqrscas1s, d.iqrscas2 = (d.iqrscas2 -
  d.iqrscas21), d.iqrscas2s = d.iqrscas2s, qrsca1 = qrsca1, qrsca2 = qrsca2)
z
}

```

APPENDIX J

“VQRSDEP” PROGRAM LISTING

```
function(ecg1, ecg2, fin, rq = 15, rs = 15, nfft = 8192, sr = 500, decim = 25,
        wait = T, title = "")
{
  print(paste("creating vectors"))
  minq <- vector("numeric", 0)
  mins <- vector("numeric", 0)
  qrscal <- vector("numeric", 0)
  minx1 <- vector("numeric", 0)
  qrscal2 <- vector("numeric", 0)
  minx2 <- vector("numeric", 0)
  pkx <- fin$pk
  print(paste("checking ecgs"))
  if(pkx[1] < rq) {
    pkx <- pkx[2:length(pkx)]
  }
  if(length(ecg1) < (pkx[length(pkx)] + rs)) {
    pkx <- pkx[1:(length(pkx) - 1)]
  }
  print(paste("sampling rate of ecgs = ", sr))
  print(paste("decim = ", decim))
  sr2 <- sr/decim
  print(paste("sr2 = ", sr2))
  print(paste("detrending ecgs"))
  lwf1 <- lowess(1:length(ecg1), ecg1, f = 110/length(ecg1), iter = 2, delta = 0.1)$y
  ecg1 <- ecg1 - lwf1
  lwf2 <- lowess(1:length(ecg2), ecg2, f = 110/length(ecg2), iter = 2, delta = 0.1)$y
  ecg2 <- ecg2 - lwf2
  print(paste("shifting ecgs"))
  minecg1 <- min(ecg1)
  minecg2 <- min(ecg2)
  if(minecg1 < 0) {
    ecg1 <- ecg1 + 1.1 * abs(minecg1)
  }
  if(minecg2 < 0) {
    ecg2 <- ecg2 + 1.1 * abs(minecg2)
  }
  print(paste("Detecting Q-waves"))
  for(i in 1:length(pkx)) {
    minq1 <- ((pkx[i] - rq):(pkx[i] - 2))[(ecg1[(pkx[i] - rq):(pkx[i] - 2))]]
  }
}
```



```

        <= min(ecg1[(pkx[i] - rq):(pkx[i] - 2)])]
    if(length(minq1) > 1) {
        minq1 <- minq1[length(minq1)]
    }
    minq <- c(minq, minq1)
}
if(length(pkx) != length(minq)) {
    print(paste("Number of Q's is not equal to that of R's"))
    print(paste("Q's:", length(minq)))
    print(paste("R's:", length(pkx)))
    stop( )
}
print(paste("Detecting S-waves"))
par(mfrow = c(2, 1), mar = c(6.1, 6.1, 4.1, 4.5))
for(i in 1:length(pkx)) {
    mins1 <- (pkx[i):(pkx[i] + rs))[(ecg1[pkx[i):(pkx[i] + rs)])
        <= min(ecg1[pkx[i):(pkx[i] + rs)])]
    if(length(mins1) > 1) {
        mins1 <- mins1[length(mins1)]
    }
    mins <- c(mins, mins1)
}
if(length(pkx) != length(mins)) {
    print(paste("Number of S's is not equal to that of R's"))
    print(paste("S's:", length(mins)))
    print(paste("R's:", length(pkx)))
    stop( )
}
for(i in 10:14) {
    plot((minq[i] - 10):(mins[i] + 10), ecg1[(minq[i] - 10):(mins[i] + 10)])
    abline(v = pkx[i])
    abline(v = minq[i])
    abline(v = mins[i])
    plot((minq[i] - 10):(mins[i] + 10), ecg2[(minq[i] - 10):(mins[i] + 10)])
    abline(v = pkx[i])
    abline(v = minq[i])
    abline(v = mins[i])
    if(wait)
        scan( )
}
print(paste("Calculating areas"))
for(i in 1:length(pkx)) {
    cols1 <- ecg1[minq[i]:mins[i]]
    cols2 <- ecg2[minq[i]:mins[i]]
    ca1 <- sum(cols1)

```

```

ca2 <- sum(cols2)
minx1[i] <- min(ecg1[minq[i]:mins[i]])
minx2[i] <- min(ecg2[minq[i]:mins[i]])
window <- round(mins[i] - minq[i])
base1 <- minx1[i] * window
base2 <- minx2[i] * window
rca1 <- ca1 - base1
rca2 <- ca2 - base2
qrscal <- c(qrsca1, rca1)
qrscal2 <- c(qrsca2, rca2)
# par(mfrow=c(2,1))
# plot((minq[i] - 10):(mins[i] + 10), ecg1[(minq[i] - 10):(mins[i] + 10)])
# abline(v = pkx[i])
# abline(v = minq[i])
# abline(v = mins[i])
# plot((minq[i] - 10):(mins[i] + 10), ecg2[(minq[i] - 10):(mins[i] + 10)])
# abline(v = pkx[i])
# abline(v = minq[i])
# abline(v = mins[i])
# if(wait)
# scan( )
}
n <- length(ecg1) + 100
f1 <- 0.3
f2 <- 0.2
d <- 1
xf <- ((1:330) - 1)/nfft * sr2
iqrscal <- spline(pkx, qrscal, n)
iqrscal <- iqrscal$y
d.iqrscal <- iqrscal[seq(1, length(iqrscal), decim)]
par(mfrow = c(1, 1))
plot(qrscal, ylab = "ecg1 areas uninterpolated", main = title)
if(wait)
scan( )
plot(d.iqrscal, type = "l", xlab = "Time", ylab = "ecg1 Deriv Resp (vQRSdep)",
main = title)
if(wait)
scan( )
d.iqrscal1 <- lowess(1:length(d.iqrscal), d.iqrscal, f = f2, iter = 2,
delta = ceiling((length(d.iqrscal) * 0.3)/8))$y
d.iqrscals <- spect(d.iqrscal - d.iqrscal1, nt = nfft, ns = 6)
par(mfrow = c(1, 1), mar = c(6.1, 6.1, 4.1, 4.5))
plot(xf, fin$isp[1:330], type = "l", xlab = "Frequency Number", ylab = "Power",
main = title)
par(new = T)

```

```

plot(xf, d.iqrscals[1:330], type = "l", lty = 3, axes = F, xlab = "", ylab = "")
axis(4)
mtext("ecg1 Deriv Resp(vQRSdep) Power - - ", side = 4, line = 3)
if(wait)
  scan( )
iqrsc2 <- spline(pkx, qrsca2, n)
iqrsc2 <- iqrsc2$y
d.iqrsc2 <- iqrsc2[seq(1, length(iqrsc2), decim)]
par(mfrow = c(1, 1))
plot(qrsca2, ylab = "ecg2 areas uninterpolated", main = title)
if(wait)
  scan( )
plot(d.iqrsc2, type = "l", xlab = "Time", ylab = "ecg2 Deriv Resp (vQRSdep)",
      main = title)
if(wait)
  scan( )
d.iqrsc2l <- lowess(1:length(d.iqrsc2), d.iqrsc2, f = f2, iter = 2, delta =
  ceiling((length(d.iqrsc2) * 0.3)/8))$y
d.iqrsc2s <- spect(d.iqrsc2 - d.iqrsc2l, nt = nfft, ns = 6)
par(mfrow = c(1, 1), mar = c(6.1, 6.1, 4.1, 4.5))
plot(xf, fin$isp[1:330], type = "l", xlab = "Frequency Number", ylab =
  "Power", main = title)
par(new = T)
plot(xf, d.iqrsc2s[1:330], type = "l", lty = 3, axes = F, xlab = "", ylab = "")
axis(4)
mtext("ecg2 Deriv Resp(vQRSdep) Power - - ", side = 4, line = 3)
if(wait)
  scan( )
qrsca <- (atan(qrsca2/qrsca1) * 180)/pi
plot(qrsca, ylab = "Arctan (ecg2/ecg1) uninterpolated", main = title)
if(wait)
  scan( )
iqrsc <- spline(pkx, qrsca, n)
iqrsc <- iqrsc$y
d.iqrsc <- iqrsc[seq(1, length(iqrsc), decim)]
plot(d.iqrsc, type = "l", xlab = "Time", ylab = "Arctan (ecg2/ecg1) Deriv Resp
  (vQRSdep)", main = title)
if(wait)
  scan( )
d.iqrscal <- lowess(1:length(d.iqrsc), d.iqrsc, f = f2, iter = 2, delta =
  ceiling((length(d.iqrsc) * 0.3)/8))$y
d.iqrscas <- spect(d.iqrsc - d.iqrscal, nt = nfft, ns = 6)
par(mfrow = c(1, 1), mar = c(6.1, 6.1, 4.1, 4.5))
plot(xf, fin$isp[1:330], type = "l", xlab = "Frequency Number", ylab =
  "Power", main = title)

```

```

par(new = T)
plot(xf, d.iqrscas[1:330], type = "l", lty = 3, axes = F, xlab = "", ylab = "")
axis(4)
mtext("Arctan (ecg2/ecg1) Deriv Resp (vQRSdep) Power - - ", side = 4, line = 3)
if(wait)
  scan( )
plot(xf, d.iqrscas[1:330], type = "l", xlab = "frequency", ylab = "Power")
par(new = T)
plot(xf, d.iqrscals[1:330], type = "l", lty = 2, col = 2, axes = F)
par(new = T)
plot(xf, d.iqrscas2s[1:330], type = "l", lty = 3, col = 3, axes = F)
if(wait)
  scan( )
par(mfrow = c(3, 1), mar = c(6.1, 6.1, 4.1, 3.1))
plot((d.iqrscas2 - d.iqrscas2l), type = "l", xlab = "Time", ylab = "ecg2", main = title)
plot((d.iqrscas1 - d.iqrscas1l), type = "l", xlab = "Time", ylab = "ecg1")
plot((d.iqrscas - d.iqrscal), type = "l", xlab = "Time", ylab = "Arctan (ecg2/ecg1)",
      sub = "Derived with vQRSdep")
if(wait)
  scan()
par(mfrow = c(2, 1), mar = c(6.1, 6.1, 4.1, 4.5))
plot(d.iqrscas1[1:(length(d.iqrscas1)/2)], type = "l", main = title, xlab = "Time",
      ylab = "ecg1 (solid), ecg2 (dashed)", sub = "First Minute : Derived
      with vQRSdep")
par(new = T)
plot(d.iqrscas2[1:(length(d.iqrscas2)/2)], type = "l", xlab = "", axes = F,
      ylab = "", col = 2, lty = 2)
plot(((length(d.iqrscas1)/2):length(d.iqrscas1)), d.iqrscas1[(length(d.iqrscas1)/2):
length(d.iqrscas1)], type = "l", main = title, xlab = "Time", ylab = "ecg1
(solid), ecg2 (dashed)", sub = "Second Minute : Derived with vQRSdep")
par(new = T)
plot(((length(d.iqrscas2)/2):length(d.iqrscas2)), d.iqrscas2[(length(d.iqrscas2)/2):
length(d.iqrscas2)], type = "l", xlab = "", axes = F, ylab = "", col = 2,
lty = 2)
print(paste("length of d.iqrscas1=", length(d.iqrscas1)))
print(paste("length of d.iqrscas2=", length(d.iqrscas2)))
print(paste("length of d.iqrscas=", length(d.iqrscas)))
z <- list(qrscas1 = qrscas1, qrscas2 = qrscas2, d.iqrscas = (d.iqrscas - d.iqrscal),
d.iqrscas = d.iqrscas, d.iqrscas1 = (d.iqrscas1 - d.iqrscas1l), d.iqrscals =
d.iqrscas1s, d.iqrscas2 = (d.iqrscas2 - d.iqrscas2l), d.iqrscas2s = d.iqrscas2s)

z
}

```

APPENDIX K

S-PLUS PROGRAM DEVELOPED TO CALCULATE CROSS CORRELATION

```
function(x, y)
{
# The length of x, y data must be the same
  if(length(x) %% 2 > 0) {
    x <- x[1:(length(x) - 1)]
  }
  if(length(y) %% 2 > 0) {
    y <- y[1:(length(y) - 1)]
  }
  if(length(x) > length(y)) {
    x <- x[1:length(y)]
  }
  if(length(y) > length(x)) {
    y <- y[1:length(x)]
  }
  x <- x - mean(x)
  y <- y - mean(y)
  n <- length(x)
  autox <- sqrt(sum(x * x))
  autoy <- sqrt(sum(y * y))
  autoxy <- autox * autoy
  r <- c(1:n)
  cross <- c(1:2 * n)
  print(paste("calculating cross-correlation"))
  for(i in 1:n) {
    xshift <- x[(length(x) - i + 1):length(x)]
    ywindow <- y[1:i]
    p <- xshift * ywindow
    r[i] <- sum(p)
    cross[i] <- r[i]/autoxy
  }
  for(i in 1:n) {
    xshift <- x[1:(length(x) - i + 1)]
    ywindow <- y[i:length(x)]
    p <- xshift * ywindow
    r[i] <- sum(p)
    cross <- c(cross, (r[i]/autoxy))
  }
}
```

```
}  
print(paste("maximum cross-correlation=", max(cross)))  
print(paste("minimum cross-correlation=", min(cross)))  
par(mfrow = c(3, 1), mar = c(6.1, 6.1, 4.1, 3.1))  
par(cex = 1)  
plot(x, type = "l", ylab = "", xlab = "")  
plot(y, type = "l", ylab = "", xlab = "")  
plot(cross, type = "l", ylab = "", xlab = "")  
}
```

APPENDIX L

S-PLUS PROGRAM DEVELOPED TO CALCULATE COHERENCE

```
function(x, y, nfft = 8192, Fs = 20, nwind = 700, noverlap = 350, taper = 0.2, title = "")
{
  if (any(is.na(x)))
    stop("NA's not allowed - some found in x")
  if (any(is.na(y)))
    stop("NA's not allowed - some found in y")
  if (taper < 0 | taper > 1)
    stop("taper must be between 0 & 1")
  if (length(x) != length(y)) {
    print(paste("lengths of x and y must be the same!!!!"))
    print(paste("automatically adjusting to the size of the smallest signal"))
    if(length(x) %% 2 > 0) {
      x <- x[1:(length(x) - 1)]
    }
    if(length(y) %% 2 > 0) {
      y <- y[1:(length(y) - 1)]
    }
    if(length(x) > length(y)) {
      x <- x[1:length(y)]
    }
    if(length(y) > length(x)) {
      y <- y[1:length(x)]
    }
  }
  x <- x - mean(x)
  y <- y - mean(y)
  n <- length(x)
  k <- trunc((n - noverlap)/(nwind - noverlap))
  index <- 1:nwind
  Pxx <- rep(0, nfft)
  Pyy <- rep(0, nfft)
  Pxy <- rep(0, nfft)
  Pxx2 <- rep(0, nfft)
  Pyy2 <- rep(0, nfft)
  Pxy2 <- rep(0, nfft)
  print(paste("Windowing is done with a Hanning window"))
  window <- 0.5 * (1 - cos((2 * pi * (1:nwind))/(nwind + 1)))
  for(i in 1:k) {
    xw <- window * x[index]
```

```

yw <- window * y[index]
index <- index + (nwind - noverlap)
if(nfft < length(xw)) {
  xw <- xw[1:nfft]
}
if(nfft < length(yw)) {
  yw <- yw[1:nfft]
}
if(nfft > length(xw)) {
  xw <- c(xw, rep(0, nfft - length(xw)))
}
if(nfft > length(yw)) {
  yw <- c(yw, rep(0, nfft - length(yw)))
}
Xx <- fft(xw, nfft)
Yy <- fft(yw, nfft)
Xx2 <- abs(Xx)^2
Yy2 <- abs(Yy)^2
Xy2 <- Yy * Conj(Xx)
Pxx <- Pxx + Xx2
Pxx2 <- Pxx2 + abs(Xx2)^2
Pyy <- Pyy + Yy2
Pyy2 <- Pyy2 + abs(Yy2)^2
Pxy <- Pxy + Xy2
Pxy2 <- Pxy2 + Xy2 * Conj(Xy2)
}
if(nfft %% 2 > 0) {
  select <- (1:((nfft + 1)/2))
}
else {
  select <- (1:((nfft/2) + 1))
}
Pxx <- Pxx[select]
Pxx2 <- Pxx2[select]
Pyy <- Pyy[select]
Pyy2 <- Pyy[select]
Pxy <- Pxy[select]
Pxy2 <- Pxy2[select]
Coh <- (abs(Pxy)^2)/(Pxx * Pyy)
xf <- ((1:330) * Fs)/nfft
plot(xf, Coh[1:330], type = "l", xlab = "Frequency", ylab = "Coherence", main =
  title)
x <- locator()
print(paste("y value of coherence=", x$y))
}

```


REFERENCES

- [1] A.J. Vander, J.H. Sherman, and D.S. Luciano. *Human Physiology*. New York: McGraw-Hill Publishing Company. Sixth Edition. 1994.
- [2] A.C. Guyton. *Textbook of Medical Physiology*. Philadelphia: W.B. Saunders Company. Eighth Edition. 1991.
- [3] J. Wartak. *Simplified Vectorcardiography*. J.B. Lippincott Company. 1970.
- [4] D. Cheng. *Field and Wave Electromagnetics*. New York: Addison-Wesley Publishing Company. Second Edition. 1989.
- [5] G.B. Moody, R.G. Mark, A. Zoccola, and S. Mantero, "Derivation of respiratory signals from multi-lead ECGs," *IEEE Comp. in Cardiol.*, vol. 12, pp. 113-116, 1985.
- [6] F. Netter. *The CIBA Collection of Medical Illustrations Volume 5, The Heart*. CIBA Pharmaceutical Company. 1981
- [7] M.D. Kamath and E.L. Fallen, "Power spectral analysis of heart rate variability: A noninvasive signature of cardiac autonomic function," *Crit. Rev. in Biomed. Eng.*, vol. 21, no. 3, pp. 245-311, 1993.
- [8] A.L. Goldberger, D.R. Rigney, and B.J. West, "Chaos and fractals in human physiology," *Scientific American*, vol. 262, pp. 42-49, 1990.
- [9] R. Ziemer and W. Tranter. *Principles of Communication Systems, Modulation, and Noise*. Boston: Houghton Mifflin Company. Third Edition. 1990.
- [10] G.G. Berntwon, J.T. Cacioppo, and K.S. Quigley, "Respiratory sinus arrhythmia: Autonomic origins, physiological mechanisms, and psychophysiological implications," *Psychophysiology*, vol. 30, pp. 183-196, 1993.
- [11] S.J. Shin, W.N. Tapp, S.S. Reisman, and B.H. Natelson, "Assessment of autonomic regulation of heart rate variability by the method of complex demodulation," *IEEE Trans. on Biomed. Eng.*, vol. 36, no. 2, pp. 274-282, 1989.
- [12] M. Pagani, F. Lombardi, S. Guzzetti, O. Rimoldi, R. Furlan, P. Pizzinelli, G. Sandrone, G. Malfatto, S. Del' Orto, E. Piccaluga, M. Turiel, G. Baselli, S. Cerutti, and A. Malliani, "Power spectral analysis of heart rate and arterial pressure variabilities as a marker of sympatho-vagal interaction in man and conscious dog," *Circulation Res.*, vol. 59, pp. 178-93, 1986.

- [13] I. O'Brien, P. O'Hare, and R. Corral, "Heart rate variability in healthy subjects: effect of age and the derivation of normal ranges for tests of autonomic function," *Bristol Heart Journal*, vol. 55, pp. 348-354, 1986.
- [14] M. Pagani, G. Malfatto, S. Pierini, R. Casati, A.M. Masu, M. Poli, F. Guzzetti, F. Lombardi, S. Cerutti, and A. Malliam. "Spectral analysis of heart rate variability in the assessment of autonomic diabetic neuropathy," *Journal of Autonomic Nervous System*, vol. 23, pp. 143-149, 1988.
- [15] R.E. Kleiger, J.P. Miller, J.T. Jr. Bigger, A.J. Moss, and the Multicenter Post-Infarction Research Group, "Decreased heart rate variability and its association with increased mortality after acute myocardial infarction," *Am. J. Cardiol.*, vol. 59, pp. 256-264, 1987.
- [16] J.T. Jr. Bigger, R.E. Kleiger, J.L. Fleiss, L.M. Rolintzky, R.C. Steinman, J.P. Miller, and the Multicenter Post Infarction Research Group, "Components of heart rate variability measured during healing of acute myocardial infarction," *Am. J. Cardiol.*, vol. 61, pp. 208-215, 1988.
- [17] J. Hayano, Y. Masami, Y. Sakakibara, T. Fujinami, K. Yokoyama, Y. Watanabe, and K. Takata, "Short- and long-term effects of cigarette smoking on heart rate variability," *Am. J. of Cardiol.*, vol. 65, pp. 84-88, 1990.
- [18] J.T. Jr. Bigger, R. Goldsmith, R. Steinman, and J. Fleiss, "Comparison of 24-hour parasympathetic activity in endurance-trained and untrained young men," *J. Am. College of Cardiol.*, vol. 20, no. 3, pp. 552-558, 1992.
- [19] A. Pellegrini, F. Pinciroli, R. Rossi, and L. Vergani, "Virtual leads for the ambulatory ECG monitoring: remarks on the persistency of their direction," *Comp. and Biomed. Research*, vol. 18, pp. 62-78, 1985.
- [20] F. Pinciroli, R. Rossi, and L. Vergani, "Detection of electrical axis variation for the extraction of respiratory information," *IEEE Comp. in Cardiol.*, vol. 12, pp. 113-116, 1985.
- [21] G.B. Moody, R.G. Mark, M. Bump, J. Wienstein, A. Berman, J. Mietus, and A. Goldberger, "Clinical validation of the ECG-derived respiration (EDR) technique," *IEEE Comp. in Cardiol.*, vol. 13, pp. 507-510, 1986.
- [22] L. Zhao, "Derivation of respiration from electrocardiogram during heart rate variability studies," thesis presented to the biomedical engineering committee at NJIT, May, 1994.

- [23] L. Zhao, S. Reisman, T. Findley, "Derivation of respiration from the electrocardiogram during heart rate variability studies," *IEEE Comp. in Cardiol.*, vol. 21, pp. 53-56, 1994.
- [24] L. Zhao, S. Reisman, and T. Findley, "Derivation of respiration from electrocardiogram during heart rate variability studies," *Proceed. Ann. Conf. of IEEE Eng. in Med. and Biol. Soc.*, Baltimore, Md. Nov, 1994.
- [25] J. Nilsson. *Electric Circuits*. New York: Addison-Wesley Publishing Company. Third Edition. 1990.
- [26] R. Ziemer, W. Tranter, and R. Fannin. *Signals and Systems: Continuous and Discrete*. New York: Macmillan Publishing Company. Second Edition. 1989.
- [27] R.C. Gonzalez and R.E. Woods. *Digital Image Processing*. New York: Addison-Wesley Publishing Company. 1992.
- [28] R.E. Challis and R.I. Kitney, "Biomedical signal processing, part 1: Time domain methods," *Med. & Biol. Eng. & Comput.*, vol. 28, pp. 509-524, 1990.
- [29] R.E. Challis and R.I. Kitney, "Biomedical signal processing, part 3: The power spectrum and coherence function," *Med. & Biol. Eng. & Comput.*, vol. 29, pp. 225-241, 1991.
- [30] J. Rosell and J.G. Webster, "Signal-to-Motion Artifact Ratio Versus Frequency for impedance pneumography," *IEEE Trans. on Biomed. Eng.*, vol. 42, no. 3, pp.321-323, 1995.
- [31] J. Rosell, K.P. Cohen, and J.G. Webster, "Reduction of motion artifacts using a two-frequency impedance plethysmograph and adaptive filtering," *IEEE Trans. on Biomed. Eng.*, vol. 42, no. 10, pp. 1044-1048, 1995.